Civil and Environmental Theses   Civil and Environmental Engineering

10-2016

Characterization of the Interfacial Behavior of Hybrid Fiber-Steel Lap Connections Fastened by Steel on FRP Anchors

Omnia Ragab Abou El-Hamd

UAEU

جامعة الإمارات العربية المتحدة
United Arab Emirates University

United Arab Emirates University

College of Engineering

Department of Civil and Environmental Engineering

CHARACTERIZATION OF THE INTERFACIAL BEHAVIOR OF HYBRID FIBER-STEEL LAP CONNECTIONS FASTENED BY STEEL OR FRP ANCHORS

Omnia Ragab Mohamed Abou El-Hamd

This thesis is submitted in partial fulfilment of the requirements for the degree of Master of Science in Civil Engineering

Under the Supervision of Dr. Amr M.I. Sweedan

October 2016

Declaration of Original Work

I, Omnia Ragab Mohamed Abou El-Hamd, the undersigned, a graduate student at the United Arab Emirates University (UAEU), and the author of this thesis entitled *"Characterization of the Interfacial Behavior of Hybrid Fiber-steel Lap Connections Fastened by Steel or FRP Anchors"*, hereby, solemnly declare that this thesis is my own original research work that has been done and prepared by me under the supervision of Dr. Amr M.I. Sweedan, in the College of Engineering at UAEU. This work has not previously been presented or published, or formed the basis for the award of any academic degree, diploma or a similar title at this or any other university. Any materials borrowed from other sources (whether published or unpublished) and relied upon or included in my thesis have been properly cited and acknowledged in accordance with appropriate academic conventions. I further declare that there is no potential conflict of interest with respect to the research, data collection, authorship, presentation and/or publication of this thesis.

Student's Signature: _____   Date: ___5/12/2016___

Advisory Committee

1) Advisor: Dr. Amr M.I. Sweedan

Title: Associate Professor

Department of Civil and Environmental Engineering

College of Engineering, UAE University

2) Co-advisor: Prof. Khaled M. El-Sawy

Title: Professor

Architecture Department

College of Architecture and Design, Effat University, KSA

Approval of the Master Thesis

This Master Thesis is approved by the following Examining Committee Members:

1) Advisor (Committee Chair): Dr. Amr M.I. Sweedan

   Title: Associate Professor

   Department of Civil and Environmental Engineering

   College of Engineering

   Signature _____ Date _Oct 27, 2016_

2) Member (Internal Examiner): Dr. Bilal El-Ariss

   Title: Associate Professor

   Department of Civil and Environmental Engineering

   College of Engineering

   Signature _____ Date _OCTOBER 27, 2016_

3) Member (External Examiner): Prof. James M. Ricles

   Title: Bruce G. Johnston Professor

   Department of Civil and Environmental Engineering

   Lehigh University, USA
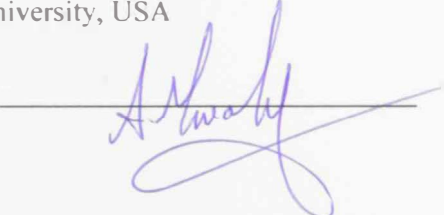
   Signature _____ Date _Oct 27, 2016_

This Master Thesis is accepted by:

Dean of the College of Engineering: Professor Sabah Alkass

Signature _____Sabah_____ Date _5/12/2016_____

Dean of the College of the Graduate Studies: Professor Nagi T. Wakim
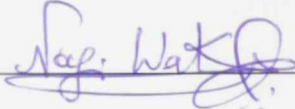
Signature _Nag. Wak_____ Date _5|12|2016_____

Copy _8_ of _9_

Abstract

Fiber reinforced polymers (FRP) are extensively used in several engineering fields due to their superior properties. In structural engineering applications, fiber polymers have been recently used for retrofitting and strengthening of existing structures. A common technique for strengthening steel structures involves bonding FRP composites to targeted steel elements. However, bonding practices and researches revealed undesirable brittle failure of the adhesive at the FRP-steel interface. A recent research program conducted at UAE University validated the effectiveness of using mechanically fastened hybrid FRP (HFRP) laminates in strengthening steel beams. Outcomes of the research program revealed that the fastening technique could provide a good alternative to overcome the unfavorable brittle failure of bonded FRP composites. In addition, the study was enlightening and showed promising results in terms of both yield and ultimate load capacities of the strengthened steel beams. However, a limited range of fastening parameters was examined in the above mentioned research program.

The current research study is motivated by the need to investigate the influence of wider range of fastening parameters and geometrical configurations on the interfacial behavior of fastened HFRP-steel connections. An extensive experimental program was carried out on 62 fastened connections on two phases. In the first phase, the effect of different number of washers-per-bolt, clamping torque, bolt-hole diameter and bolt spacing were investigated on connections formed using steel bolts. While the second phase was conducted using FRP anchors to examine the effect of fastener type and diameter along with the sheared edge distance on the performance of the connections. Test results recommended to snug-tight the steel bolts after placing them in standard hole-diameters with the use of 2 washers-per-bolt. Bolt spacing was proven to have insignificant effect on both failure modes and load carrying capacity of the HFRP-steel connections. The study also suggested the use of FRP anchors with 13 mm diameter with a sheared edge distance that is three times the hole-diameter for optimal performance in terms of ductility and load carrying capacity. Recorded experimental measurements were utilized to develop nonlinear load-slip models which were integrated in developing nonlinear 3D finite

element (FE) models using ANSYS software. FE models were used to simulate the behavior of the fastened connections and to accurately predict their load carrying capacity. Numerical predictions were in excellent agreement with the experimental findings which verified the accuracy of the proposed nonlinear load-slip models.

Keywords: Hybrid fiber reinforced polymers (HFRP), fastened connection, HFRP-steel connections, washers, clamping torque, bolt-hole diameter, FRP anchors, finite element method.

Title and Abstract (in Arabic)

توصيف السلوك البيني لوصلات تراكبية من الألياف الهجينة و الفولاذ المثبتة باستخدام مسامير من الفولاذ أو الألياف

الملخص

تستخدم الألياف الهجينة (FRP) على نطاق واسع في العديد من المجالات الهندسية وذلك بسبب خصائصها المتفوقة. مؤخراً تم استخدام الألياف الهجينة في التطبيقات الهندسة الإنشائية لإعادة ترميم وتقوية المنشآت القائمة. وتتضمن الوسيلة السائدة لتقوية المنشآت الفولاذية لصق الألياف الهجينة بالهياكل الفولاذية المستهدفة. وقد كشفت البحوث التي أجريت على الألياف الهجينة الملصقة بهياكل الفولاذ عن انهيار سريع غير مرغوب فيه للمادة اللاصقة. وقد أثبت برنامج بحثي أجري حديثاً في جامعة الإمارات العربية المتحدة فعالية استخدام الألياف الهجينة المثبتة ميكانيكيا على الفولاذ من أجل تعزيز الدعامات الفولاذية. وكشفت الدراسة أن تقنية الربط يمكن أن توفر بديلا جيدا للتغلب على الانهيار السريع الغير مرغوب فيه للمادة اللاصقة في وصلات الألياف الملصقة بالفولاذ. بالإضافة إلى ذلك، فقد أظهرت الدراسة نتائج واعدة من حيث قدرة تحمل الدعامات الفولاذية المدعمة باستخدام تقنية الربط، ولكن مع الأخذ في الاعتبار محدودية عوامل الربط التي تمت دراستها في البرنامج البحثي السابق ذكره.

الدافع الرئيسي وراء إجراء الدراسة الحالية هو الحاجة إلى دراسة تأثير مجموعة واسعة من عوامل الربط والتشكيلات الهندسية على السلوك البيني للوصلات التراكبية من الألياف الهجينة المثبتة بالفولاذ. تم تنفيذ الأولى، تمت دراسة تأثير عدد مختلف من ورذ التثبيت ، وقطر فتحة المسمار، والتباعد بين المسامير باستخدام مسامير من الفولاذ. في حين أجريت المرحلة الثانية باستخدام مسامير من الألياف لدراسة تأثير نوع المسمار وقطره بالإضافة إلى تأثير مسافة القص من الحرف على أداء الوصلات التراكبية المثبتة. أوصت نتائج الاختبار بحكم مسامير الفولاذ بعد وضعها في فتحة قياسية القطر مع استخدام وردتين تثبيت لكل مسمار. وقد ثبت أن تباعد المسامير له أثر ضئيل على كل من طرق انهيار و قدرة تحمل الوصلات التراكبية الهجينة. واقترحت الدراسة أيضا استخدام مسامير من الألياف قطرها 13 مم مع مسافة قص من الحرف تساوي ثلاثة أضعاف قطر حفرة المسمار لتحسين أداء الوصلات التراكبية من حيث الليونة وطاقة التحميل الاستيعابية. واستخدمت القياسات العملية لتطوير نماذج غير خطية للتحميل و الانزلاق والتي تم استخدامها لبرمجة نماذج محاكاة ثلاثية الأبعاد باستخدام برنامج ANSYS. استخدمت نماذج العناصر المحددة (FE) لمحاكاة سلوك الوصلات التراكبية المثبتة والتنبؤ بدقة بطاقتها الاستيعابية. أظهرت نتائج المحاكاة توافق ممتاز مع النتائج العملية مما أكد دقة نماذج التحميل و الانزلاق المطورة في هذا البحث.

مفاهيم البحث الرئيسية: ألياف هجينة مقواه (HFRP)، وصلات مثبتة، وصلات الألياف و الفولاذ، ورذ التثبيت، الدوران، قطر فتحة المسمار، مسامير من الألياف، طريقة العناصر المحددة.

Acknowledgements

Dedication

I dedicate my thesis work to the soul of my father, Dr. Ragab Mohamed Abou-ElHamd, who would have been happy to see me follow in his steps as a researcher. I also devote this thesis to my mother, Dr. Noura Ali Khalil, my brother, Eng. Ahmed Ragab, and my sisters, Eng. Amira Ragab and Eng. Aya Ragab.

Table of Contents

List of Tables

List of Figures

List of Abbreviations and Symbols

2D	Two Dimensional
3D	Three Dimensional
Al	Aluminum
BSR	Block Shear Rupture
CFRP	Carbon Fiber Reinforced Polymers
D	Bolt-Hole Diameter
E	Young's Modulus
ERSG	Electrical Resistance Strain Gauges
E_t	Tangential Modulus
FB10	FRP Anchor (FIBREBOLT[R]) with 10 mm Diameter
FB13	FRP Anchor (FIBREBOLT[R]) with 13 mm Diameter
FE	Finite Element
FEM	Finite Element Method
FRP	Fiber Reinforced Polymers
GFRP	Glass Fiber Reinforced Polymers
HFRP	Hybrid Fiber Reinforced Polymers
LVDT	Linear Variable Differential Transducers
R	Rolled Edge Distance
S	Spacing between Bolts
SG	Strain Gauge
Sh	Sheared Edge Distance
ST	Snug-tight
T	Clamping Torque
W	Number of Washers-per-Bolt
σ_u	Ultimate Stress
σ_y	Yield Stress

Chapter 1: Introduction

For over 70 years, steel has been widely used in several structural applications for its high ductility, stiffness-to-weight ratio, strength-to-weight ratio and ease of constructability. However, steel structures are susceptible to deteriorations due to the exposure to repeated cyclic loading and moist environments which consequently limit their serviceability. Recent strengthening practices involve the use of fiber reinforced polymers (FRP) as an alternative to conventional rehabilitation methods of steel structures. FRP composites are favored in several structural applications due to their high strength-to-weight ratio and efficiency in resisting flexural and fatigue loads. The commonly used FRP composites in structural rehabilitation applications are Carbon Fiber Reinforced Polymers (CFRP) and Glass Fiber Reinforced Polymers (GFRP). Despite the very high strength-to-weight ratio offered by CFRP, their corrosion induced problems when connected to steel limits their applications in metallic structures. Meanwhile, the use of GFRP provides better corrosion resistivity with lower strength than the CFRP when connected to steel. Hybrid CFRP-GFRP composites (HFRP) combine both CFRP and GFRP and utilize their advantages in an efficient manner. It should be noted that the utilization of CFRP in the HFRP composites promotes for high tensile strength of the composites and increases their stiffness. In addition, the incorporation of GFRP enhances the corrosion resistivity of HFRP and prevents their splitting when drilled.

Regular strengthening techniques of steel structures involve bonding FRP composites to steel elements. However, research studies revealed brittle failure of the system before the full utilization of the strength of the composites. Therefore, recent studies were directed towards using fastened FRP-steel systems. This current study is

motivated by the need to investigate the effect of various fastening parameters on the performance and load carrying capacity of fastened HFRP-steel system. Experimental and numerical investigations are performed in order to assess the interfacial behavior of the fastened system with respect to the studied parameters.

This introductory chapter includes five sections starting by presenting the problem to be investigated and the objectives of the study, followed by the adopted methodology to execute the research. Finally, the structure of the thesis and its contribution to the area of rehabilitation of steel structure are described.

1.1 Problem Statement

Fiber reinforced polymers (FRP) are extensively used in several engineering fields due to their superior properties of corrosion resistivity, lightweight, high strength-to-weight ratio and easy handling. In structural engineering applications, fiber polymers have been recently used for retrofitting and strengthening of existing structures. A common technique of strengthening steel structures involves bonding FRP composites to targeted steel elements. However, bonding practices and researches revealed undesirable brittle failure of the adhesive at the FRP-steel interface. Very limited studies were conducted recently to investigate the effectiveness of mechanically fastened hybrid fiber reinforced polymers (HFRP) in strengthening steel elements. These studies validated the use of fastened HFRP-steel technique and proposed it as a good alternative to overcome the unfavorable brittle failure of bonded FRP-steel systems. Reported experimental and numerical results by Sweedan et al. (2014, 2016) revealed significant improvements in both ultimate and flexural capacities of steel beams strengthened using fastened HFRP laminates. Obtained results established a potential interest to investigate the effect of different

geometrical and fastening parameters on the behavior of the fastened HFRP-steel system. Another study by Sweedan et al. (2013) examined the effect of selected geometrical parameters on fastened HFRP-steel connections. Promising results, in view of both yield and ultimate load capacities, were reported in the study. However, the study considered a limited range of fastening parameters.

The current thesis is motivated by the need to investigate the influence of wider range of fastening parameters and geometrical configurations on the interfacial behavior and response of fastened HFRP-steel connections. A wide spectrum of design parameters is examined including fastener type and diameter, sheared edge distance, spacing between fasteners, number of washers-per-bolt, clamping torque and bolt-hole diameter. Both experimental and numerical approaches are utilized in conducting the study in order to propose preferred configurations for optimum performance of multi-fastened HFRP-steel lap connections.

1.2 Objectives of the Study

The main objective of the current research work is to identify the influence of major fastening parameters on the interfacial behavior of fastened HFRP-steel connections. The conducted research includes experimental and numerical investigations. The experimental program is divided into two main phases depending on the fastener type. The first phase is conducted on double-lap HFRP-steel connections fastened using steel bolts. The effect of different number of washer-per-bolt, clamping torque, bolt-hole diameter and bolt spacing on the fastened connections is investigated in this phase. Meanwhile, the second phase utilizes FRP anchors with different diameters to assess the effectiveness of using FRP anchors in structural applications. Outcomes of the experimental program are used to

recommend fastening configurations that would result in optimum performance of similar connections. The responses of the tested configurations are used to establish load-slip models, for each fastener type, that are capable of describing the interfacial behavior of the connections considering the different failure modes. The research then proceeds by performing numerical modeling and analysis of the fastened HFRP-steel connections. The developed load-slip models are used to model three dimensional (3D) nonlinear finite element (FE) models to simulate the behavior of the tested connections. The developed FE models are validated against the experimental results. Numerically predicted load-displacement curves and strains in the HFRP are compared to the experimental measurements to verify the accuracy of the proposed load-slip models.

1.3 Methodology and Approach

The current study is conducted experimentally and numerically. The experimental program aims at investigating the interfacial behavior of fastened HFRP-steel double-lap connections. Designed direct shear connections are subjected to tensile loading using a displacement-controlled Universal Testing Machine. The experimental investigation includes two main phases based on the type of fasteners. Steel bolts are used in the first phase in order to examine the effect of the number of washers-per-bolt on the response of the HFRP-steel connections. Recommended configuration is then used in designing the next set of connections which focuses on examining the effect of clamping torque on the tested connections. After that, the performance of the HFRP-steel connections under various bolt-hole diameters and spacing values is assessed. The second experimental phase highlights the use of non-corrosive fiber fasteners as replacement of the steel bolts. FRP anchors with different

diameters are used to form the connection between the HFRP laminates and steel plates. In this phase, the influence of the bolt diameter along with the sheared edge distance on the response of the HFRP-steel connections is investigated. Linear variable displacement transducer (LVDTs) and strain gauges are used to monitor the in-plane and out-of-plan deformations of the tested connections. Recorded measurements, along with the corresponding applied loads, enable tracking the behavior of the fastened connections. Experimental measurements are also used to develop nonlinear load-slip models that account for the different failure modes controlling the interfacial behavior of tested connections. Fastening configurations which resulted in optimum performance of the tested connections in each phase are recommended and modeled numerically.

Three-dimensional nonlinear FE models of the fastened HFRP-steel connections with the recommended configurations are developed. The interfacial behavior between the HFRP laminates and steel plates is taken into consideration through the implementation of the load-slip models developed in the experimental phase into the FE model. Finite element simulations are carried out using the general purpose finite element software package ANSYS. The FE models are designed to simulate the behavior of the tested connections and predict the load distribution between bolts in multi-bolt connections. Resulted numerical predictions are compared to the experimental findings in order to ensure the accuracy of the proposed load-slip models. The developed load-slip models should serve as tools to accurately predict the load carrying capacity of the fastened HFRP-steel connections.

1.4 Organization of the Thesis

The current research thesis consists of five chapters. Brief description of the contents of each chapter is provided in this section.

Chapter 1 discusses the problem statement of the current research, followed by an illustration of the objectives of the study and the methodology adopted in conducting the experimental and numerical work. The chapter proceeds by presenting the organization of the thesis and concludes by the contribution of this study to the structural engineering field.

Chapter 2 addresses the previously published research work related to the use of FRP composites. The pros and cons of bonded FRP-steel system are displayed in this chapter followed by a summary of research studies on the behavior of fastened FRP composites with respect to various fastening parameters: presence of washers, clamping torque, bolt-hole diameter, bolts spacing and fastener diameter and type. Finally, the latest experimental and numerical researches evaluating the performance of fastened FRP-steel system in strengthening steel structures are discussed.

Chapter 3 discusses in details the experimental work performed on fastened HFRP-steel double-lap connections. The executed experimental procedures to investigate the behavior of fastened HFRP-steel connections with respect to different fastening parameters using steel and fiber bolts are displayed. Obtained experimental results in terms of load-displacement curves and strain measurements are also reported in this chapter. Developed nonlinear load-slip models reflecting the interfacial behavior of the tested HFRP-steel connections using both types of fasteners are also presented and discussed in details.

Chapter 4 focuses on the development of finite element models based on the nonlinear load-slip models obtained from the experimental findings in order to accurately predict the behavior of the fastened HFRP-steel connections. Detailed descriptions of the geometries. materials, boundary conditions and loading system of the 3D finite element models are also presented. Numerically predicted load-displacement curves and strain measurements of each model are verified against their experimental counterparts.

At the end of this thesis. chapter 5 provides a summary of the work carried out in the thesis: it also presents conclusions regarding the interfacial behavior of the fastened HFRP-steel connections. Conclusions related to the influence of each tested parameter on the behavior of the fastened connections are also drawn. Technical recommendations of the preferred configurations for optimum performance of similar multi-fastened HFRP-steel connections in terms of ductility and strength are presented. Finally. the chapter provides recommendations for future researches based on the findings of the study.

1.5 Study Contribution

The outcomes of the current study enrich the literature with technical data related to the use of fastened HFRP-steel systems in the structural engineering field. The study provides better understanding of the interfacial behavior between steel and HFRP laminates considering different types of fasteners. Furthermore. the wide range of design parameters considered in the study provides reliable database for engineers to produce safe and economical design of similar connections. The developed and verified nonlinear load-slip models allow designers to accurately consider the partial composite action taking place at the HFRP-steel interface.

Outcomes of the study are expected to provide code developers with practical design recommendations for safe and optimum design of fastened HFRP-steel connections.

Chapter 2: Literature Review

2.1 Introduction

Fiber reinforced polymers (FRPs) are extensively used in several engineering applications due to their superior properties compared to conventional construction material. Their marvelous characteristics of corrosion resistivity, lightweight, high strength-to-weight ratio and easy handling enabled them to be used in aerospace and military applications. In the mid-1980's, an urgent need for the implementation of FRP composites in retrofitting and strengthening deteriorated concrete and steel structures erected after the Second World War had emerged (Hollaway and Teng, 2008). FRP composites have been a good replacement for steel plates used in conventional structural steel repairing techniques. A common technique of strengthening steel structures involves bonding FRP composites to targeted steel elements. Although bonded FRP-steel systems have proven effectiveness in strengthening steel members, steel beams strengthened with bonded FRP strips were found to fail in a brittle mechanism due to debonding of the FRP. Recently, an alternative strengthening technique was proposed in which FRP composites are fastened to targeted steel members. Despite the proved efficiency of the fastened FRP-steel system, very few researchers attempted to investigate the effect of fastening parameters on its performance.

This chapter summarizes the pros and cons of the bonded FRP-steel strengthening system. After that, it reviews various research studies which were conducted on fastened FRP composite systems in different engineering applications. The effect of the fastening parameters (i.e., clamping torque, spacing, …, etc.) on the performance of the connections is discussed. Research studies on each parameter are

presented in a historical order. Finally, the latest studies that address utilizing fastened FRP sheets in strengthening steel elements are presented.

2.2 Bonded FRP-Steel Connections

Conventional structural steel repairing techniques involve the use of steel plates either bonded or fastened to the metallic structure. Many disadvantages are associated with the traditional method since the additional plates are susceptible to corrosion, difficult to shape, transport and install, prone to buckle and impose extra loads on the existing structure. Bonded steel plates require careful surface preparations and expensive false work to stabilize the steel plates until they are fully bonded to the structure.

With the evolution of FRP composites, they have been introduced to replace the steel plates in strengthening applications due to their excellent properties. Three fibers are commonly used in the construction industry: glass, aramid and carbon fibers (Hollaway, 2010). The mechanical and physical properties of carbon fibers (CFRP) make them excellent alternative for the rehabilitation of steel structures. Their high strength-to-weight ratio enables 2 kg of FRP to equate, approximately in 2016, the strength of 47 kg of steel. Although the initial cost of fiber composites is generally higher than that of steel (4 to 20 times), their installation savings can overcome their high cost. Considering the facilitated transportation and long-term performance of FRP composites, they can result in cost savings by 17.5% (Hollaway and Cadei, 2002). Practical steel retrofitting techniques involve bonding FRP strips to steel elements by an adhesive. Earlier researches classified six different failure modes for bonded FRP-steel systems: failure of steel and adhesive interface, failure of FRP and adhesive interface, adhesive layer failure, FRP delamination, FRP

rupture and steel yielding. Usually the last two failure modes (i.e.. FRP rupture and steel yielding) are avoided by using normal modulus FRP (i.e.. elastic modulus between 100 GPa and 250 GPa) and sufficient steel thickness (Zhao and Zhang. 2007). A schematic view of the described failure modes is shown in Fig. 2.1. Generally. the performance of bonded FRP-steel systems depends on the effectiveness of the adhesive and the pre-treatment of the bonded surfaces. Unlike FRP-concrete bonded system where concrete presents the weak link. epoxy adhesive is the weak link in bonded FRP-steel connections. It is clear that the failure of bonded FRP-steel connections significantly depends on the adhesive properties and thicknesses. As bond length affects the failure of bonded FRP composite system. Xia and Teng (2005) proposed a bi-linear bond-slip model that can be used in predicting the effective bond length in bonded FRP-steel connections.
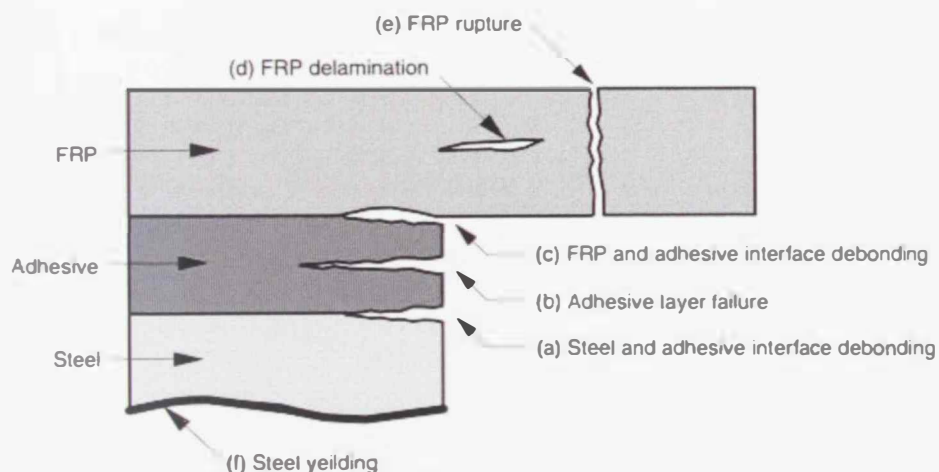
Figure 2.1: Schematic view of the failure modes [after Zhao and Zhang (2006)]

The quality of bonded FRP-steel composites depends on the surface preparations prior to the application of the adhesive which is considered one of the drawbacks of bonded connections. Therefore. skilled labors are required to prepare

the surface and mix the adhesive in a proper manner. Basic principles of surface preparations include providing a bonding surface that is: free from contamination, chemically reactive to enable reliable chemical bond between the adhesive and the steel and resistant to environmental deteriorations.

Durability is a common concern in the bonded connections since they are expected to withstand a wide range of environmental conditions including high temperature, high humidity, freezing-and-thawing cycles, chloride and de-icing salts penetration. Water can adversely affect the durability of the bonded connections if diffused through the adhesive, transported along the interface or by capillary action through adhesive cracks. Bonded connections could experience a reduction in their strength if exposed to liquid water, high temperature and/or high humidity. They are also sensitive to thermal changes. At high temperature, the adhesive can soften resulting in a reduction in the mechanical performance of the connection. Freezing-and-thawing cycles can induce moisture into the bond facilitating the de-bonding process of the laminates. A comprehensive state-of-the-art review performed by Heshmati et al. (2015) addressed the effect of moisture and temperature on the durability of adhesively bonded FRP-steel connections. Although FRP composites are corrosion resistant, their contact with metallic materials can initiate a galvanic interaction between them. Practical applications highlight the importance of the use of glass fiber layer as corrosion barrier between the CFRP plate and the steel during bonding to prevent galvanic action (Hollaway and Cadei, 2002).

Several research studies were conducted to investigate the performance of bonded FRP-steel system under variable factors. An experimental investigation was conducted by Sen et al. (2001) to examine the feasibility of using CFRP in repairing

steel members. Steel specimens were loaded until yielding then high modulus CFRP laminates were bonded to the tension flange and tested to failure. Results showed significant gain in the ultimate strength by 21% (for 2 mm thick CFRP laminates), however, small enhancement in the elastic stiffness was observed. The study recommended increasing the capacity of the adhesive by using fasteners to ensure yielding of steel members before failure. It also highlighted that bonded steel-FRP composites do not fully utilize the ductility of the steel member.

The discussed drawbacks of bonded FRP-steel strengthening system provoke researchers to consider the potential use of fastened composite connections in steel construction applications.

2.3 Fastened Composite Connections

A summary of research work on the behavior of fastened FRP composites is presented in this section. Focus will be placed on studies that investigate the effect of selected parameters (i.e., clamping torque, bolt-hole diameter,…etc.) on the behavior of fastened FRP composite connections. The majority of these research papers was directed to aerospace applications, while a limited number was implemented in the area of structural engineering. It should be noted that the performance of fastened FRP-steel connections is discussed separately in section 2.4.

Coelho and Mottram (2015) reported four main failure modes for statically loaded fastened composite plate connection with steel plate through a single bolt as shown in Fig. 2.2. Bearing failure (Fig. 2.2(a)) occurs close to the contact region, while net-tension is characterized by sudden cracks transverse to the loading direction (Fig. 2.2(b)). In some cases, bearing failure causes shear-out failure (Fig.

2.2(c)) of the connections which, when joined with net-tension, produces the cleavage failure (Fig. 2.2(d)). Experimental researches indicated that bearing failure is a progressive damage that allows for ductile behavior of the connections, therefore, most connections are rather designed to fail in bearing.
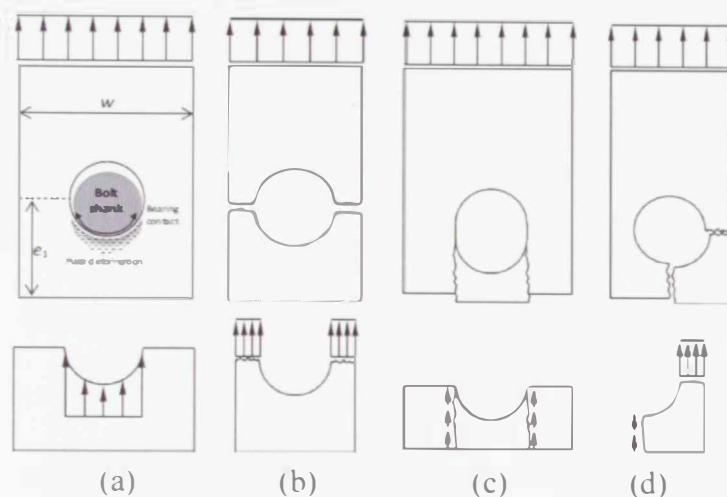
Figure 2.2: Failure modes of fastened plate-to-plate connections: (a) bearing, (b) net-tension, (c) shear-out and (d) cleavage. [after Coelho and Mottram (2015)]

2.3.1 Effect of Washers

To the best of the author's knowledge, no one had yet investigated the effect of the presence of washers and their thickness on the behavior of mechanically fastened FRP-metal connections. However, few researchers studied washers' effect on FRP-concrete and FRP-FRP fastened connections as outlined hereunder.

A numerical study was performed by Feo et al. (2012) to examine the influence of the presence of washers on the bearing stresses of GFRP-GFRP connections formed using 14 mm steel bolts. Straus7 software was used to perform the finite element analysis in which connections were modeled using eight-node elements, while the contact between the bolts and the FRP was simulated by one-dimensional point-contact elements. Numerical results revealed that the presence of

washers reduced the bearing stresses of the fastened connections and influenced their failure modes. The FE analysis showed dominant bearing failure of the modeled connections with the presence of washers due to the compression stresses around and under the washers. The numerical results were validated through an experimental investigation for selected connections in the University of Salerno.

The effect of washers on mechanically fastened FRP-concrete connections was investigated by Realfonzo et al. (2013). The experimental program tested 17 specimens of different layouts with the presence of washers and 17 other specimens without washers. Test specimens were made of 150×200 mm^2 concrete prisms fastened to FRP laminates using 6 mm diameter steel bolts. Results revealed that specimens with washers had greater load carrying capacity than those without washers. Such behavior can be referred to the fact that washers provided larger contact area for the applied clamping pressure, therefore enhancing the bearing strength of the connections. The absence of washers caused early damage of the outer surface of the FRP laminates as evident by the observed punching of the laminates due to the rotation of the bolt head which, consequently, reduced the capacity of the connection. The presence of washers kept the post-peak response of the connection almost stable for wide range of slip values. Specimens without washers showed remarkable softening after the peak load which led to collapse of the connections at lower slip values. Using washers in single-fastener connections slightly enhanced the strength of the connections; however, it almost doubled the slip at the peak load providing more ductility of the connections. On the other hand, the use of washers in multi-fastener FRP-concrete connections significantly increased the peak loads by about 38% and showed higher displacements at failure. Simplified FEM models were developed by Martinelli et al., (2012) using SAP2000 to simulate

and verify the experimental results. The authors used the findings of the experimental program to propose an inverse numerical procedure for identifying the interfacial behavior of mechanically fastened FRP-concrete connections.

2.3.2 Clamping Torque

Several studies since the 1970's have investigated the effect of clamping torque on the behavior of fastened composite connections. Different terminologies have been used to identify the clamping torque such as: tightening torque, clamping pressure and pre-loading moment. Stockdale and Matthews (1976) examined the effect of clamping pressure on the bearing failure of bi-directional E-glass fiber-reinforced polymeric connections. A special bolt was placed in a 6.3 mm hole-diameter in single shear setup. The specimens were tested under four clamping loads: 0, 4905, 9810 and 14715 N using washers of different outer diameters. Test results were also compared to pin testing condition where washers were excluded from the setup without clamping pressure. Experimental results revealed a significant increase in the failure loads of the specimens associated with increasing the clamping loads. An enhancement of 75% in the load carrying capacity of the specimens was obtained for the examined range of clamping loads. Failure of the zero clamped specimens was located near the hole; however, with the increase of the clamping loads, failure was characterized by cracking in the hole and compression at the washer edge. One of the remarkable highlights of the research was the observed post peak sudden brittle failure with the increase of the clamping loads. It is worth noting that the failure load of pin type connection was 40% lower than the zero clamping condition (with restraining washer) with noticeable fiber delamination.

Another study by Crews (1981) investigated the torque effect on mechanically fastened composites using 2.24 mm thick $[0/45/90/-45]_{2s}$ graphite/epoxy laminates fastened using 6.35 mm steel bolts with 0.15 mm clearance. Tested torque values include: 0, 2.82, 5.65, 8.48 and 11.3 N.m. Experimental results revealed that increasing the torque delayed the onset of failure of the assembly and increased its ultimate strength. Significant improvements in the bearing strength were observed at higher torque values. It was also observed that the applied torque considerably affected the failure modes of the composites and combined modes were detected at increased clamping. Typically, the noticed failure modes were shear-out under washer and bearing failure beyond it. A 100% improvement in the ultimate strength of specimens torqued to 11.3 N.m. was observed relative to the pin-bearing condition. The research concluded that strength improvements caused by increasing the applied torque were reflected on the associated failure modes.

In the early 1990's, Horn and Schmitt (1994) examined the influence of clamping force on the bearing strength of multi-directional fiber composite material. A total of 32 single-shear connections were prepared using composite material and titanium fasteners. Net-fit holes were drilled in the composites with diameter of 6.35 mm and edge distance of 19.05 mm. The effect of fastener types (in terms of bolt-head type) on the strength of the connections was also investigated using protruding and countersink head fasteners. The study concluded that increasing the clamping force enhanced the bearing strength of the composite connections. Assemblies with protruding head fasteners showed higher strength than those with countersink fasteners.

Another experimental investigation was conducted by Cooper and Turvey (1995) using double-lap-single-bolt connections made of 6.35 mm thick layered GFRP sheets in order to examine the effect of bolt clamping torque. Specimens were tested under three clamping conditions: pin-bearing (zero clamping torque), lightly clamped (3.0 N.m.) and fully clamped condition (30.0 N.m.). Connections were connected by M10 grade 8.8 bolts. Increasing the applied torques from zero to 3 N.m. resulted in 30% improvement in the average failure loads. Meanwhile, 96% enhancement in the failure loads was obtained with the use of 30 N.m. torque. Although the applied torque had almost negligible effect on the stiffness of the connections, it had significant effect on the composite plate critical edge-to-diameter and width-to-diameter ratios to ensure bearing behavior of the tested connections.

Further study performed by Wang et al. (1996) aimed at evaluating the effect of clamping pressure on the bearing response and strength of fastened composite connections. Double-lap connections were designed using high strength steel and carbon composites with bolt-hole clearance of 0.002 inches. The study was conducted using carbon composites of bi- and multi-directional fibers. A pre-designed load cell was used to measure the clamping force generated from the applied torque. Different clamping forces were tested ranging from "finger tight" to "1.2 kips". Specimens were tested using MTS machine in tensile mode at a loading rate of 0.05 inch/min. Two failure modes were observed: bearing failure (for specimens with W/D greater than 8 and E/D greater than 6) and shear-out failure. Results revealed that increasing the clamping pressure improved the bearing strength of the connections. Increasing the clamping force reduced the visible cracks under the washer since the clamping pressure reduced the probability of transverse expansion of the laminates. It was also observed that bearing damage under washers

depended on the applied clamping condition. As bearing load increased, damage accumulated under the washers and shear cracks were formed until it over-passed the washers and cracks appeared on the laminate surface. The researches interpreted the enhanced bearing strength associated with increasing the clamping pressure to the friction between washers and the laminates.

Three years later, Yan et al. (1999) examined the effect of clamping pressure on composite-focused level using composite-bolted laminates. The experimental study tested the response of graphite/epoxy laminates with different fiber orientations under various clamping forces. Laminates which were prone to fiber-matrix splitting and delamination exhibited decreased tensile strength at higher clamping pressure. Although splitting of fiber-matrix could improve the tensile strength around the hole through releasing stress concentrations in the 0-degree plies around the bolt-hole, applied clamping pressure restrained fiber-matrix splitting leading to higher stress concentrations in the 0-degree plies associated with lower tensile strength around the hole. Nevertheless, laminates which were not prone to fiber-matrix splitting were insensitive to the clamping conditions. Tested laminates were then used in double-lap fastened connections to examine the effect of clamping pressure on the tensile strength of the connections. Results revealed enhancement in the strength of the connections with the increase of the clamping pressure.

In 2000, Tong investigated the effect of clamping torque along with the relative positions of bolt and washer on bearing failure of composite connections. CFRP laminates, with carbon fibers oriented in a quasi-isotropic sequence, with width of 38.1 mm and thickness of 1.72 mm were fastened in a double-lap setup using 6.25 mm bolt diameter. Tested specimens had edge distance of 38.1 mm, hole-

diameter of 6.35 mm and length of 178 mm. The tested configuration resulted in hole-bolt clearance of 0.1 mm and hole-washer clearance of 0.65 mm. Two offsets were studied: positive offset; where the center of the washers had offset in the direction of the load leaving a gap between the inner surface of the washer and the upper surface of the hole and (b) negative offset, where washer offset is assumed in the opposite direction of that in the positive offset. Specimens with positive offset were tested under 3 torque values (0, 6.4 and 12.88 N.m.), while those with negative offset experienced 5 torque values (0, 6.4, 11.88, 17.19 and 19.77 N.m.). Experimental results showed increase in the initial and ultimate failure loads with increasing the applied torques regardless of the setup offset. Local delamination buckling was observed around the edge of the washer at ultimate failure loads.

A more recent experimental program by Khashaba et al. (2006) studied the effect of clamping torque on the performance of single-bolt connections using GFRP composites. Glass fibers were arranged in an angle-ply of $[0/\pm45/90]_s$ with a thickness of 5.2 mm. Typical 0.1 mm clearance of aircraft connections was selected in designing the connections. Results of the investigated torque values (0, 5, 10 and 15 N.m.) showed an improvement in the stiffness of the connection with increasing the applied torque from finger-tight to 15 N.m. This improvement was attributed to the increase in the contact pressure between the washer and the laminate. Increasing the applied torque enhanced the bearing strength of the connection and allowed it to carry higher ultimate loads, hence, enhancing its load carrying capacity. The observed failure modes were similar for most of the specimens starting by delamination between the laminate layers followed by a net-tension failure in the 90° layers, then shear-out of the 0° layers and finally bearing failure in the 45° layers.

Kapti et al. (2010) conducted experimental and numerical investigations to explore the failure mechanisms of carbon/epoxy composite connections under different pre-loading moments (torques). Carbon/epoxy laminates with thickness of 1.6 mm and lay-up of [90/0]$_s$ were used to form fastened connections using 8 mm bolts. Specimens were tested under 3 N.m. and 6 N.m. preloading moments. Testing was performed on Instron-1114 Tensile Machine at a rate of 1 mm/min. Three main failure modes were observed depending on the dimensions of the tested specimens: shear-out, net-tension and bearing. Increasing the pre-loading moment enhanced the bearing strength of the connections. Specimens tested under 3 N.m. and 6 N.m. exhibited enhancement of the bearing strength by of 152% and 241%, respectively, compared to non-pre-loaded specimens.

Another study by Ozen and Sayman (2011) examined the effect of torque on the load carrying capacity of rectangular glass fiber composite laminates. Connections were tested under 0, 3 and 6 N.m. in tension with a displacement rate of 1 mm/min. Experimental results showed improvement in the load capacity of the connections with increasing the clamping torque. Net-tension and bearing failure modes were observed for connections with zero torque, while only net-tension failure was detected for higher torque values. A two dimensional finite element model was developed on ANSYS 11.0 software using the SHELL181 element. Predicted failure loads were close to the experimental ones with a maximum error of 10%.

2.3.3 Bolt-Hole Diameter

Bolt-hole diameter is one of the principle parameters considered in designing mechanically fastened connections. The effect of the clearance between the bolts and the drilled holes is of great interest especially for aerospace applications. McCarthy

et al. (2002) investigated the effect of bolt-hole diameter on the stiffness and bearing strength of single-lap composite connections with a single-bolt using protruding and countersunk bolts. 8 mm diameter bolts made of titanium alloy were utilized in the study along with graphite/epoxy composites of multi-directional fibers. Four different clearances were examined in the experimental program: net-fit, 80 μm, 160 μm and 240 μm. Connections were loaded in tension in a displacement-controlled manner with a rate of 0.1 mm/min. Resulting load-displacement curves showed delayed initial load take-up of the connections with increasing the bolt-hole diameter. Experimental observations revealed initial bearing failure of all connections, while the final failure was characterized by bolt failure. It was also noted that bolt-hole diameter affected the ductility of the connections as net-fit assemblies failed at lower displacements than others. For finger-tight connections with protruding head bolts, a reduction of about 10% in the stiffness of the connections was observed with increasing the clearance to 240 μm. This decrease in the stiffness was attributed to the reduced bolt-hole contact area associated with increasing the bolt-hole diameter. One of the most important findings of this study is the insignificant effect of bolt-hole diameter on the ultimate strength of the connections, despite its inverse effect on the initial bearing of the connections. Connections with protruding head bolts were stiffer than those fastened with countersunk bolts.

In 2004, Kelly and Hallström conducted experimental and numerical studies on the effect of geometrical parameters, lateral clamping load and bolt-hole clearance on the bearing strength of laminated multi-directional carbon fibers. The experimental program tested three different clearance levels: 0%, 1.55% and 3.05% as percentage increase of the bolt diameter (d_b = 6.35 mm). Specimens were prepared with different edge-to-diameter, width-to-diameter and thickness-to-diameter values

and were tested under a universal testing machine with a constant cross-head speed of 1 mm/min. Test results revealed that bolt-hole clearance inversely influences the bearing strength of the laminates. For finger-tightened laminates, a reduction of 7% and 19% of the bearing strength was observed for clearances of 1.55% and 3.05%, respectively. However, the percentage reduction was slightly improved with the use of lateral clamping of 5 N.m. to 4% and 12% for clearance levels of 1.55% and 3.05%, respectively. One of the most important highlights of the study was the insignificant effect of bolt-hole clearance on the ultimate bearing strength of the connection. However, it was suggested to use of a small bolt-hole clearance for better bearing strength of the connections.

The effect of different bolt-hole clearances on load distribution between bolts was examined by Lawlor et al. (2005) using double-lap multi-bolt connections. Graphite/epoxy specimens with width of 48 mm, thickness of 4.16 mm, edge distance of 24 mm and bolt diameter of 8 mm were prepared. The composite laminates had quasi-isotropic lay-up of [45/0/-45/90]. Bolts were torqued to 0.5 N.m. to present a finger-tight condition. Selected clearances used in the experimental study were: net-fit, 80 µm, 160 µm and 240 µm. Small clearances were considered to reflect practical application of aircraft connections. Six different clearances cases were examined: one connection with all neat-fit holes, four connections with one loose-fit hole and a sixth connection with two loose-fit holes. Eight strain gauges were installed on each specimen to trace the load distribution between the bolts. Test results revealed that clearances had a remarkable effect on load distribution in multi-bolt connections. Generally, loads were transferred to net-fit bolts first due to their high stiffness. In all net-fit connections, the outer two bolts carried the majority of the load. However, connections having one loose-fit hole placed at one end showed

different behavior since the two net-fit holes shared the entire load initially, then at a later stage the loose-fit bolt started contributing in carrying the load. At the described case of one loose-fit hole located at one end, load tried to be equally distributed among all bolts but material failure occurred first. The analysis of the results showed that net-fit connections were the stiffest and underwent the shortest deflections. The experimental findings indicated that bolt-hole clearance had insignificant effect on the ultimate failure loads; however, it influenced the initial failure loads of the specimens. Connection with all net-fit clearance showed 25% increase in the initial failure loads than those with two loose holes.

The findings of the above mentioned experimental study were used to validate a 3D FE model developed by McCarthy et al. (2005). The nonlinear finite element software ABAQUS was used in modeling and predicting load distributions and redistributions between bolts when bearing failure occurred. The validation of the model was performed through comparing the load-displacement characteristics and surface strains of the connections with the experimental results. Results revealed that bolt-hole diameter affected the initial failure loads of the connections but had insignificant effect on their ultimate load capacity.

Esendemir and Oendueruecue (2011) performed an experimental investigation to examine the effect of bolt-hole diameter on the bearing strength of mechanically fastened connections. Specimens with different widths and edge distances were tested to set limits for width-to-diameter (W/d) and edge distance-to-diameter (E/d) ratios that are necessary to avoid the undesirable net tension failure. Glass fiber composites were used in preparing a total of 20 specimens with thickness of 1.45 mm and length of 80 mm. All bolts used in the investigation had diameter of

5 mm and torqued to 0 N.m. to present finger-tight conditions. The setup of the experiment identified two types of clearances: Type-I had hole-diameter of 5 mm (net-fit), while Type-II had hole-diameter of 5.2 mm (loose-fit). Each specimen was loaded to ultimate failure and failure modes and loads were recorded. Three failure modes were observed in each clearance type: net tension, cleavage with net tension and bearing with net tension. Results showed that bolt-hole diameter had insignificant effect on the failure mode of the connections. However, clearance was shown to inversely affect failure loads of the connections, where connections with smaller clearances withstood more loads before failure. Results showed 35.72% increase in the bearing strength of connections with Type-I than Type-II.

Another experimental study by Rosales-Iriarte et al. (2011) examined the effect of bolt-hole diameter on carbon fiber laminates under bearing and bypass loads. Tested specimens were made of layered uni-directional carbon fibers. Three different clearances were tested: net-fit, 160 μm and 240 μm. Obtained bearing-bypass-load curves revealed a reduction in the load carrying capacity of the connection with increasing the clearance when bearing loads govern the behavior of the connection. On the other hand, increasing the clearance improved the capacity of the connection when bypass stresses controlled. The presence of clearance reduced the bolt-hole contact area under bearing conditions generating higher stresses which, in-turn, reduced the carrying capacity of the connection. In conditions where bypassing stresses were dominant, the clearance reduced the stresses produced between the hole-edge and the pin allowing the connection to carry more loads. Also, the experimental program investigated the effect of clamping torque on the capacity of the connection. Results showed enhancements in the bearing strength of the connection with increasing the clamping forces from finger-tight to 15 N.m.

2.3.4 Spacing and Bolt Diameter

The term 'Spacing' is used in this study to describe the row spacing between connecting bolts along the same gauge line in the loading direction. To the best of the author's knowledge, only one research work was conducted by Chutima and Blackie (1996) to explore the effect of row spacing on fastened composite connections. A two dimensional FE model was developed to examine the effect of row spacing and bolt diameter on the stress distribution at the bolt-hole interface and load transfer between bolts in a multi-fastened composite plate. The modeled connection consisted of laminated multi-directional CFRP fastened to a rigid fixture using 6.35 mm titanium bolts loaded in tension. Integer multiples of the hole-diameter from 2 to 4 were modeled to investigate the effect of spacing on the connection, while the selected range of bolt-diameter varied between 5 mm and 16 mm. The developed FE model was verified against pervious experimental data and showed reliable predictions. Resulted simulations revealed more uniform load distribution across the rows of the connection at higher spacing. Meanwhile, varying the spacing had negligible effect on load transfer between bolts. Increasing the bolt-diameter resulted in lower stresses at the hole boundary and non-uniform load distribution across the connection. For the range of bolt diameter investigated in this study, bolt diameter of 8 mm was selected for ideal performance of the modeled connection.

The effect of bolt diameter was also investigated experimentally by Ascione et al. (2010). The study was conducted using mono-directional and bi-directional GFRP laminates with three different bolt diameters: 18 mm, 19 mm and 20 mm. Increasing the bolt diameter in fastened GFRP laminates was shown to have a direct linear relation with the pin-bearing capacity of tested composite laminates. The

experimental outcomes were then used to propose a design formula that predicts the pin-bearing failure load of similar connections as a function of the bolt diameter and fiber inclination angle.

2.3.5 Bolt Type

Researchers investigated the use of different bolt types on the behavior of the fastened connections in several applications. Generally, metal bolts were used with different shapes (i.e., countersunk, hexagonal, ...etc.). Few researchers designed their own composite bolts for research purposes. Erki (1995) compared the use of two types of fasteners: GFRP threaded rods and steel threaded rods. The experimental program examined the effect of 19 mm diameter rods on the strength of composite-composite double lap connections. It was noted that GFRP threaded rods reduced the capacity of the composite connections by half since they were weaker than the connected composite plate. However, the failure of connections fastened using the steel threaded rods was governed by the mechanical properties of the composite laminates.

Another experimental study by Starikov and Schön (2001) investigated the use of composite (ACF) bolts made of carbon reinforced polymers on the mechanical behavior of multi-bolt CFRP-CFRP connections. The composite plates were made of carbon fibers with quasi-isotropic lay-up. The behavior of connections with composite bolts was compared to that of connections made using titanium bolts: torque-set and Hunk-comp. Composite bolts were designed so that the part where torque was applied broke after attaining an average torque of 2.7 N.m. Constant bolt diameter of 6 mm was maintained throughout the investigation for all types of bolts. Each connection was equipped with ten strain gauges to monitor the transfer of load

between three rows of bolts. Five strain gauges were placed between the first and second rows of bolts while the remaining were placed between the second and third rows of bolts. Connections were exposed to static tensile loading with a constant displacement rate of 1 mm/min. Experimental results showed better load carrying capacity for connections with titanium bolts than those with ACF bolts. Connections fastened using both torque-set and Hunk-comp titanium bolts had the same ultimate strength and failure mode which was characterized by sudden post peak net-section failure. The load-displacement curve for connection with ACF bolts showed two failure modes. Fracture of the composite bolts was the dominant failure mode, followed by late bearing damage resulted from the left fractured pieces in the bolt-hole which created a pin loading set-up. The tested multi-bolt connections allowed the authors to examine the load distribution between bolts using the torque-set and ACF bolts. Results indicated that the row of bolts closer to the loading direction transferred the maximum amount of the applied loads, while the other two rows of bolts shared the remaining loads almost equally. Connections with the same configurations were tested under fatigue loading by Starikov and Schön (2002). The main difference in the behavior of the connections was the observed failure modes, where all connections failed in bolt fracture regardless of their type.

In 2005, Riccio and Marciano conducted an experimental study in order to examine the effect of bolt type and bolt diameter on the behavior of fastened composite-composite connections. Titanium bolts and nuts were used to connect the CFRP laminates, with lay-up of $[(0/\pm45/90)_4]_s$, in a single-lap setup. Protruding 4.8 mm diameter bolts were utilized in the study along with 4.8 mm and 6.4 mm countersunk bolts. Connections were loaded statically in tension with a displacement rate of 1 mm/min. The study results indicated that increasing the bolt diameter

enhanced the load carrying capacity of the connections, while changing the bolt type had insignificant effect on the failure load of the CFRP-CFRP connections. It was also concluded that the protruding bolts delayed the failure onset of the connection compared to countersunk bolts. Selected connections were numerically modeled by Riccio (2005) using a 3D progressive damage approach for the CFRP laminate. ANSYS software was utilized in developing the model, where brick elements (BRICK 45) and (BRICK 46) were used to model the bolts and the composite laminates, respectively. Numerical load-displacement curves were in good agreement with the experimental results, which validated the predictions of the FE model. Also, numerical strain predictions were compared to their experimental counterparts and showed acceptable match. The developed model was able to give detailed information on matrix cracking, fiber breakage and delamination at the damage onset of the joints which can be hardly identified using the non-destructive ultrasonic evaluations.

2.4 Fastened FRP-Steel Connections

A very limited number of research studies were found in the literature related to fastened FRP-steel connections. Hai and Mutsuyoshi (2012) performed experimental study to investigate the behavior of double-lap connections of steel splices fastened to hybrid CFRP-GFRP (HFRP) laminates. Eighty millimeter wide HFRP laminates were cut from the flanges of manufactured HFRP I-beams with a thickness of 14 mm. HFRP laminates were connected to the splices plates using steel bolts of 10 mm diameter. Connections were loaded in tension using a universal testing machine with 500 kN load capacity. Analysis of the resulted load-displacement curves of the fastened connections indicated initial negligible slip

resistance between the splice plate and the HFRP laminates, followed by gradual slip of the bolts toward the bearing region. After that, bearing failure and bending of the bolts took place reaching the ultimate load capacity of the connection before failure. The study also examined the effect of end-distance on the failure loads and failure modes of the steel-HFRP connections. Fastened connections with end-distances that are two-to-four times the nominal bolt diameter were tested. The lowest failure load was recorded for connections with end-distance that is double the bolt diameter with shear-out failure. The study suggested the use of end-distance that is four-times the bolt diameter to fully utilize the load capacity of the fastened connections with ductile bearing failure.

In 2013, an experimental study was conducted by Sweedan et al. to examine the effect of sheared and rolled edge distances and bolts' spacing on the behavior of FRP-steel connections. Two hybrid GFRP-CFRP laminates with thickness of 3.17 mm were fastened to 10 mm thick steel plates in a double-lap setup using M6 hexagonal steel zinc coated bolts. Connections were loaded in tension following a displacement-controlled manner in a rate of 1 mm/min. Tested connections experienced combination of failure mechanisms including: bearing at the bolts-FRP interface, followed by bending in bolts and folding of washers and finally tear out of the FRP laminates. All specimens failed in a ductile manner verifying the ability of mechanically fastened systems to overcome the undesirable brittle failure of bonded FRP-steel systems. The experimental findings recommended the use of sheared edge distance that is six to seven times the hole-diameter for better ductility and carrying capacity of the connections. The study had shown the insignificant influence of rolled edge distance on the behavior of the FRP-steel connections. For the examined range of spacing (100, 125 and 168 mm), the study revealed negligible effect of bolt

spacing on both failure loads and modes. The experimental outcomes were used to develop a simplified load-slip model for the various mechanisms taking place at the steel-FRP interface. The interfacial behavior of the fastened system was modeled numerically using ANSYS software. Predicted peak loads were in agreement with those obtained experimentally with error range between 0.25% and 8.87%, which validated the accuracy of the proposed load-slip model.

Validated load-slip model was further used by Sweedan et al. (2014) to simulate the behavior of steel beams strengthened with FRP laminates that are fastened to the bottom flange. Material and geometrical nonlinearities were considered in the simulation along with the relative slip at the FRP-steel interface. Resulted FE predictions revealed a ductile behavior of the strengthened beams and showed excellent agreement with the experimental measurements which confirmed the reliability of the developed model. An additional beam was simulated where the FRP laminates covered the total span of the beam. Stress distribution in the steel fasteners and the FRP laminates were studied in addition to the composite action of the mechanically strengthened beams. The main conclusions of the conducted numerical study highlighted the ductile behavior of the mechanically strengthened beams with the use of sufficient number of fasteners. The contribution of the FRP laminates in carrying the applied loads became apparent after yielding of the extreme fibers of the steel beams. Numerical results indicated that reducing the length of the FRP laminates required less number of fasteners and hence inducing more shear forces in each fastener risking the ductility of the strengthened system. However, increasing the stiffness of the fasteners enabled them to withstand higher shear forces. It was also concluded that increasing the thickness of the FRP laminates enhanced the load carrying capacity of the FRP-steel beams.

An extensive experimental investigation of the behavior of full-scale steel beams externally reinforced with fastened FRP composites was conducted by Sweedan et al. (2016). Eleven UB203×102×23 steel beams were reinforced using hybrid GFRP-CFRP composite strips which were fastened to the bottom flange of the beams using 6 mm diameter zinc coated steel bolts. The experimental program examined the influence of various lengths and thicknesses of the FRP laminates along with different number of fastening bolts. Yield flexural capacities and failure modes of the strengthened beams were assessed. Test matrix involved using three lengths of FRP laminates: 1200 mm, 1800 mm and 2200 mm with single and double layers of the FRP laminates corresponding to thicknesses of 3.175 mm and 6.35 mm, respectively. Reinforced beams were tested in three-point loading system and their behavior was compared to un-strengthened control beams. The experimental results revealed enhancements of both yield and ultimate loads of the strengthened beams compared to the control beams. Increasing the length of the FRP laminates showed slight improvement in the yield loads of the beams ranging between 1.8% and 6.4%. However, the strengthened beams exhibited significant enhancement in their ultimate flexural capacity by 11.1%, 16.7% and 19.4% for FRP lengths of 1200 mm, 1800 mm and 2200 mm, respectively. Moreover, doubling the thickness of the FRP laminates with maintaining sufficient number of bolts improved the yield and ultimate load carrying capacities of the beams by 9.1% and 30.6%, respectively. It's worth noting that all beams strengthened using single FRP laminate failed in a ductile manner by combination of bearing in the FRP laminates, rupture of the FRP fibers and local buckling in the compression steel flange. The same failure modes were observed with doubling the thickness of the FRP laminates while preserving adequate number of bolts. Using insufficient number of fastening bolts caused

sudden failure in the beams by shear fracture of the bolts before utilizing the full strength of the laminates.

2.5 Concluding Remarks

The research studies reviewed in this chapter covered a wide-range of the existing literature relevant to bonded and fastened FRP-Steel and FRP-FRP connections. The review included experimental and numerical research work that investigated the effects of main parameters controlling connection behavior such as use of washers, clamping torque, bolt-hole diameter, bolt diameter, spacing between bolts and fastener type. The review indicated that the response and strength of fastened composite connections are highly influenced by several failure modes including bearing at the FRP-bolt interface, bending in connecting bolts and tear out of FRP laminate. The few cited research studies devoted to structural applications of FRP-steel connections were limited to connections formed using 6 mm diameter steel bolts with bolt spacing that ranged between 100 mm to 168 mm. The sensitivity of connection behavior and the controlling failure mechanism to bolt spacing values beyond this limit needs to be investigated carefully. Other factors such as bolt-hole diameter, washers thickness and clamping torque need also to be explored. Moreover, the possible use of FRP anchors to enhance corrosion resistivity of the connections need to be addressed. Irrespective to the fastener material, the nature of the prevailing failure mechanism is of significant concern that needs to be carefully explored to avoid undesirable brittle failure of the FRP-steel connection. This literature review indicates that several aspects of fastened FRP-steel connections have not yet been extensively explored. This greatly emphasizes the importance of conducting the current study which also embarks upon the promising results reported

by Sweedan et al. (2013, 2014 and 2016) on the efficiency of the fastened FRP-steel strengthening system.

Chapter 3: Experimental Program

3.1 Introduction

The former literature showed an evident potential of the fastened FRP-steel system in strengthening steel members. The fastening technique was proven to present a ductile behavior of the composite hybrid fiber reinforced polymers-steel (HFRP-steel) system with significant enhancements in the load carrying capacity of the strengthened steel elements. However, no information was found in the literature discussing the effect of various fastening parameters on the response of HFRP-steel fastened system. Thus, the aim of this study is to investigate the effect of different fastening parameters on the interfacial behavior of the fastened HFRP-steel system. The current chapter presents the experimental program that was carried out to achieve the main goal of this study with emphasis on the materials used and the experimental methodology, procedures and results. The experimental study was performed to investigate the effect of several parameters including: fastener type and diameter, sheared edge distance, spacing between fasteners, number of washers-per-bolt, clamping torque and bolt-hole diameter on the response of the fastened HFRP-steel connections. The obtained experimental results were reported in view of the load-displacement curves and measurements of strain gauges for all the specimens.

3.2 Material and Instrumentation

The experimental program involved testing two main types of direct shear connections. The first type employs steel bolts to connect the HFRP laminates to steel plates. Meanwhile, in the second type, fiber anchors are utilized to form the connection between the HFRP laminates and steel plates. Materials and components

that were used to assemble the tested specimens are fully described in this section along with used measuring devices to allow for better understanding of the testing procedures.

3.2.1 Hybrid FRP Laminates

Hybrid CFRP-GFRP (HFRP) laminates produced by STRONGWELL[R] were used in this study. The hybrid laminates were supplied in rolls of 30 m length, 101.6 mm width and 3.175 mm thickness. The HFRP laminates are composed of carbon tows sandwiched between fiberglass mats bonded by highly corrosion resistant resin. Carbon tows enhance the strength of the composite while fiberglass provides better bearing strength. The special composition of the used laminates makes it the only available drillable type of FRP. Additionally, a synthetic surfacing veil is incorporated into the HFRP laminates to prevent corrosion at the interface between the HFRP and the steel plates. A cross-sectional view of the HFRP laminates, as provided by the manufacturer, is presented in Fig. 3.1.

Figure 3.1: Cross-section of the HFRP laminate used in the experimental study

The tensile properties of the HFRP laminates were identified by the manufacturer in accordance with ASTM D638-10 standards (2010) as displayed in Table 3.1.

Table 3.1: Tensile properties of HFRP Laminates (Provided by the Manufacturer)

Property	Average Value (MPa)	Design Value (MPa)
Tensile Strength	852	640
Tensile Modulus	62,190	62,190

In order to confirm the accuracy of the HFRP tensile properties reported in Table 3.1, three coupons were uniaxially tested in tension using a 100 kN MTS hydraulic testing machine with a displacement rate of 1 mm/min. These coupons were cut from the same material of the HFRP laminates and the tensile properties were determined according to ASTM D3039-14 standards (2014). The typical dimensions of the rectangular tested coupons are shown in Fig. 3.2. Each coupon has an overall length of 250 mm and a cross-sectional area of 79.375 mm^2 (see Fig. 3.2). Aluminum (Al) tabs with thickness of 3 mm were bonded using M-Seal adhesive to both ends of the HFRP coupon to allow for proper fixation with the grips of the tensile machine (see Fig. 3.3). Each coupon was instrumented with two electrical strain gauges at the front and backsides of the coupon for calculation of the stresses induced in the gauge section of the coupon as displayed in Fig. 3.3.
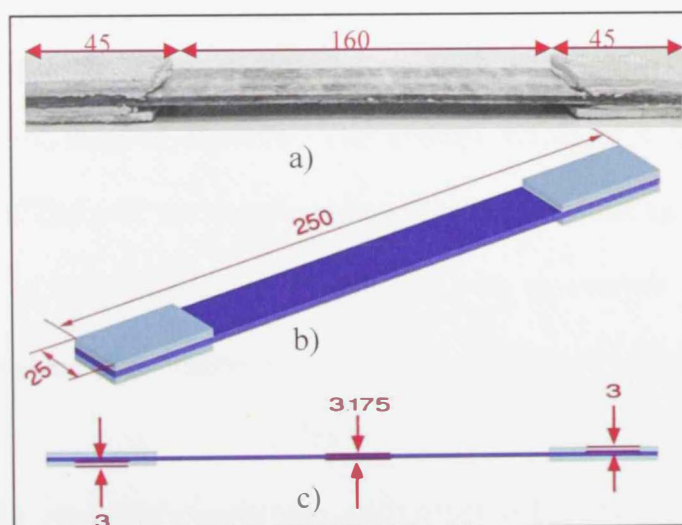
Figure 3.2: (a) Photo of the HFRP coupon, (b) Schematic view and dimensions of HFRP Coupon (c) Side view of the HFRP coupon (mm) [According to ASTM D3039]
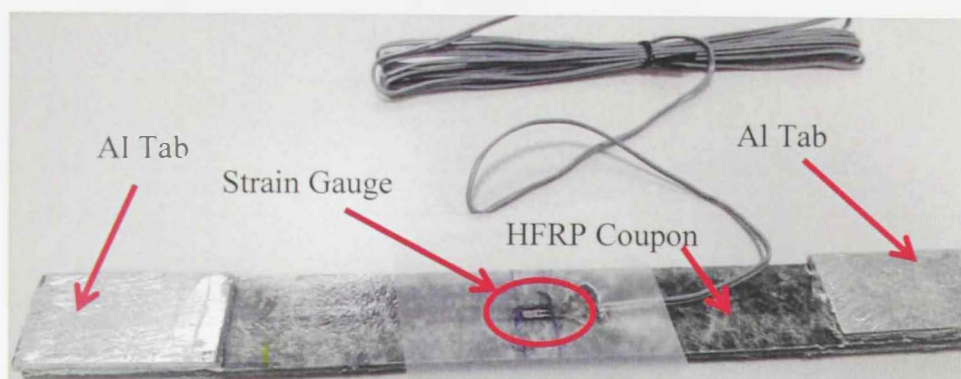
Figure 3.3: Location of the strain gauges in the tested coupons

Test coupons were gripped from their enlarged ends using rough wedges in order to prevent slippage of the coupons before failure occurs. The used MTS electromechanical machine was connected to a computer where the applied loads were automatically recorded as the test was being carried out. Strains gauges were connected to a data acquisition system for strain measurements. Figure 3.4 shows a photo for a coupon during the progress of the tensile test, whereas Fig. 3.5 illustrates the shape of a typical coupon after failure, which was characterized by edge delamination failure at the gauge length. The stress-strain curve for each coupon was then plotted and the ultimate tensile stress and elastic modulus were calculated. The tensile properties obtained from the three tests were very close as displayed in Table 3.2. The average properties showed 867.6 MPa for ultimate tensile strength and 63,519 MPa for the modulus of elasticity. The average values of both the tensile strength and elastic modulus of the tested coupons were in excellent agreement with those recommended by the manufacturer (Table 3.1) with an average difference in the order of 2%. Given that manufacturer values are always less than their experimental counterparts, it has been decided to use the manufacturer recommended values throughout the study for consistency with other published literature of the same HFRP.

Table 3.2: Tensile properties of the tested HFRP coupons

Tested Coupon	Tensile Strength (MPa)	Elastic Modulus (MPa)
1	881.5	63,142
2	861.3	64,679
3	860.1	62,735
Average	**867.6**	**63,519**
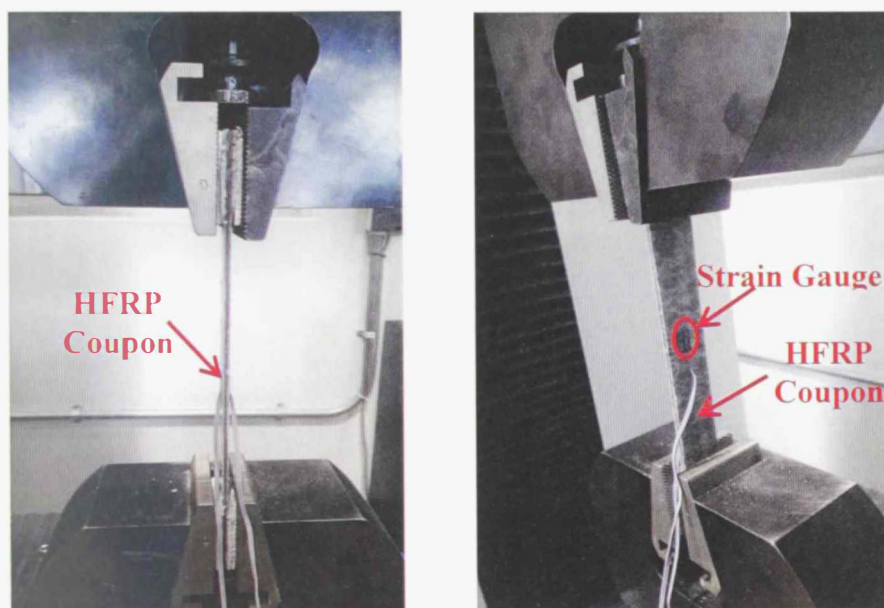
Figure 3.4: HFRP Coupon being tested in MTS machine

Figure 3.5: Photo of the HFRP coupon after failure

3.2.2 Steel Plates

The steel plates used in the experimental program were prepared, cut and drilled using the computerized cutting and drilling equipment at Al Fara'a Steel Structures located in Al-Ain, UAE. The plates had uniform cross-section with 10 mm thickness and 100 mm width. However, the length of the plates varied depending on the different specimen configurations as explained in section 3.3. Three steel coupons were prepared and tested according to the ASTM A370 standards (2014). Obtained mechanical properties from the tested coupons were very close and, therefore, average values were used in modeling the connections. Average yield and tensile strength of the steel plates were 300 MPa and 460 MPa, respectively. Furthermore, an average value of 200 GPa was calculated for the modulus of elasticity of the tested coupons.

3.2.3 Steel Bolts

The conducted experimental investigations involved using two different types of fasteners to connect HFRP laminates to steel plates. The first type of fasteners was hexagonal galvanized zinc coated steel bolts provided by Hilti. The used M6x40 bolts had a diameter of 6 mm and threaded length of 40 mm. Bolts were made of high tensile steel of grade 8.8 according to DIN ISO 4017 (2011) standards with 375 MPa shear strength. A photo and sketch illustrating the dimensions of the steel bolt are shown in Fig. 3.6.
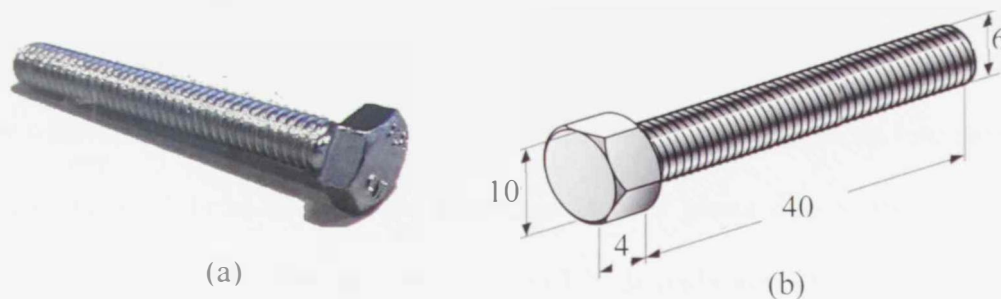
Figure 3.6: (a) Photo of the M 6x40 steel bolt used in the experimental study.
(b) Sketch and dimensions of the used steel bolt (mm)

3.2.4 Steel Washers and Nuts

Galvanized zinc coated flat washers manufactured by Hilti were utilized in this study. The used washers have thickness of 2 mm, inner diameter of 8.4 mm and outer diameter of 28 mm as shown in Fig. 3.7.
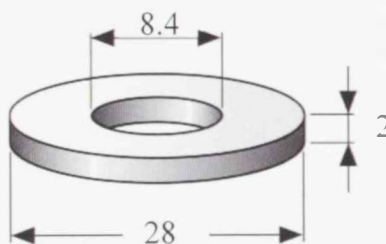
Figure 3.7: Galvanized steel washer used in the
experimental study (Dimensions are in "mm")

M6 zinced hexagonal steel nuts were used to firmly tighten washers to the steel bolts. The thickness of the nuts is 5 mm with an inner diameter of 6 mm and outer diameter of 10 mm as presented in Fig. 3.8.
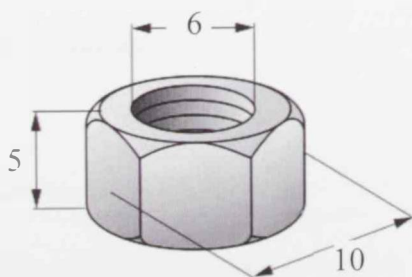
Figure 3.8: Galvanized steel nut (Dimensions are in "mm")

3.2.5 FRP Anchors

FRP anchors, FIBREBOLT[R], provided by STRONGWELL[R] manufacturer were used in the second phase of the study. They were proposed as an alternative to replace the steel bolts used in the first experimental phase due to their corrosion resistivity, low conductivity and resistivity to UV degradation. The FRP anchors are composed of fiberglass studs, washers and nuts. It should be noted that the washer is readily attached to the nut (i.e., nut and washer come in one piece) as can be seen in Fig. 3.9.

Figure 3.9: Photo of the FIBREBOLT[R] studs, washers
and nuts used in the second experimental phase

Pultruded fiberglass vinyl ester rods were machined by the manufacturer to form the studs, which were then lubricated to facilitate the movement of the thermoplastic hexagonal fiberglass nuts through them. The fiberglass studs and nuts were easily assembled using six point socket wrench. The experimental program adopted two sizes of the FRP anchors in order to examine the effect of anchor diameter on the response of fastened HFRP-steel lap connections. FRP anchors of 13 mm nominal diameter were utilized to provide shear strength of 11.6 kN which is almost equal to the 10.6 kN strength of the M6 steel bolt discussed in section 3.2.3. Moreover, FRP anchors with smaller nominal diameter (10 mm) were used to minimize the reduction in the original cross-sectional area of the connected elements

due to drilling of bolt-hole. All FRP anchors were provided in a length of 120 mm. In order to differentiate between the two sizes of the used studs. designations of FB10 and FB13 were used to refer to the 10 mm and 13 mm anchor-diameters. respectively. Table 3.3 summarizes the mechanical properties of the used FRP anchors as provided by the manufacturer.

Table 3.3: Mechanical properties of FIBREBOLT® (Provided by the Manufacturer based on the nominal diameter)

Properties	FB10	FB13
Ultimate Tensile Stress (MPa)	65.5	70.2
Transverse Shear Stress (double shear) (MPa)	187.3	175.6

Given the fact that FRP anchors are sensitive to the applied torque. caution was required during tightening the nuts. A breaking type torque wrench was used to apply the proper tightening torque in accordance with the ultimate and recommended values provided by the manufacturer as displayed in Table 3.4.

Table 3.4: Ultimate and recommended torques of the used FIBREBOLT®

Torque	FB10	FB13
Ultimate Torque Strength (N.m.)	11	24
Recommended Installation Torque (N.m.)	5.5	11

3.2.6 Torque Wrench

An adjustable breaking torque wrench was purchased from Torqueleader Co.. UK. to allow for better control of the tightening process of the FRP anchors. The wrench was set to the required limiting torque value and automatically broke after reaching this limit to avoid the possibility of under- or over- tightening the fasteners. The used ATB 25A model has a sensitivity of 0.1 N.m. and accuracy of ± 0.04 with a torque range from 5 to 25 N.m. A photo of the used torque wrench is shown in Fig. 3.10.

Figure 3.10: Photo of the used breaking torque wrench

3.2.7 Strain Gauges

The HFRP-steel connections were instrumented with electrical resistance strain gauges (ERSG) which were bonded at different locations on the HFRP laminates to record the induced strains during testing. FLA-3-11-3L strain gauges purchased from TML, Japan were utilized in the experimental program. The strain gauges (SG) had a gauge length of 3 mm. gauge factor of $2.12 \pm 1\%$ and 119.6 ± 0.5 Ω electrical resistance. CN-type strain gauge adhesive was used to mount the strain gauges to the surface of the HFRP laminates. Recorded strain gauge measurements were used for different purposes at each phase of the experimental study. They were also used later to validate the performance of the developed finite element model by comparing the experimental measurements against their numerical counterparts.

3.2.8 LVDT

Linear variable differential transducers (LVDTs) were used to measure the longitudinal displacement of the tested connections during testing. These LVDTs were of CDP-100 contact type with a capacity of 100 mm. The recorded displacements were used to develop load-displacement curves for the different tested configurations.

3.3 Experimental Methodology, Procedure and Results

The purpose of the experimental program was to investigate the interfacial behavior of fastened HFRP-steel shear lap connections under variable fastening parameters. The investigation was conducted on two main phases based on the type of fasteners. Steel bolts were used in the first phase to investigate the effect of the number of washers-per-bolt, clamping torque, bolt-hole diameter and spacing between bolts on the performance of HFRP-steel connections. The second phase involved the use of FRP anchors with different diameters and sheared edge distances to form the HFRP-steel connections.

The experimental program was designed to study the influence of each individual parameter by changing one parameter at a time while keeping all other test parameters unchanged. In the first phase, the effect of different number of washers-per-bolt, referred to as (W), was examined under standard fastening conditions. After processing the results, the recommended number of washers-per-bolt was used to design the next set of tested connections that aimed at studying the effect of the clamping torque (T) on the behavior of the HFRP-steel connections. Following that, connections with different bolt-hole diameters (D) were tested using the recommended number of washers-per-bolt and tightening torque value. The configuration which revealed an optimal performance of the connection, based on the three tested parameters (W, T and D) was implemented in the design of a new set of connections that examines the effect of spacing between bolts (S) on the connection performance. Based on the results an optimum range of spacing (S) was suggested for designers.

FRP anchors were used in the second phase of the experimental program to fasten the HFRP laminates to the steel plates. This phase was conducted using two stud diameter values: 10 mm and 13 mm. For each diameter, five values of sheared edge distance (Sh) were tested. Finally, comparison was held between connections that were formed using steel bolts and those with FRP anchors. The following sections include detailed description of the experimental procedures, results and discussion of the outcomes of each phase.

3.3.1 Phase I: HFRP-Steel Connections using Steel Bolts

This section illustrates the tests carried out on various configurations of HFRP-steel connections formed using steel bolts. The test procedures and results of each tested configuration are outlined and discussed in details.

Effect of Number of Washers-per-Bolt (W)

Three different configurations were considered to examine the effect of variable number of washers-per-bolt (W) on the behavior of fastened HFRP-steel lap connections. Figure 3.11 shows schematic views of a typical connection. The connection is composed of two steel plates (clamped and loaded plates) and two HFRP laminates placed at the top and bottom of the steel plates in a double-lap arrangement. The clamped side of the connection was provided with quadruple the number of bolts installed at the loaded side in order to ensure that slippage and bearing displacements will occur at the loaded side of the connection only. The design values of rolled (R) and sheared (Sh) edge distances (R = 20 mm and Sh = 50 mm, respectively) were adopted from earlier researches to ensure bearing failure of all specimens (Sweedan et al., 2013). HFRP laminates were drilled at the specified

bolts' locations with the exact diameters at Al Fara'a Steel Structures' workshop. The details dimensions of a typical connection are presented in Fig. 3.12.
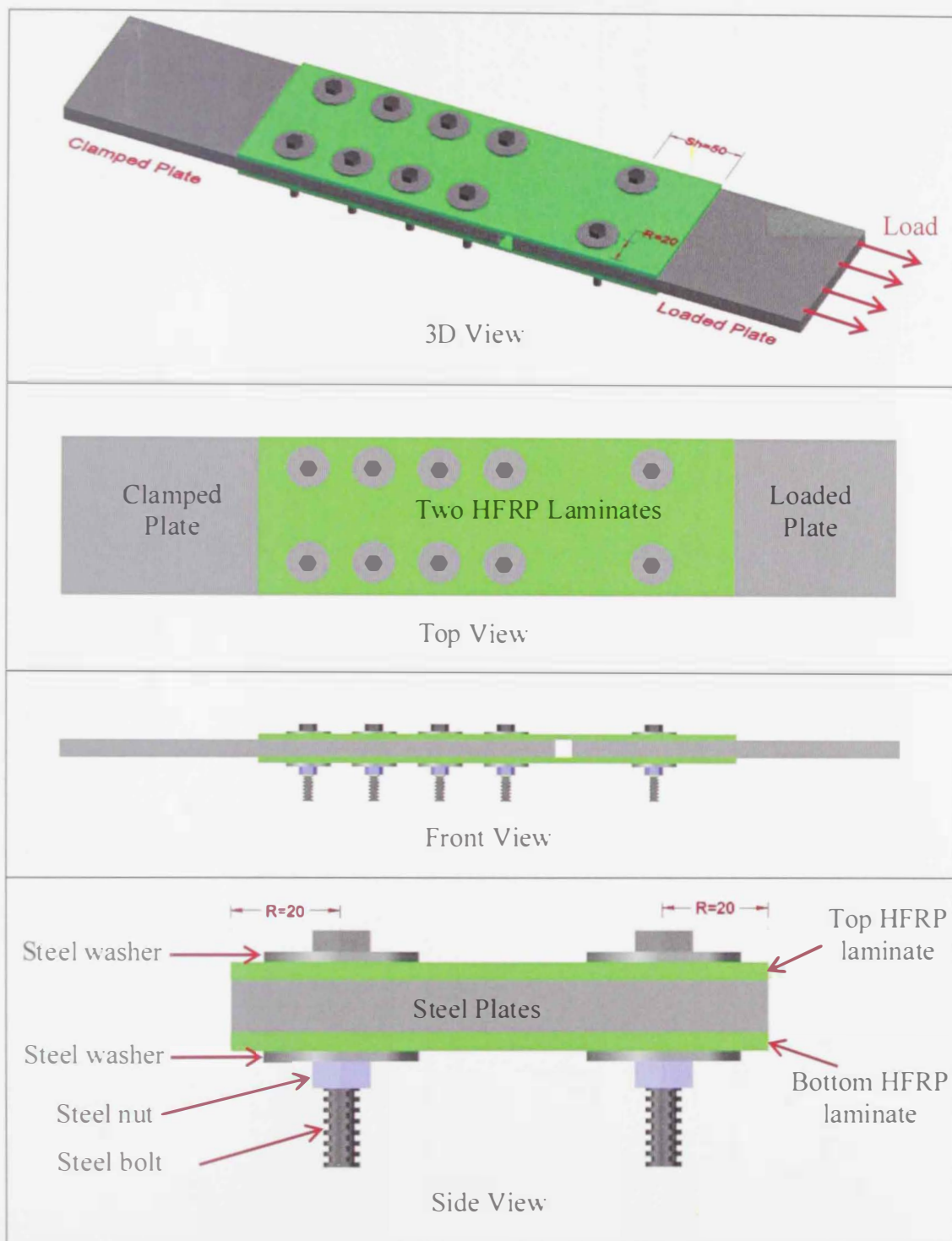
Figure 3.11: Schematic views of a typical HFRP-steel connection using steel bolts

Figure 3.12: Geometrical details of a typical HFRP-steel connection using steel bolts (Dimensions are in "mm")
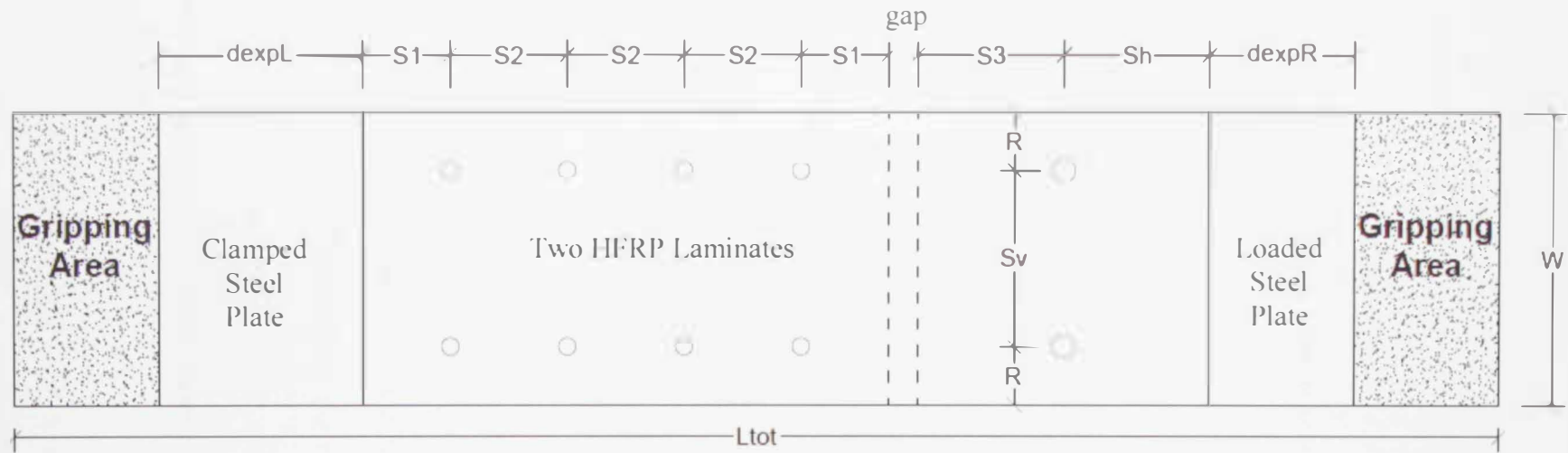
dexpL = 70	S1 = 30	S2 = 40	Sv = 61.6	R = 20	Ltot = 510
dexpR = 50	Sh = 50	S3 = 50	W = 101.6	Gap = 10	

Specimens were loaded in tension using displacement-controlled MTS Universal Testing Machine with a 100 kN capacity. The displacement-controlled test was performed in a constant cross-head speed of 1 mm/min. The in-plane displacement was measured using two LVDTs attached to metal brackets mounted to both sides of the loaded steel plate as shown in Fig. 3.13. The two LVDTs were used to enable predictions of any undesirable in-plane rotation of the specimen during testing.
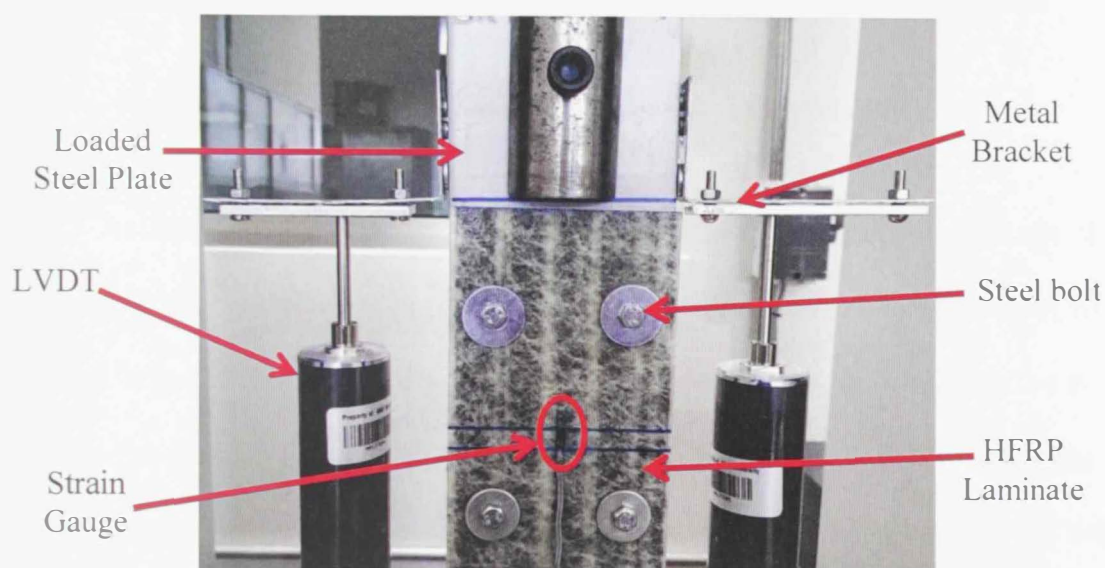
Figure 3.13: Experimental setup of the tested HFRP-steel connection using steel bolts

The longitudinal strains in the HFRP laminates were measured using two electrical strain gauges mounted at the center of the 10 mm gap between the two steel plates as presented in Figs. 3.13 and 3.14. One strain gauge was glued to the outer face of each HFRP laminate to monitor any out-of-plane bending during testing (Fig. 3.14). This particular location was selected for being relatively away from the bolts' locations where it is most likely to experience uniform stress distribution.
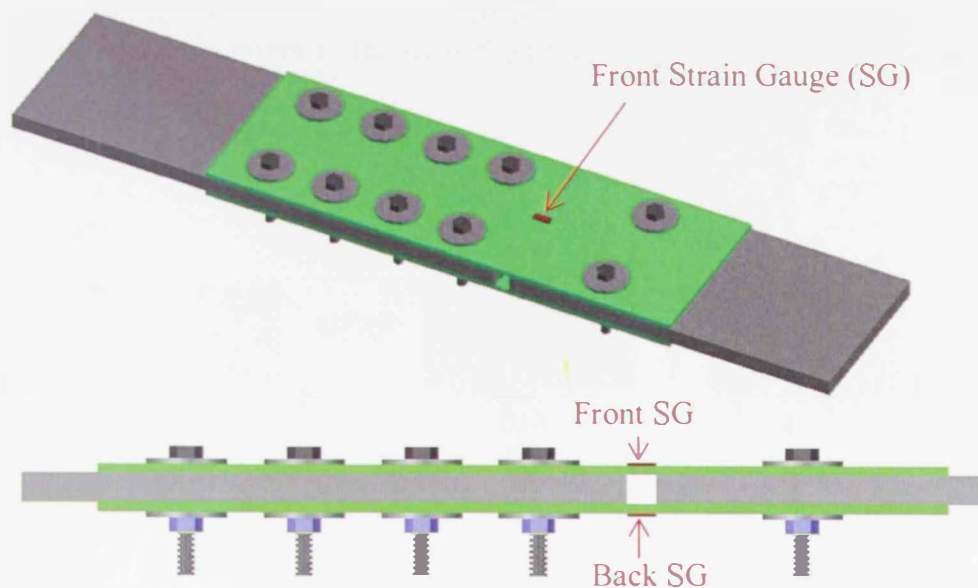
Figure 3.14: Locations of the strain gauges in the tested HFRP-steel connection using steel bolts

As mentioned earlier, three configurations were selected to evaluate the response of the specimens with respect to variable number of washers-per-bolt (W0, W2 and W4). In the first configuration (W0), no washers were used with the two bolts at the loaded side of the connection as shown in Fig. 3.15(a). The second configuration (W2) used two washers-per-bolt; one of which was placed at the bolt head while the other one was used at the nut side as shown in Fig. 3.15(b). The third configuration (W4) examined the use of four washers-per-bolt (two on each side of the connected plates) as displayed in Fig. 3.15(c). While bolts at the clamped side of HFRP-steel connection of all configurations utilized two washers-per-bolt. Bolts were installed through standard holes of 8 mm diameter and snug tightened after the full effort of a worker with an ordinary spud wrench (AISC, 2010). Each test configuration was replicated three times to ensure the repeatability and accuracy of the obtained results. Each connection is referred to as (W#_D8_ST_X). In this designation, (W#) represents the number of washers-per-bolt, (D8) denotes the bolt-

hole diameter. (ST) refers to the snug-tight torque and (X) defines the index of the replicate in the tested group of specimens.
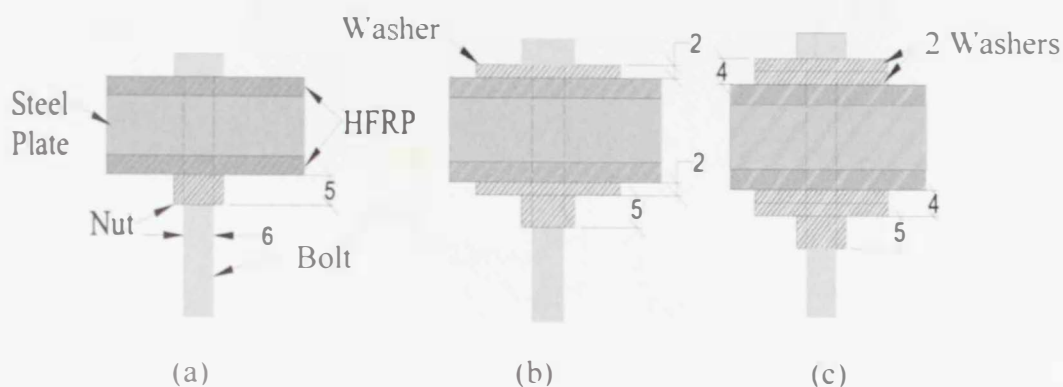
Figure 3.15: Number of washers-per-bolt for:(a) no washers. (b) two washers and (c) four washers. (Dimensions are in mm)

Discussion of Results of Number of Washers-per-bolt Specimens

The load-displacement curves of the three replicates of W0_D8_ST specimens are shown in Fig. 3.16. These plots reveal a slight increase in the load till 2.5 kN at a displacement of about 1 mm due to the initial friction between the HFRP laminates and the steel plates. At this load value, relative slippage started to take place between the HFRP laminates and the steel plates due to the 2 mm standard bolt-hole clearance. After that, the load value increased in a linear trend until it reached a value of about 26.5 kN at an average displacement of about 8 mm. This load increase was associated with a noticeable bearing between the bolts and the HFRP laminates as shown in Fig. 3.17. Once the peak load was reached, bolts started to punch through the HFRP laminates along the loading direction (refer to Fig. 3.18) causing progressive rupture of the CFRP matrix and peeling of the GFRP layers. The described rupture of the HFRP led to a gradual drop in the load values until the connection failed. The softening post-peak response displayed in the load-displacement curves of W0_D8_ST connections (Fig. 3.16) indicates unfavorable

performance along with a limited load carrying capacity of this type of connections when no washers are used.
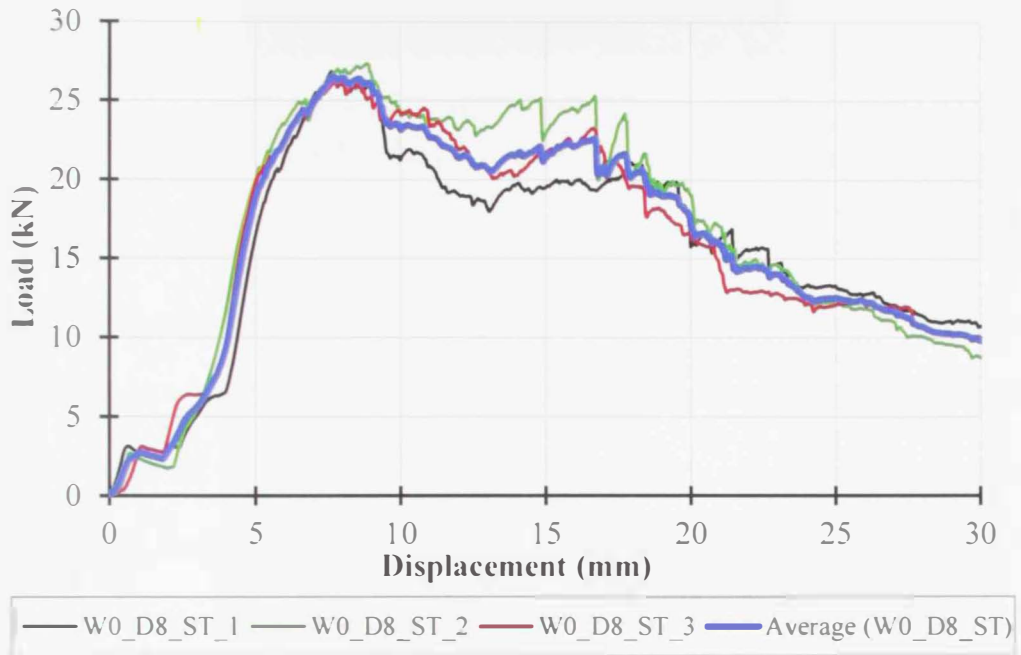
Figure 3.16: Load-displacement curves for connections without washers (W0_D8_ST)
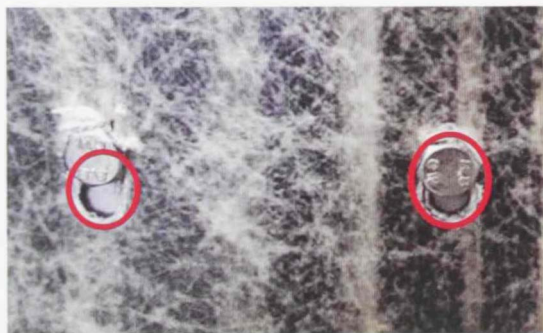
Figure 3.17: Bearing failure in W0_D8_ST_2
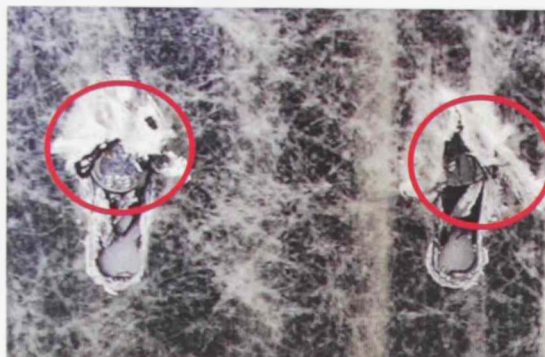
Figure 3.18: Rupture of CFRP matrix and
GFRP peeling failure in W0_D8_ST_2

A substantial improvement in the connection response was noticed upon the use of two washers-per-bolt as implied by Fig. 3.19. Initially, the connection carried a load of about 5 kN before the interfacial slippage took place at a displacement of 1 mm. Following that, the load value increased significantly in a nearly linear manner until it reached a value of about 25 kN at a corresponding displacement value of about 5 mm. At this stage, small parts of the HFRP fibers around the fastened bolts started to rupture causing a noticeable bearing damage associated with low clicking noise heard during the test as exhibited in Fig. 3.20. Following that, the load values continued to increase at a lower rate as observed by the relative reduction in the slope of the load-displacement curve for load values that range between 25 kN and about 45 kN. A significant increase in the peak load, relative to (W0) configuration, was evident with the peak load reaching a value of about 45 to 47 kN for all specimens. This stage was characterized by noticeable bending in the bolts with remarkable clicking noises indicating peeling of the GFRP layers which was associated with folding of the washers as shown in Fig. 3.21.
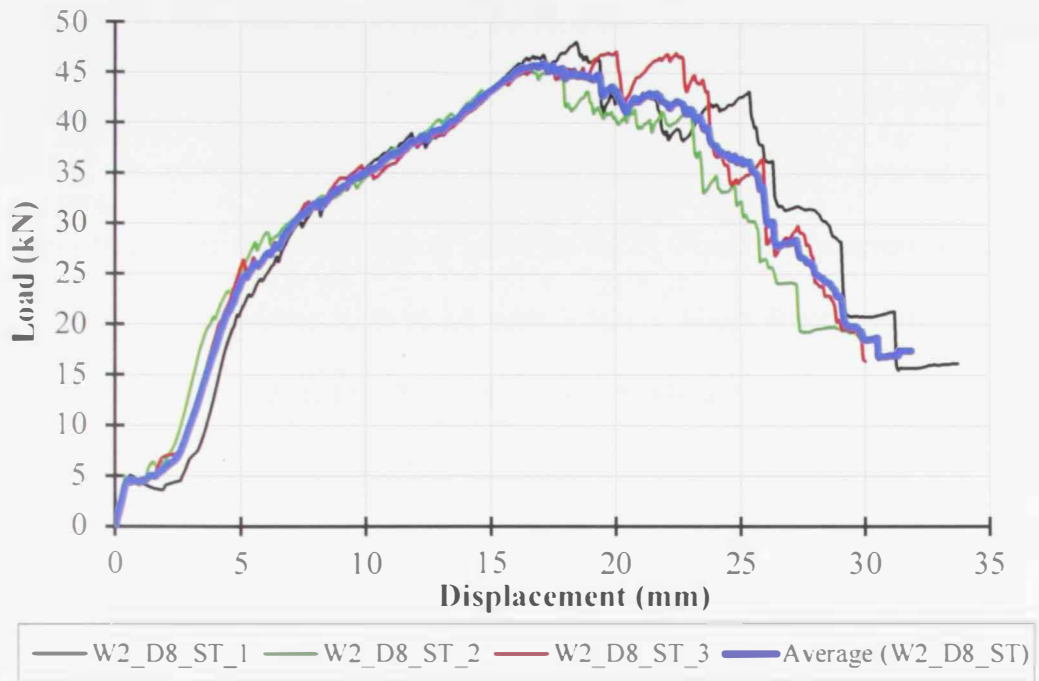
Figure 3.19: Load-displacement curves for connections with two washers-per-bolt (W2_D8_ST)

Figure 3.20: Bearing failure in W2_D8_ST_2
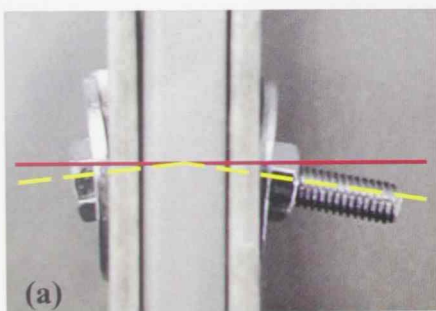
Figure 3.21: (a) Bending in the connecting bolts, (b) Folding of washers in W2_D8_ST_1

Once the peak load was reached, the load carrying capacity of the connection started to decrease gradually. A reduction in the load carrying capacity of the connection was observed beyond peak point as result of excessive bearing damage and initial tearing of the CFRP layers (see Fig. 3.22). Finally, a progressive tearing out of the HFRP laminates took place with a Block Shear Rupture (BSR) of the intact fibers as displayed in Fig. 3.23. However, bending of the bolts failure mode depended on the strength of the bolt material. The steel bolts bended due to the combined effects of the induced shear and flexural stresses which were associated with the slip in the double lap-connections. Bending of the bolts along with the accumulation of peeled GFRP layers underneath the washers led to folding of the washers. It is worth mentioning that all tested (W2) specimens, i.e., with two washers-per-bolt, showed a clear ductile behavior as they underwent significantly large displacement of about 16 mm before onset of reduction in their load carrying capacity, as implied by Fig. 3.19.

Figure 3.22: Initial tearing out failure in
W2_D8_ST_2
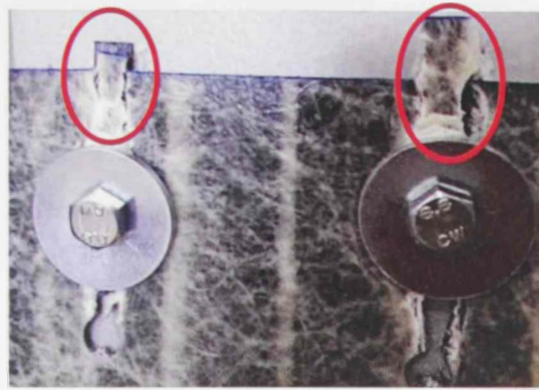
Figure 3.23: Block shear rupture of the HFRP laminates in W2_D8_ST_2

The load-displacement response curves of the connections with four washers-per-bolt (W4) followed a similar trend to those with two washers-per-bolt (W2), with an increased peak load of about 49±1 kN at a displacement of about 18±1 mm as shown in Fig. 3.24. It should be noted that, unlike all other (W4) specimens, the (W4_D8_ST_1) specimen failed by excessive shear in bolts (Fig. 3.24). For this particular specimen, no clear folding of washers was observed which could result in higher tensile stresses to be induced in the bolts. These excessive tensile stresses, when combined with shear stresses induced in the bolts, led to the immediate post-peak failure of specimen (W4_D8_ST_1).
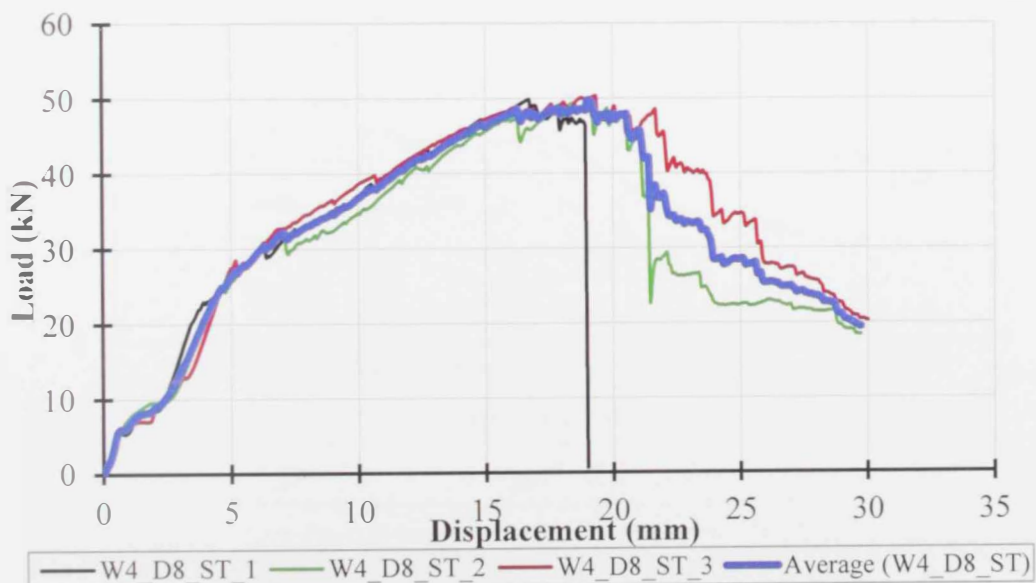
Figure 3.24: Load-displacement curves for connections with four washers-per-bolt (W4_D8_ST)

The average load-displacement curves of the three tested configurations (W0, W2 and W4) are presented in Fig. 3.25. The comparison between these curves reveal a considerable enhancement in the performance and load carrying capacity of connections that use washers (W2 and W4) over those without washers (W0). Additionally, using four washers (W4 connections) resulted in slight increase in the connection load carrying capacity compared to their counterpart connections with two washers only (W2 connections). Meanwhile, the overall behavior of both (W2) and (W4) connections is very similar as reflected by their plots in Fig. 3.25. Experimental observations revealed that utilization of washers improves the performance through the introduction of additional mechanisms that did not take place in connections with no washers including bending of bolts and folding of washers.
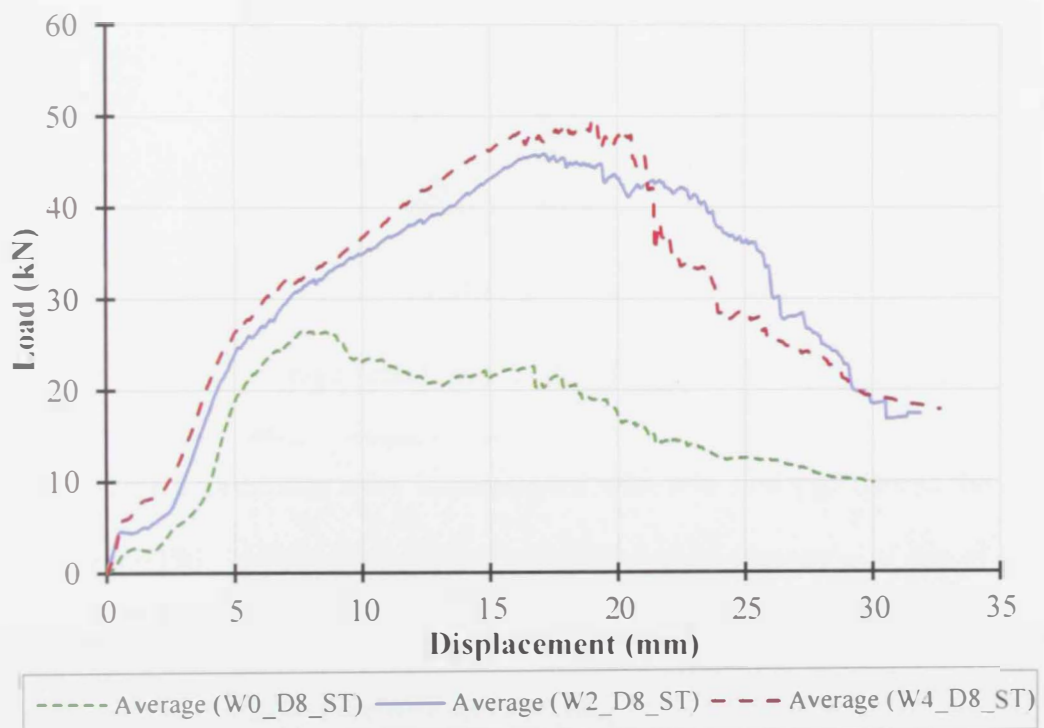
Figure 3.25: Average load-displacement response curves for each number of washers-per-bolt configurations

Figure 3.26 displays the average peak loads for the three tested configurations. Results highlight the significant effect of washers in enhancing the load carrying capacity of the connections which is consistent with the findings of Realfonzo et al. (2013). For instance, connections with two washers-per-bolt (W2) revealed 75% increase in their average load carrying capacity compared to those with no washers (W0). Meanwhile, an enhancement of 86% was obtained for connections with four washers-per-bolt (W4) relative to those without washers (W0). It is important to note that increasing the number of washers from 2 to 4 causes a slight increase (about 6.5%) in the load carry capacity of the connection. It is, therefore, recommended to use 2 washers-per-bolt (W2) for optimum performance considering economic and practical aspects.
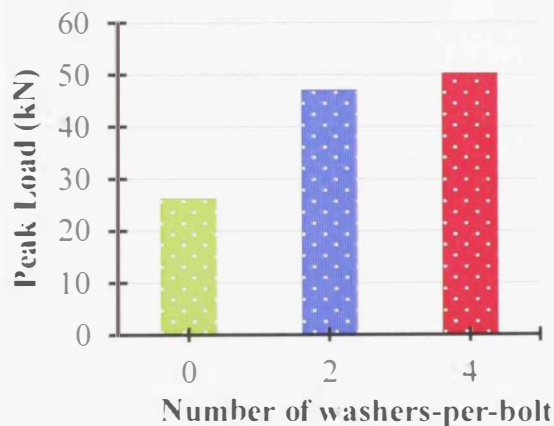
Figure 3.26: Average peak loads for the (W#_D8_ST) configurations

All tested specimens were instrumented with two strain gauges at the outer face of each HFRP laminate (Fig. 3.14) to monitor the occurrence of out-of-plane bending during testing. The strain gauges' measurements as a function of the applied loads for a representative specimen of W4_D8_ST_2 are presented in Fig. 3.27. Plotted results reveal that longitudinal tensile strains were developed in the front and back strain gauges during the test. The absence of compression strains at either

HFRP laminates imply a negligible effect for the out-of-plane bending on the response of the tested connection. The differences in the measured strains at both gauges can be referred to the non-identical effect of the combined failure modes (i.e., peeling of fibers, bolts' bending, and washers' folding) on the two HFRP laminates.
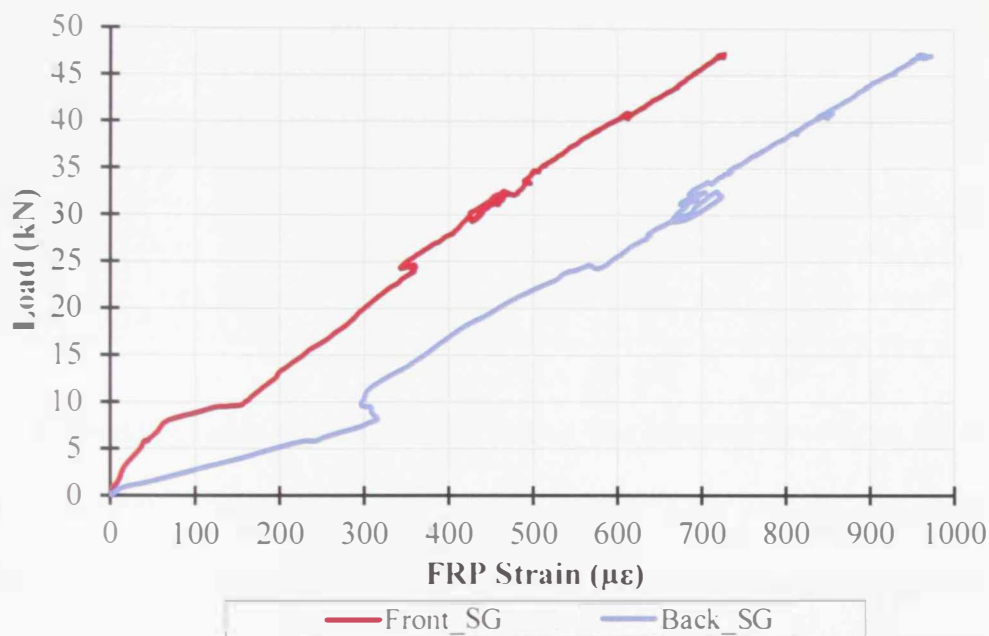
Figure 3.27: Strain gauge measurements for W4_D8_ST_2

Effect of Clamping Torque (T)

In order to investigate the effect of clamping torque on the behavior of fastened HFRP-steel lap connections, four levels of clamping torque were considered. Connections with snug-tightened (ST) bolts were considered as reference specimens (T1). Three other sets of specimens were tested with various clamping torque levels T2, T3 and T4 corresponding to 1.2 T1, 1.5 T1 and 1.8 T1, respectively. Based on the outcomes of the effect of number of washers-per-bolt study, all bolts were supplied with two washers. Bolts were installed in standard size holes to allow for investigating the pure effect of the clamping torque on the behavior of tested connections. A breaking-type torque wrench (Fig. 3.10) was

utilized to calibrate the torque equivalent to the snug-tight condition and apply all other tightening torque values. The snug-tight condition (ST) of the connections with two washers-per-bolt corresponded to a torque value of 11 N.m. The various clamping torque values considered in this phase of the study are summarized in Table 3.5.

Table 3.5: Design torque levels and values

Torque Level	Torque (N.m.)	Torque/Snug-tight
T1	11.0 (ST)	1.0
T2	13.2	1.2
T3	16.5	1.5
T4	20.0	1.8

It should be noted that each configuration was repeated three times for quality control purposes. Specimens were typically labeled (W2_D8_T#_X), where the symbol (T#) refers to the torque level and (X) indicates the index of the replicate.

Discussion of Results of Clamping Torque Specimens

Twelve specimens were tested to examine the effect of the clamping torque on the HFRP-steel connections. In these specimens two washers-pre-bolt were used along with a typical 8 mm bolt-hole size (i.e., 2 mm bolt-hole clearance). Load-displacement curves obtained experimentally for torque levels T1 through T4 are displayed in Figs. 3.28 through 3.31, respectively. The experimental results showed that for the range of applied torques covered in this study, increasing the clamping torque has insignificant effect on the failure modes of fastened HFRP-steel connections. This observation is in agreement with the results reported by Khashaba et al. (2006). All specimens followed the failure mechanisms experienced by the connections with two washers-per-bolt as explained in the previous section.
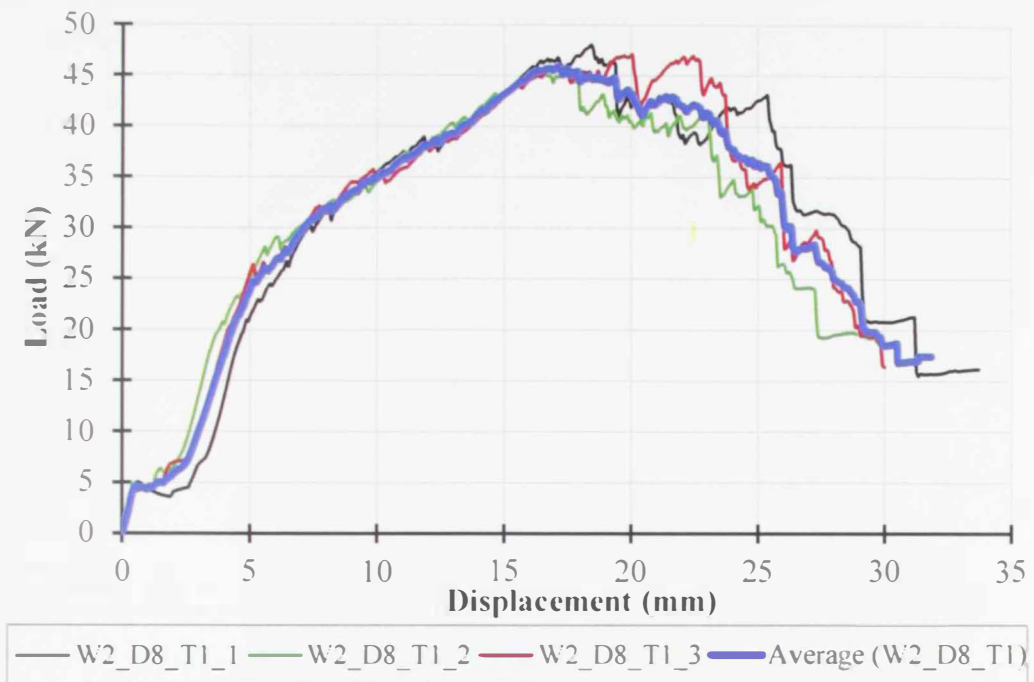
Figure 3.28: Load-displacement curves for W2_D8_T1 connections
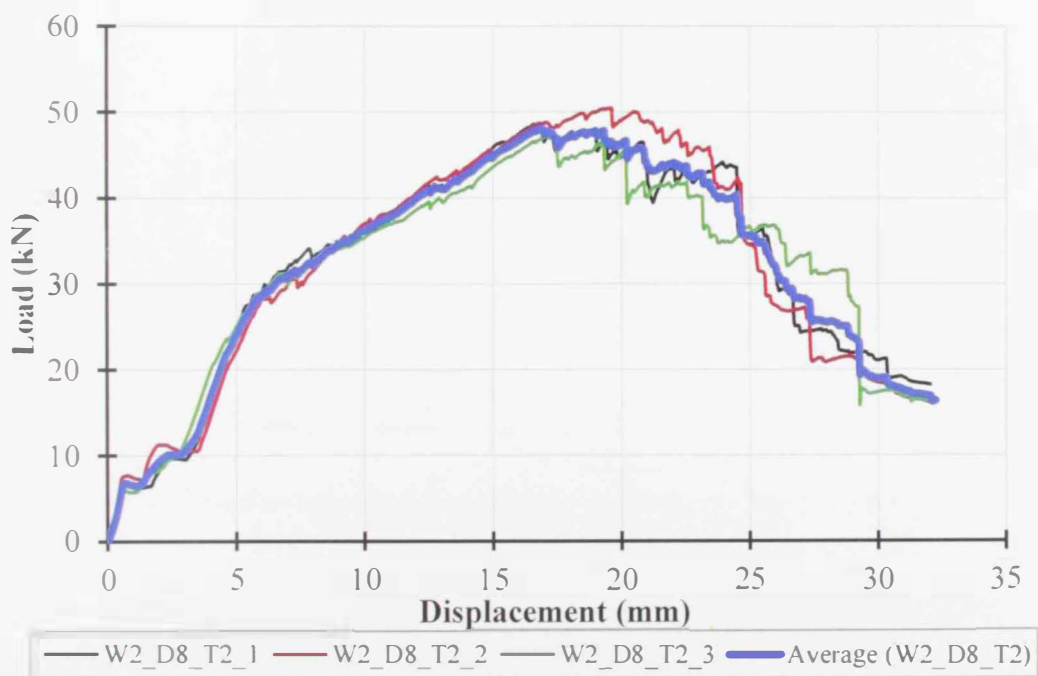
Figure 3.29: Load-displacement curves for W2_D8_T2 connections
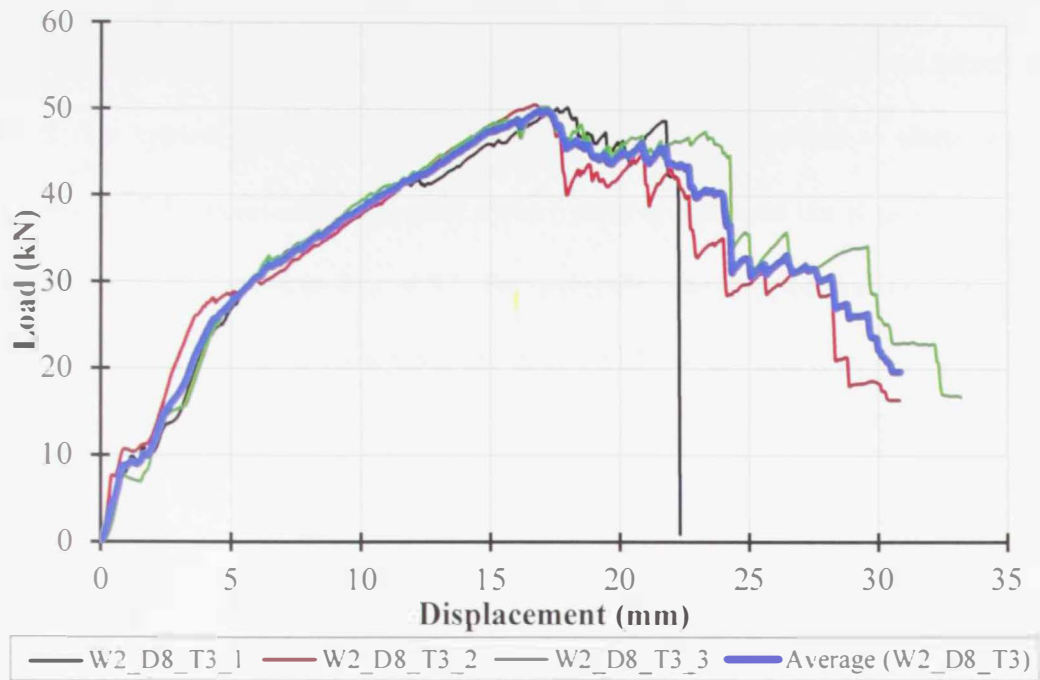
Figure 3.30: Load-displacement curves for W2_D8_T3 connections
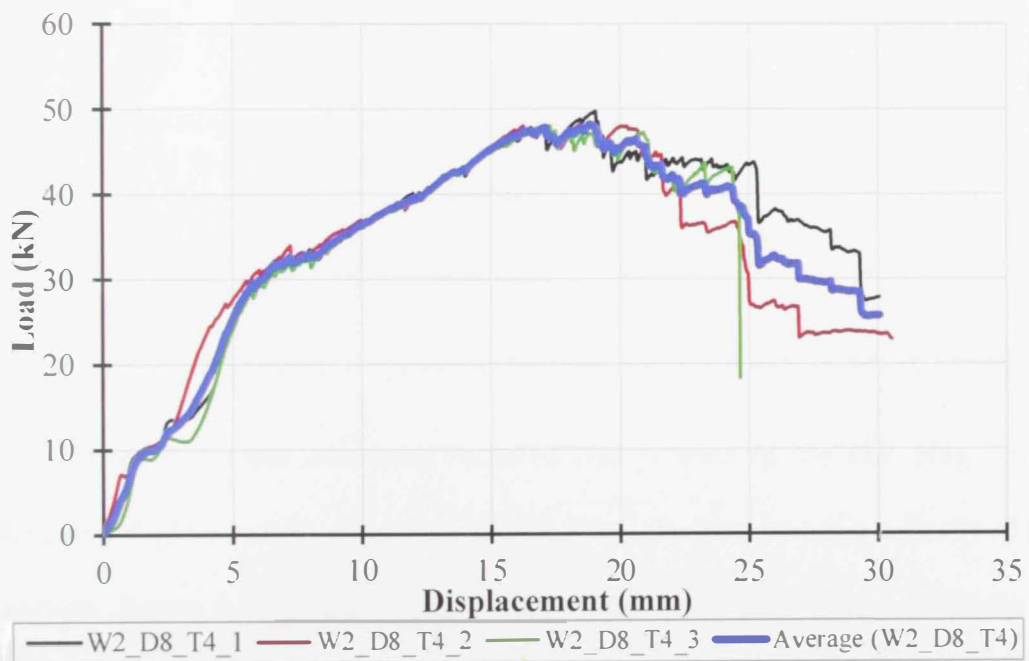
Figure 3.31: Load-displacement curves for W2_D8_T4 connections

The flat part of the response curve (enclosed in the circle in Fig. 3.32) indicates the relative slippage of the HFRP laminates relative to the steel plates due to the 2 mm typical bolt-hole clearance. Increasing the torque led to clamping the components of the connection together more tightly and caused the slippage to occur at higher loads as shown in Fig. 3.32. For example, the slippage of T1 assemblies occurred at 4.5 kN, while it took place at about 10 kN for T4 connections.
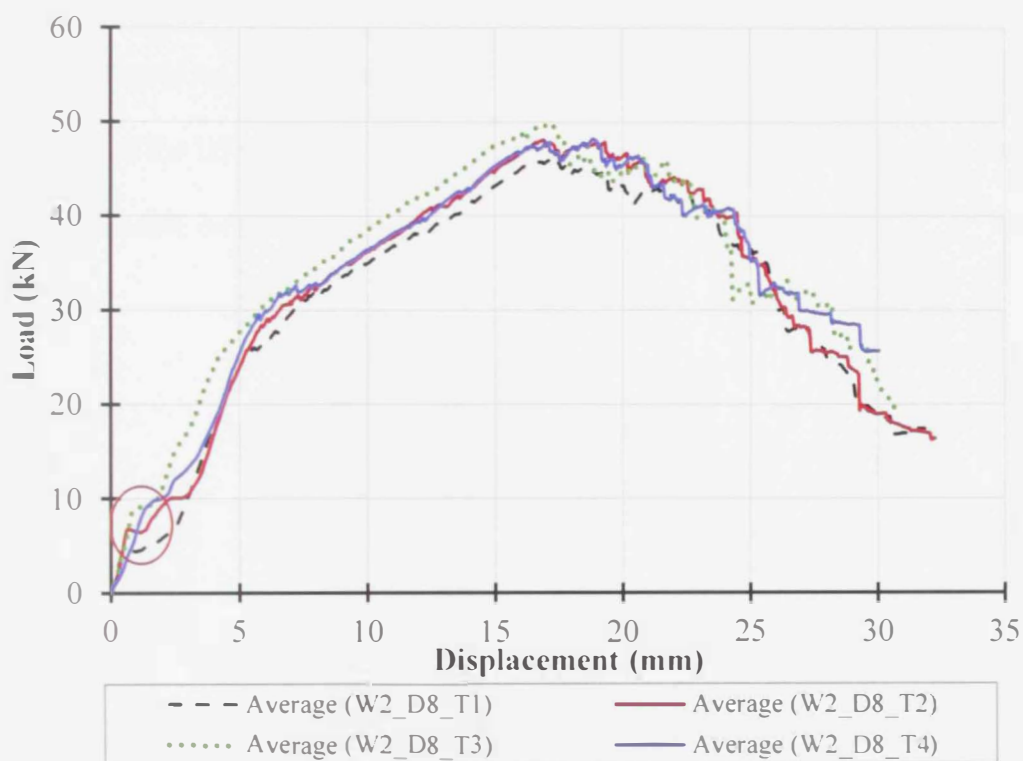
Figure 3.32: Average load-displacement curves for tested torque configurations

The experimental outcomes revealed that increasing the clamping torque resulted in a slight increase of no more than 7.5% in the load carrying capacity of the connection. Figure 3.33 illustrates the average peak loads of the three replicates of the torque configurations. The average percentage increase in the ultimate loads of T2, T3 and T4 configurations with respect to T1 are 4%, 7.5% and 4%, respectively. This slight increase implies that raising the applied torque above 50% of the snug-tight condition had inverse effect on the attained peak loads. This reversed effect

may be attributed to the micro-cracks induced in the HFRP laminates associated with increasing the tightening torque. It is clear that using a high clamping torque that is 80% higher than that of the snug-tight (test configuration T4) did not result in considerable enhancement in the load carrying capacity of the connection. It is worth noting that a significant increase in the applied torque value would lead to high tensile stresses in the bolts, which are expected to alter the failure mode of the connection to the undesirable mechanism of tensile rupture in the bolt as shown in Fig. 3.34. Therefore, it is recommended to apply the snug-tight conditions to ensure that failure of the HFRP-steel connection is controlled by bearing mechanism and the associated ductile behavior.
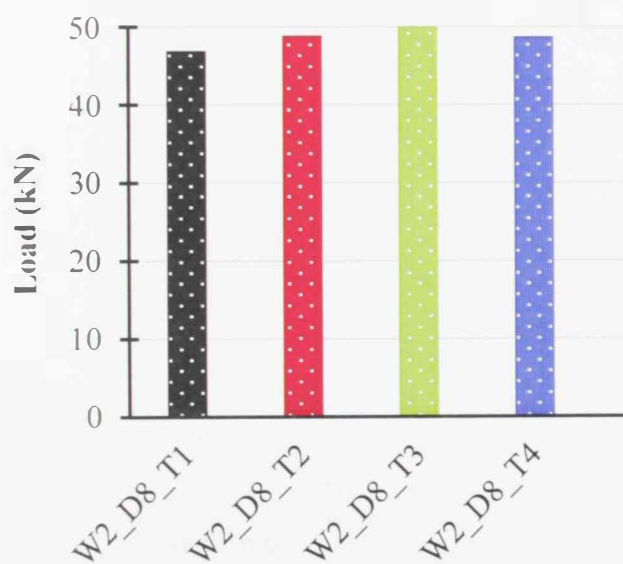
Figure 3.33: Average peak loads for the torque configurations

Figure 3.34: Shear failure in the bolts of W2_D8_T3_1

Figure 3.35 shows the strain gauge measurements for specimen W2_D8_T2_1 as a sample connection. Recorded strain measurements are used to monitor the out-of-plane bending of the fastened connection while being tested. Longitudinal tensile strains were measured in both HFRP laminates during the test. The close strain values, especially at relatively low loads, indicate that the connection experienced a negligible bending. It should, however, be noted that more diverse strain gauges measurements were recorded at high load values due to the effects of peeling of fibers, bending in bolts and washers which are not identical in the two HFRP laminates.
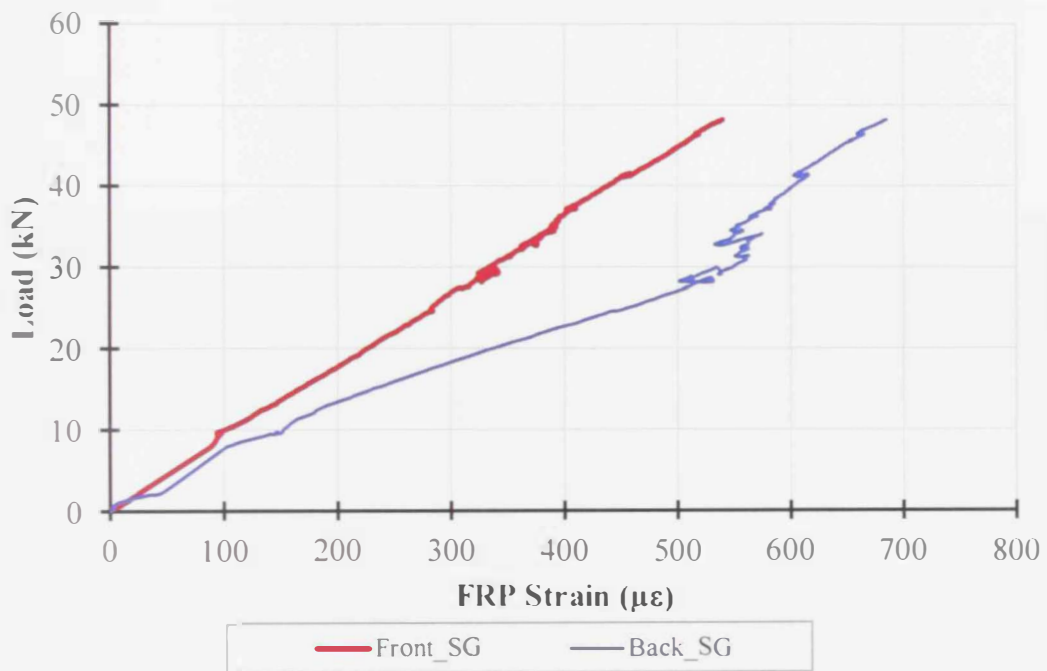
Figure 3.35: Strain gauge measurements for W2_D8_T2_1

Effect of Bolt-Hole Diameter (D)

The effect of bolt-hole diameter on the behavior of the fastened HFRP-steel connection was examined by testing three sets of specimens sharing different hole-diameters (6, 8 and 10 mm) in both the HFRP laminates and the loaded steel plates.

All tested connections were formed using two washers-per-bolt and M6 snug tightened steel bolts. Net-fit condition was attained through the 6 mm hole-diameter. Standard and loose-fit configurations were presented by 8 mm and 10 mm hole-diameters, respectively, as shown in Table 3.6. Three replicates were considered per configuration, with similar designation as described before. A schematic view of the tested assemblies is presented in Fig. 3.36.

Table 3.6: Design bolt-hole diameter values

Designation	Bolt-Diameter (mm)	Hole-Diameter (mm)	Clearance (mm)
D6	6	6 (net-fit-hole)	0
D8	6	8 (standard-hole)	2
D10	6	10 (oversized-hole)	4
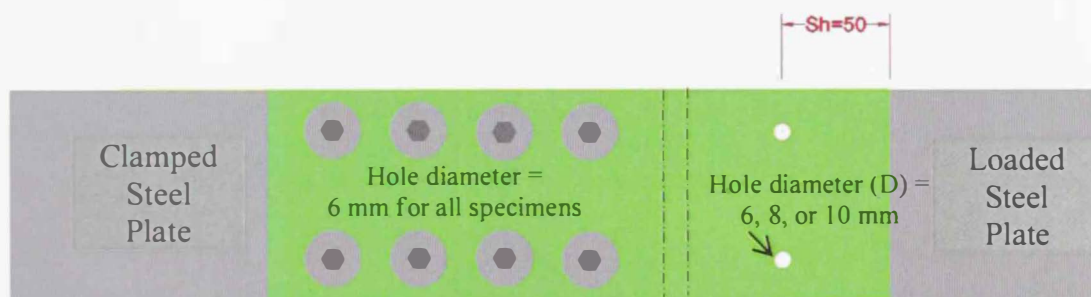
Figure 3.36: Schematic view of assemblies testing the bolt-hole diameter

Discussion of Results of Bolt-Hole Diameter Specimens

The load-displacement relations of the tested connections appeared to be sensitive to the various bolt-hole diameter values as presented in Fig. 3.37. The different response curves imply the significant impact of the hole-size on the response of the fastened HFRP-steel connections.
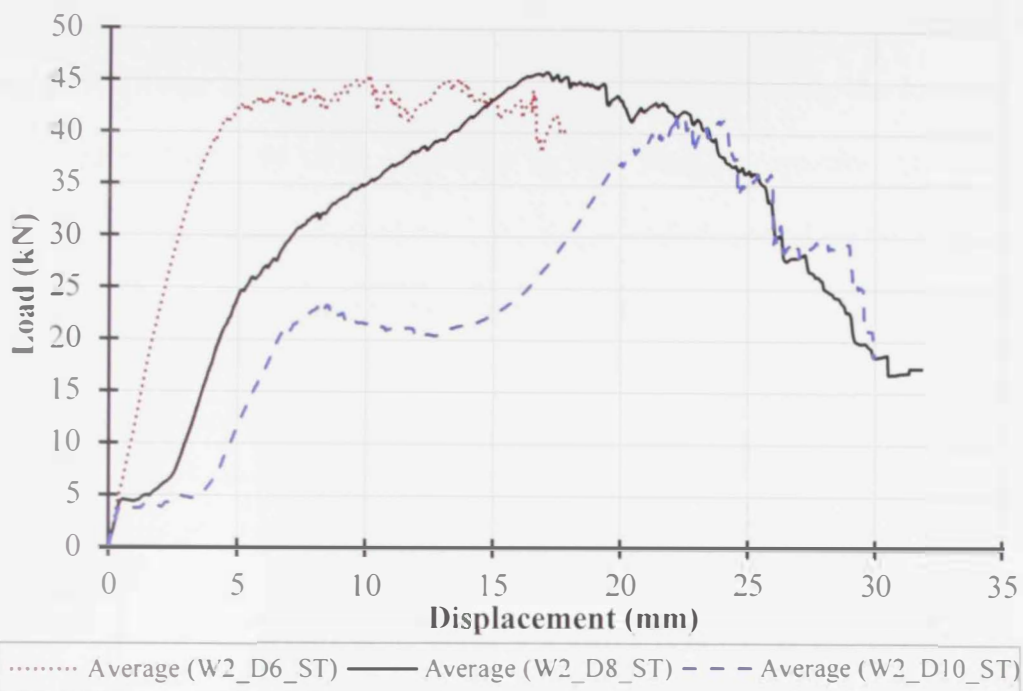
Figure 3.37: Average load-displacement curves for bolt-hole diameter
configurations

The graphical representation of the load-displacement curves for the
connections with net-fit holes (D6 with 0 mm clearance) indicated a persistent linear
trend until the load reaches a value of about 40 kN at an average displacement value
of about 4 mm as depicted by Fig. 3.38. After this stage, a fluctuation in the range of
about 3 kN was observed in the load values of the three replicates of D6 specimens
without considerable increase in the load until failure of the connection takes place at
an average displacement of about 17 mm. It is obvious that the use of net-fit holes
(D6) results in constant stiffness of the assembly (represented by the slope of the
load-displacement curve) up to a load value that is very close to the peak load as
shown in Fig. 3.38. This particular effect of the net-fit clearance on the stiffness of
the connection confirms the findings of Lawlor et al. (2005). The direct contact
between the bolts and the HFRP laminates in D6 assemblies allowed bearing to take
place once the load was applied till the peak load was attained. The post-peak

fluctuation in the load values is attributed to the continuous rupture of GFRP layers and CFRP fibers and the associated load re-distribution among the intact fibers as presented in Fig. 3.39. It is important to note that all replicates of W2_D6_ST specimens failed by bending of the bolts (Fig. 3.40) followed by bolts' shear (Fig. 3.41) without noticeable contribution of the washers in resisting the applied load.
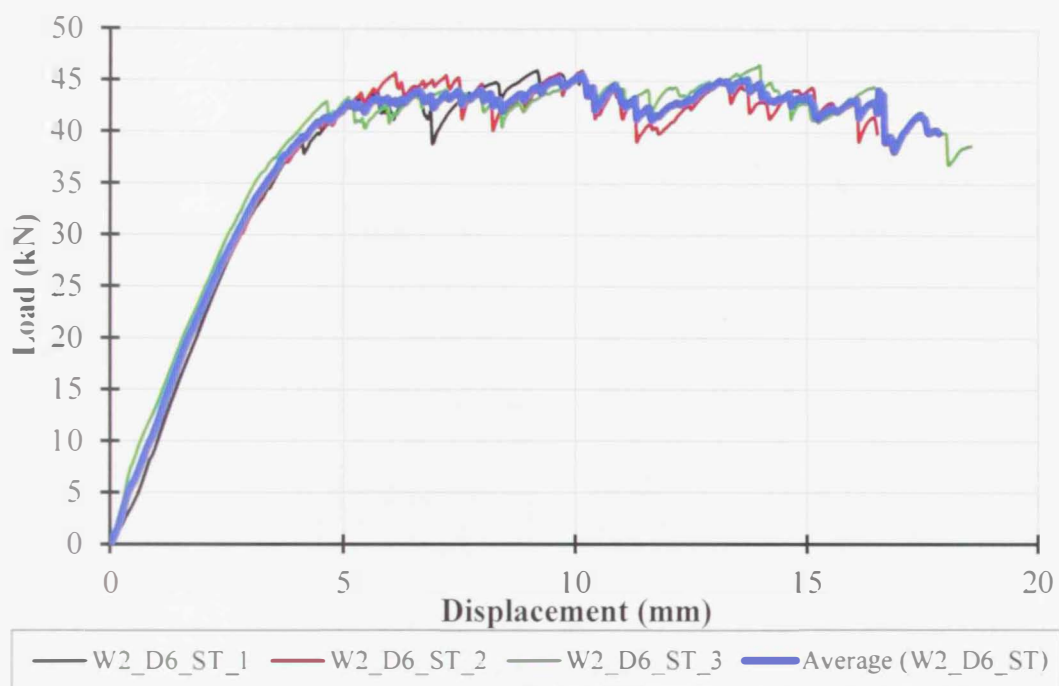
Figure 3.38: Load-displacement curves for W2_D6_ST connections

Figure 3.39: Rupture of the GFRP and CFRP in W2_D6_ST_3 connection
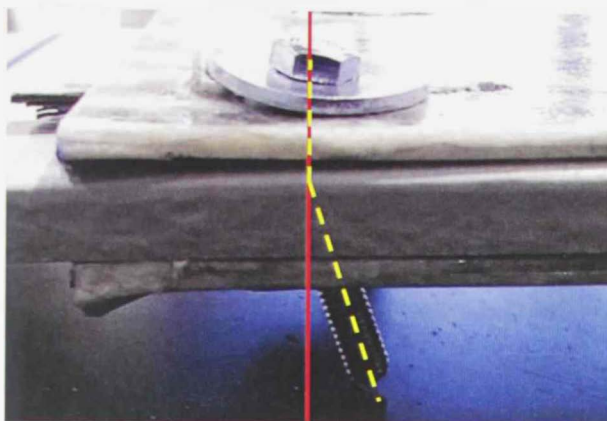
Figure 3.40: Bending of the fastened bolts of W2_D6_ST_3 connection
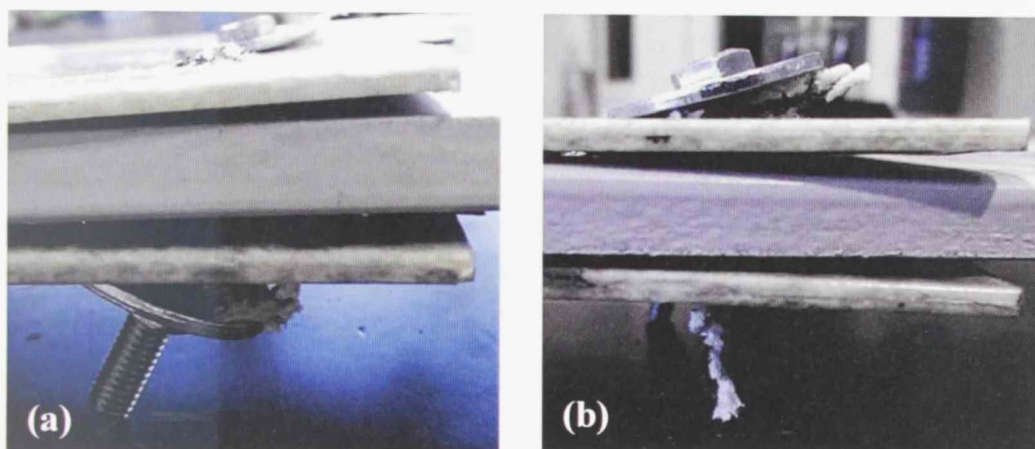
Figure 3.41: Bolt shear rupture in (a) W2_D6_ST_3 and (b) W2_D6_ST_2 connections

The D8 configuration showed more ductile behavior compared to D6 connections. Bearing effects started to take place once the gap between the bolt shank and HFRP was closed following the relative slip between HFRP and steel plate. This can be seen by the flat part of the load-displacement curves of D8 connections (in Figs. 3.19 and 3.37) of about 2 mm displacement at a load value of 5 kN. A similar behavior can be seen in the D10 connections with the only difference being that the flat part of the response curve extended to about 4 mm due to the bigger clearance in D10 connections compared to that in the D8 assemblies. The detailed behavior of D8 is presented earlier in the "Discussion of Results of Number

of Washers-per-bolt Specimens" section. The load-displacement profiles for the W2_D10_ST connections in Fig. 3.42 showed an initial increase in the carrying capacity of the connections till a load of 5 kN at a displacement of 1 mm before the load value stabilized until a displacement of 4±1 mm was reached. Following that, the load carrying capacity of the connection started to increase until a load of 22 kN was reached at a displacement of 7±1 mm. During this stage, a noticeable bearing damage was observed in the connection as displayed in Fig. 3.43.
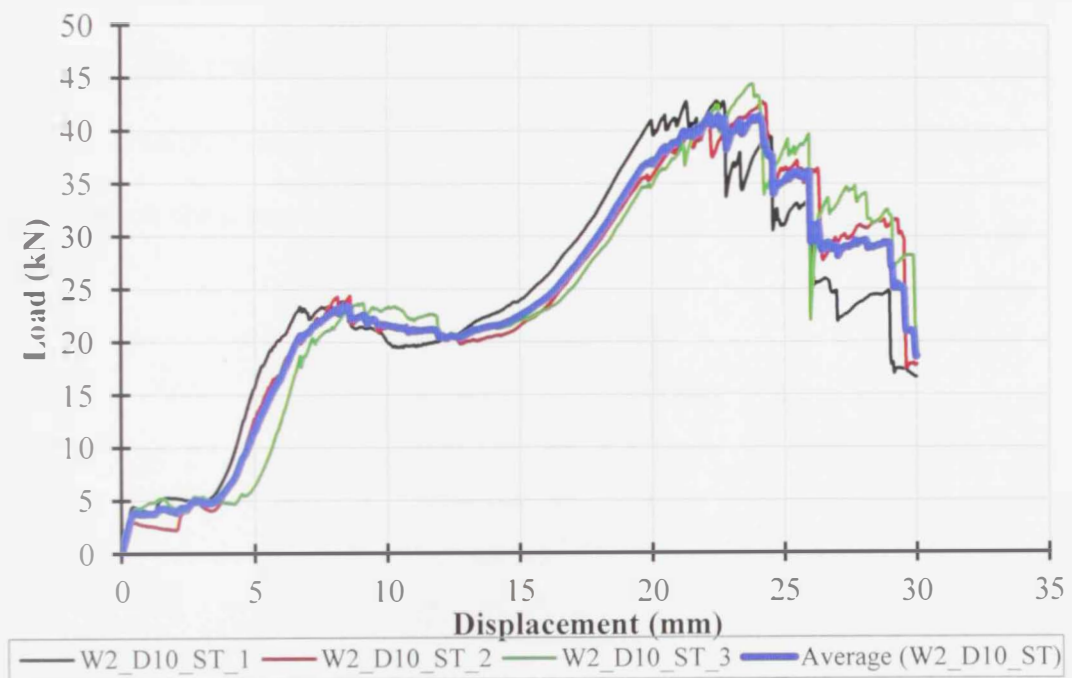
Figure 3.42: Load-displacement curves for W2_D10_ST connections

Figure 3.43: Bearing failure of W2_D10_ST_1 connection

Following the first peak of 22 kN, a significant increase in the displacement occurred (reaching a total displacement of about 15 mm) with relatively no change in the load values. This phase of the response of D10 connections was characterized by a noticeable accumulation of the GFRP layers behind the washers as shown in Fig. 3.44. Beyond the 15 mm displacement limit, the load values started to pick up again until the load carrying capacity of all specimens was almost doubled by reaching a peak value of about 41±1 kN at a total displacement of about 24 mm marking a second peak for the D10 connections. This stage was characterized by slight bending in the bolts with remarkable clicking noises which was associated with folding of the washers. Finally, excessive bearing damage took place leading to progressive tear out and block shear rupture of the connection as shown in Fig. 3.45.
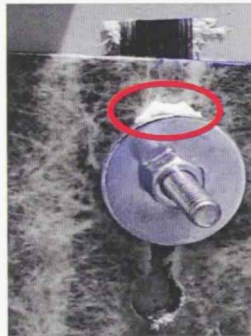
Figure 3.44: Accumulation of GFRP layers behind
the washers in W2_D10_ST_3 connection

Figure 3.45: Block shear rupture of the HFRP laminates in W2_D10_ST_2

Test results highlighted the insignificant effect of bolt-hole diameter on the ultimate load carrying capacity of the connections. This conclusion is consistent with the findings of Lawlor et al. (2005), McCarthy et al. (2005) and Kelly and Hallström (2004). Results revealed that the net-fit clearance condition (D6) maintained the carrying capacity of the connections almost unchanged compared to connections with standard hole size (D8). Meanwhile, increasing the bolt-hole clearance by 100% of the recommended standard clearance (from 2 mm in D8 to 4 mm in D10) reduced the peak load of the connections by 8%. Figure 3.46 displays the average peak loads for the three tested configurations of bolt-hole diameter (D6, D8 and D10).
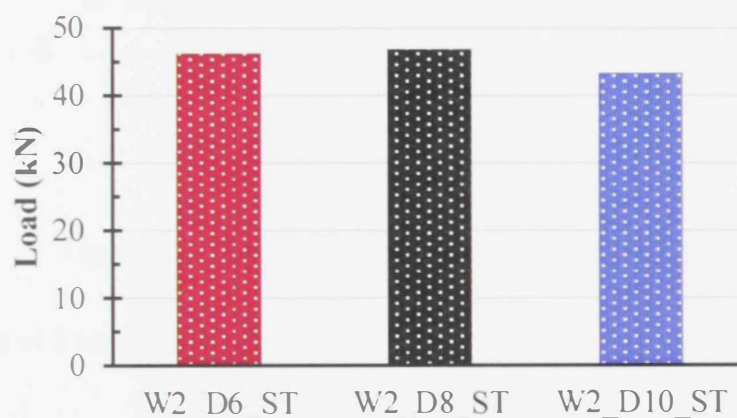
Figure 3.46: Average peak loads for the bolt-hole diameter configurations

Similar to the previously tested sets of specimens, all the bolt-hole diameter connections were instrumented with two strain gauges at both faces of the connection on the HFRP laminate (Fig. 3.14) to monitor the occurrence of out-of-plane bending during testing. The strain gauges' measurements of W2_D6_ST_3 specimen were plotted versus the applied loads in Fig. 3.47. The figure shows no sign of the connection out-of-plane bending since tensile longitudinal strains were recorded at both HFRP laminates. At low load values, measured strains at both sides of the

connection were very close. However, as the load increased, measured strains at the front side deviated from that at the backside of the HFRP laminate. This difference in the plotted strains could be referred to the combined effects of failure mechanisms which do not coincide in the two HFRP laminates.
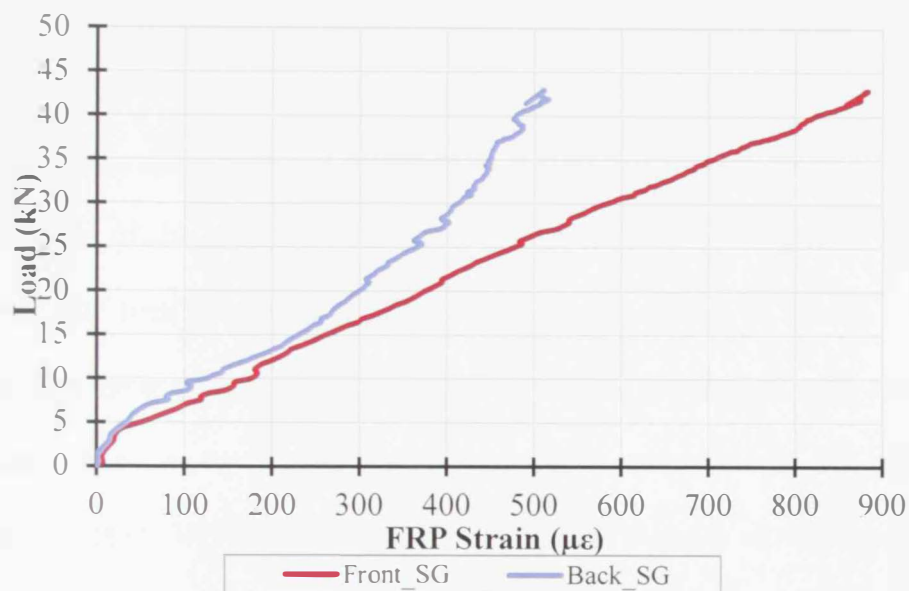
Figure 3.47: Strain gauge measurements for W2_D6_ST_3

3.3.2 Effect of Spacing between Bolts

This part of the experimental program aims at proposing a range of spacing between bolts that ensures the optimum performance of the fastened HFRP-steel connection in terms of both load carrying capacity and ductility. A test matrix including nine different spacing configurations was considered to cover a wide range of spacing values ranging between 50 mm and 300 mm as displayed in Table 3.7. The specimens were named as (S_#D), where (S) refers to the parameter being tested which is the spacing and (#D) indicates the value of the spacing as the nearest multiple integer of the bolt-hole diameter. Two replicates were tested for each configuration to ensure consistency and reliability of the experimental measurements. Based on the outcomes of section 3.3.1 of this study, the connections

were formed using M6 snug-tight steel bolts which were installed in standard 8 mm holes. Each bolt was provided with two washers: one at the head and the other at the nut. Figure 3.48 shows a schematic view of a typical spacing connection. Detailed dimensions of the nine tested configurations are presented in Fig. 3.49. Each connection included three bolts placed along a single gauge line in the loaded side of the connection. Meanwhile, eight bolts were used in the clamped side as shown in Fig. 3.49. This arrangement was followed to ensure that failure would take place in the weak side of the connection (loaded side) where various spacing values are employed. The total length of the connection varied from 610 mm to 1110 mm depending on the spacing value. It should be noted that the sheared edge distances at the loaded side of the connection was maintained 50 mm, while placing the bolts at the centerline of the HFRP width results in rolled edge distance of 50.8 mm.

Table 3.7: Bolts spacing test matrix

Designation	Spacing/Bolt-hole diameter	Spacing value (mm)
S_6D	6.25	50
S_9D	9.375	75
S_12D	12.5	100
S_15D	15.625	125
S_18D	18.75	150
S_21D	21.875	175
S_25D	25	200
S_31D	31.25	250
S_37D	37.5	300
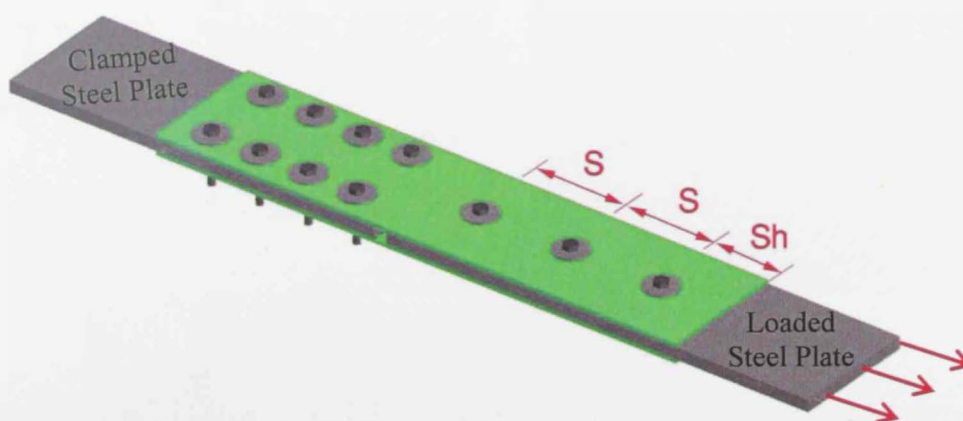
Figure 3.48: Schematic view of a typical spacing configuration
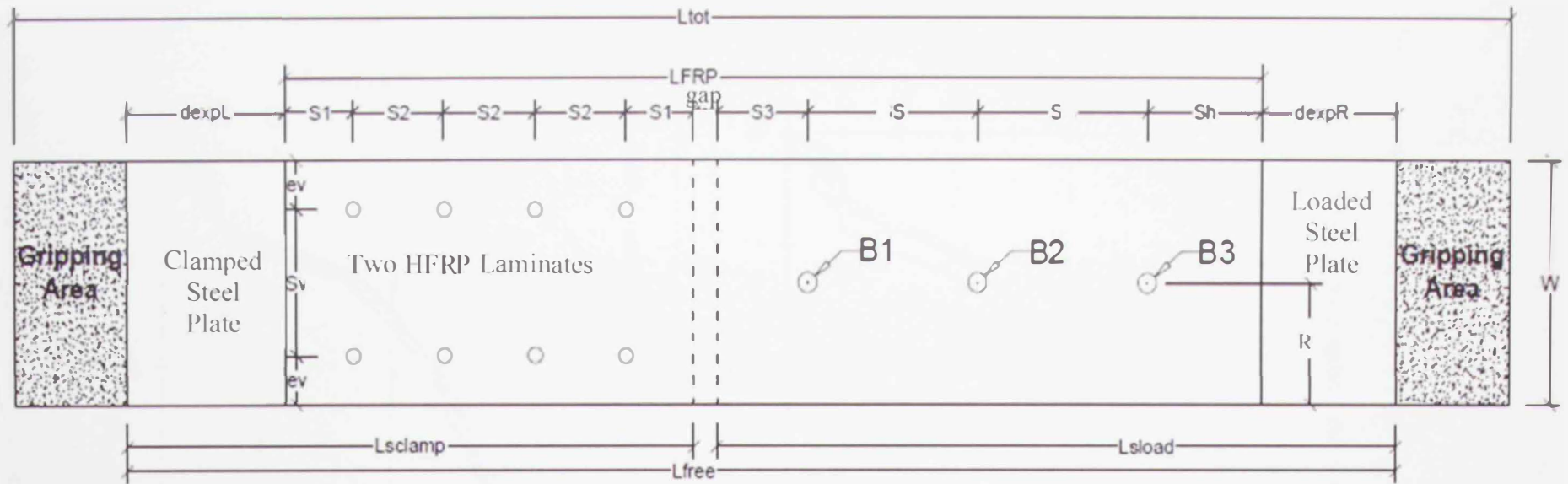
Designation	S	dexpL	dexpR	Lscalmp	Lsload	LFRP	Lfree	Ltot
S_6D	50				250	380	510	610
S_9D	75				300	430	560	660
S_12D	100				350	480	610	710
S_15D	125				400	530	660	760
S_18D	150	70	60	250	450	580	710	810
S_21D	175				500	630	760	860
S_25D	200				550	680	810	910
S_31D	250				650	780	910	1010
S_37D	300				750	880	1010	1110

S = Variable (see table)
S1 = 30
S2 = 40
S3 = 40
Sh = 50
W = 101.6
R = 50.8
Sv = 61.6
ev = 20
Gap = 10

Figure 3.49: Geometrical details of the spacing connections (Dimensions in "mm")

Discussion of Results of Spacing Specimens

For the nine tested spacing configurations, representative samples of load-displacement response curves for specimens S_6D through S_18D are presented in Fig. 3.50, while Fig. 3.51 displays the response curves for representative specimens S_18D through S_37D.
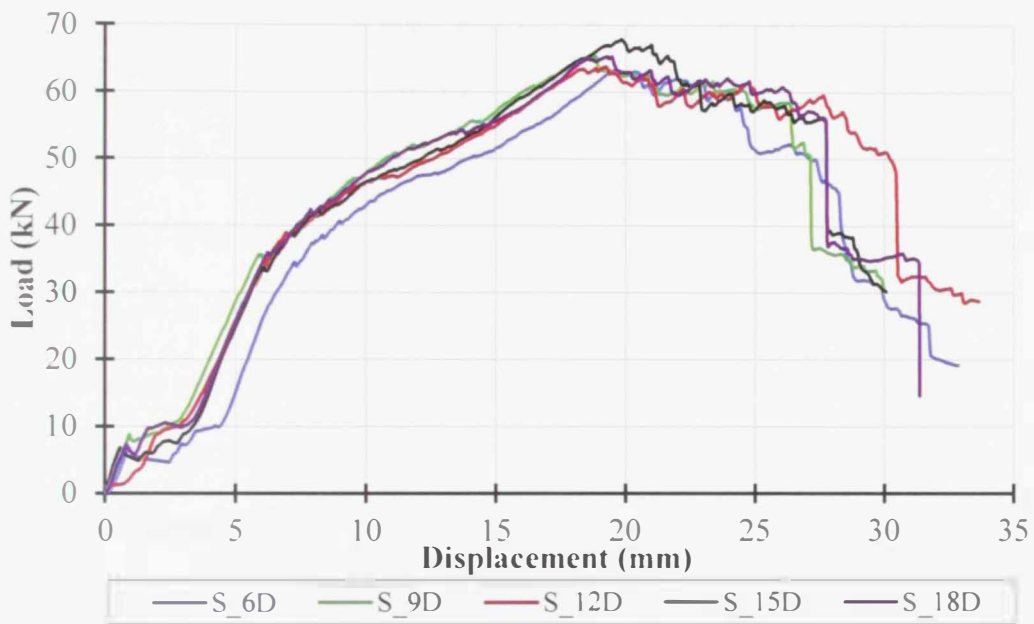
Figure 3.50: Load-displacement curves for connections from S_6D to S_18D
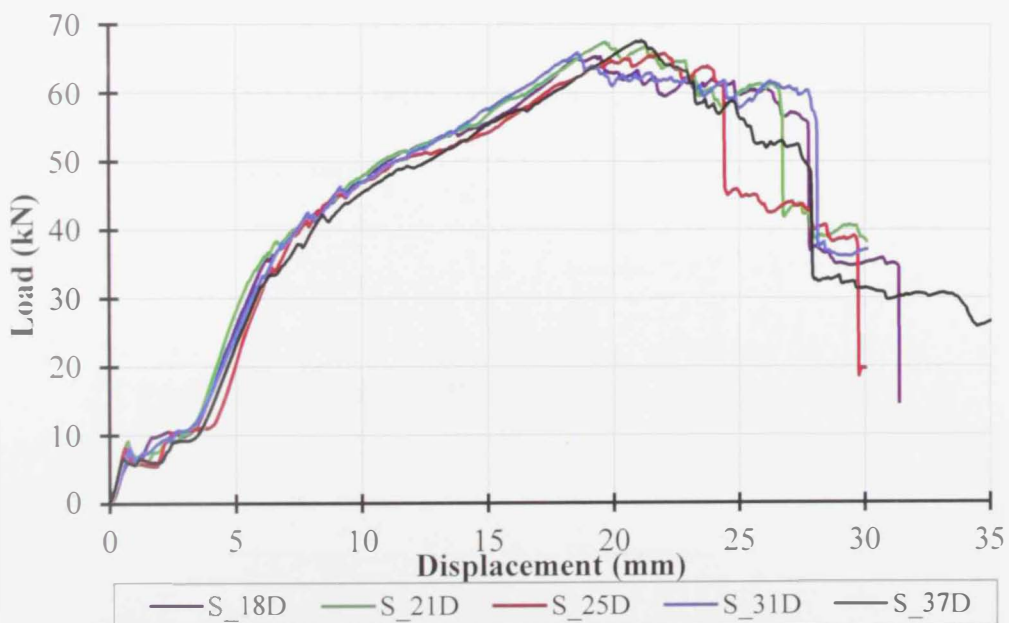
Figure 3.51: Load-displacement curves for connections from S_18D to S_37D

Both figures reveal that load-displacement curves for all specimens followed almost the same trend. Initially, the connection carried up to 8±2 kN at a displacement of about 1.5±0.5 mm. Then, the load stabilized until a displacement of 3±0.5 mm at which bearing between the bolts and the HFRP laminates took place leading to a significant linear increase in the load value till 35 kN at 6 mm displacement. The associated bearing effect observed during the test is displayed in Fig. 3.52(a). Following that, the load continued to increase with a reduced connection stiffness marking a peak of 65±1 kN at displacement of 19±1 mm. This stage was characterized by a noticeable bending in the bolts and folding of the washers as shown in Fig. 3.52(b). The load carrying capacity of the connection was then reduced by about 15% until a load value of 55 kN at a displacement of about 27±1 mm was reached. The response in this post-peak stage was associated with excessive bearing and tear out in the HFRP laminate as shown in Fig. 3.52(c). Beyond the 28 mm displacement limit, connections failed by progressive damage and BSR in the HFRP laminates as shown in Fig. 3.52(d), followed by sudden failure due to excessive shear in the bolts as displayed in Fig. 3.52(e). In general, all connections followed almost the same failure mechanisms experienced by the (W2_D8_ST) connections explained in the previous sections. This highlights the insignificant effect of considered bolts spacing on the failure modes controlling the response of the connections.
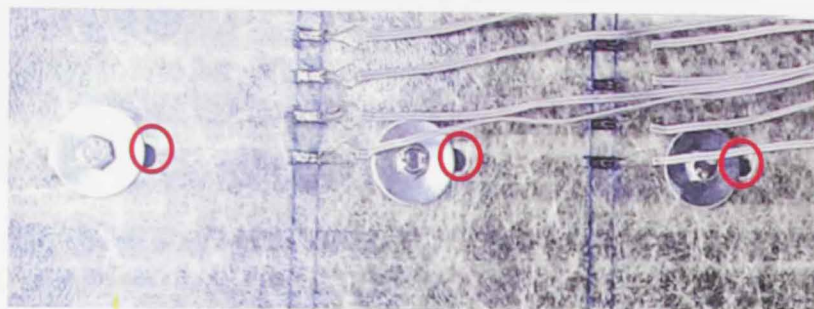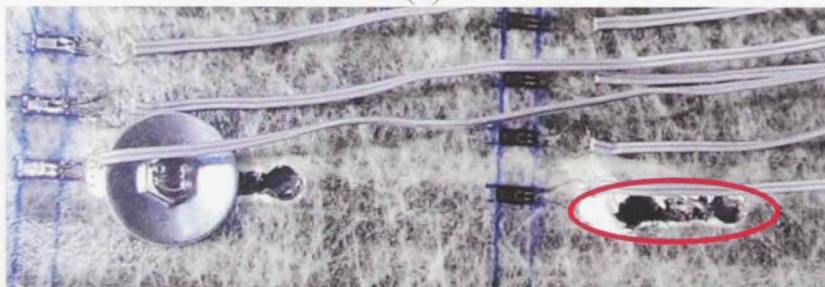
Figure 3.52: Typical behavior of S_#D connections: (a) bearing between bolts and HFRP, (b) folding of the washers, (c) excessive bearing and tear out, (d) progressive damage and BSR in HFRP and (e) bolt shear failure

Experimental measurements showed also that, for the particular range of bolts spacing considered in this study, there is no remarkable effect on the ultimate load carrying capacity of the HFRP-steel connections as reflected in Fig. 3.53. While all tested connections showed similar ductile behavior, the S_12D specimen exhibited the best performance with a displacement range that is 10% higher than all other specimen configurations. The concluded insignificant effect of bolt spacing on both failure modes and loads of the tested connections confirms the findings of Sweedan et al. (2013).
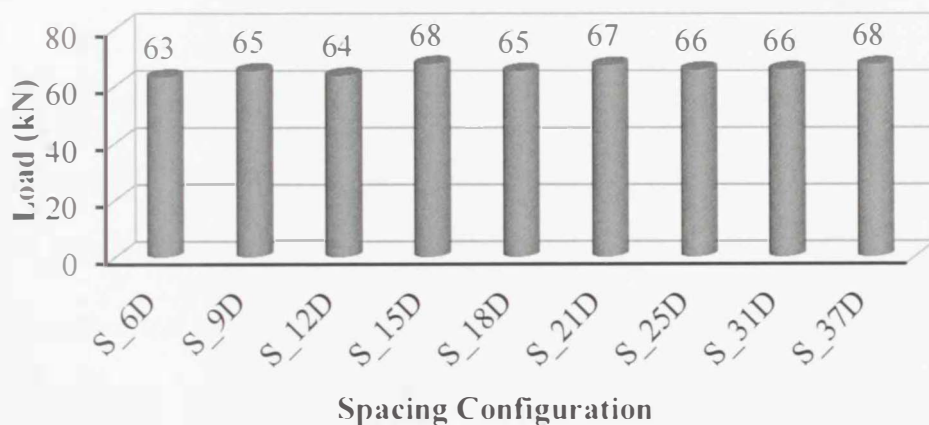
Figure 3.53: Ultimate peak loads of the different spacing configurations

Bolts loads

Strain distribution and load transfer between the bolts at the loaded steel plate was calculated experimentally in order to be used later in chapter 4 for the verification of the developed finite element model. For this purpose, each of the specimens was instrumented with eight strain gauges at one side of the connection as shown in Fig. 3.54. Four strain gauges were mounted mid-way between the first (B1) and the second (B2) bolts, while the remaining four strain gauges were attached

between the second (B2) and the third (B3) bolts as shown in Fig. 3.54. The measured strains were collected through a multi-channel digital data acquisition system.
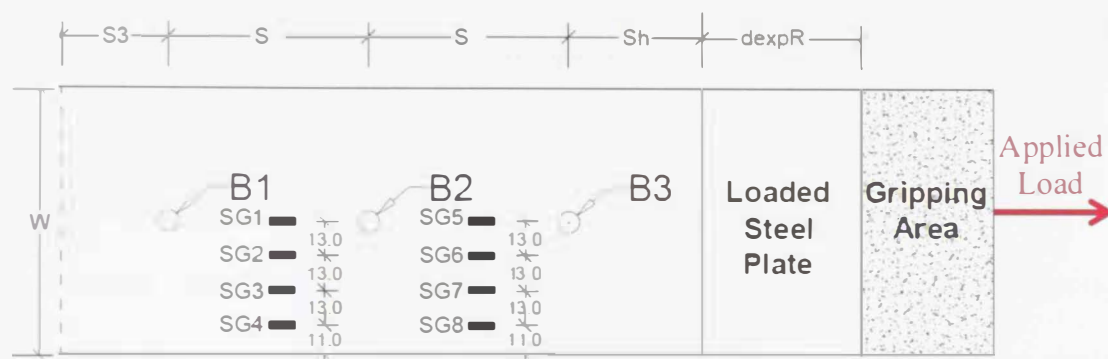
Figure 3.54: Locations of the strain gauges on the loaded side of spacing connection (Dimensions in mm)

Bolt loads were estimated using integration approach which is similar to the methods adopted by Lawlor et al. (2005) and Starikov and Schön (2002). This approach involves integrating the strain across the width of the HFRP laminate. The stresses at the cross section were calculated by multiplying the integrated strains by the elastic modulus of the laminates. The load transferred from the loaded steel plate to the HFRP laminates through bolt (B3) was estimated using strains measured by gauges (SG5 through SG8). Meanwhile, strains measured by gauges SG1 through SG4 correspond to the loads transferred from steel plate to HFRP laminates by bolts (B2) and (B3). Finally, the load induced in the segment of HFRP laminates to the left of (B1) (i.e., the HFRP width bridging the gap between the two steel plates) should be equal to the full load applied to the steel plate as a result of the static equilibrium of the connected parts.

The effect of spacing on the bolt load distribution is displayed in Fig. 3.55 for the three different loading stages: elastic, hardening and at peak loads. The load

acting on each bolt was calculated after identifying the loads induced in the cross-section of the HFRP laminates where strain gauges were attached. A numerical integration of the measured strains across the width of the laminate was performed and then multiplied by the elastic modulus and the cross-sectional area of the HFRP laminate. It is worth mentioning that the strain readings between B1 and B2 (gauges 1, 2, 3 and 4) were higher than those between B2 and B3 (gauges 5, 6, 7 and 8) because the loads bypassing (B1) are higher than those for (B2). Figure 3.55 does not indicate any specific trend for the bolt-load distribution with the change of spacing. However, the bolt-load distribution is affected by the stage of loading. At the elastic range, the three bolts shared the applied loads in a random manner as shown in Fig. 3.55a. This fluctuation of the bolt-load distribution before the yielding load can be attributed to the random distribution of the fibers and the unpredicted bearing between the bolts and the untorn fibers. At the strain hardening zone, (B1) carried the highest portion of the transferred loads from the HFRP laminates which is consistence with the findings of Starikov and Schön (2002). This is also in agreement with the results of Hanauska et al. (2001) which predicted that bolts close to the loaded side of the composite carry most of the applied loads. The remaining applied loads were distributed between bolts (B2) and (B3) randomly (see Fig. 55b). Results revealed that (B1) carried almost 60% more loads than (B2) and (B3) at the hardening zone, while it carried around 1.86 times the average loads of (B2) and (B3) at ultimate loading. A sample load distribution between bolts of S_18D specimen is presented in Fig. 3.56. At the elastic zone (i.e. before the 36 kN), the three bolts shared the applied loads almost equally, however, (B1) carried most of the loads after yielding till the failure of the specimen. The same behavior was repeated in most of the specimens as in Fig. 3.57 for S_12D.
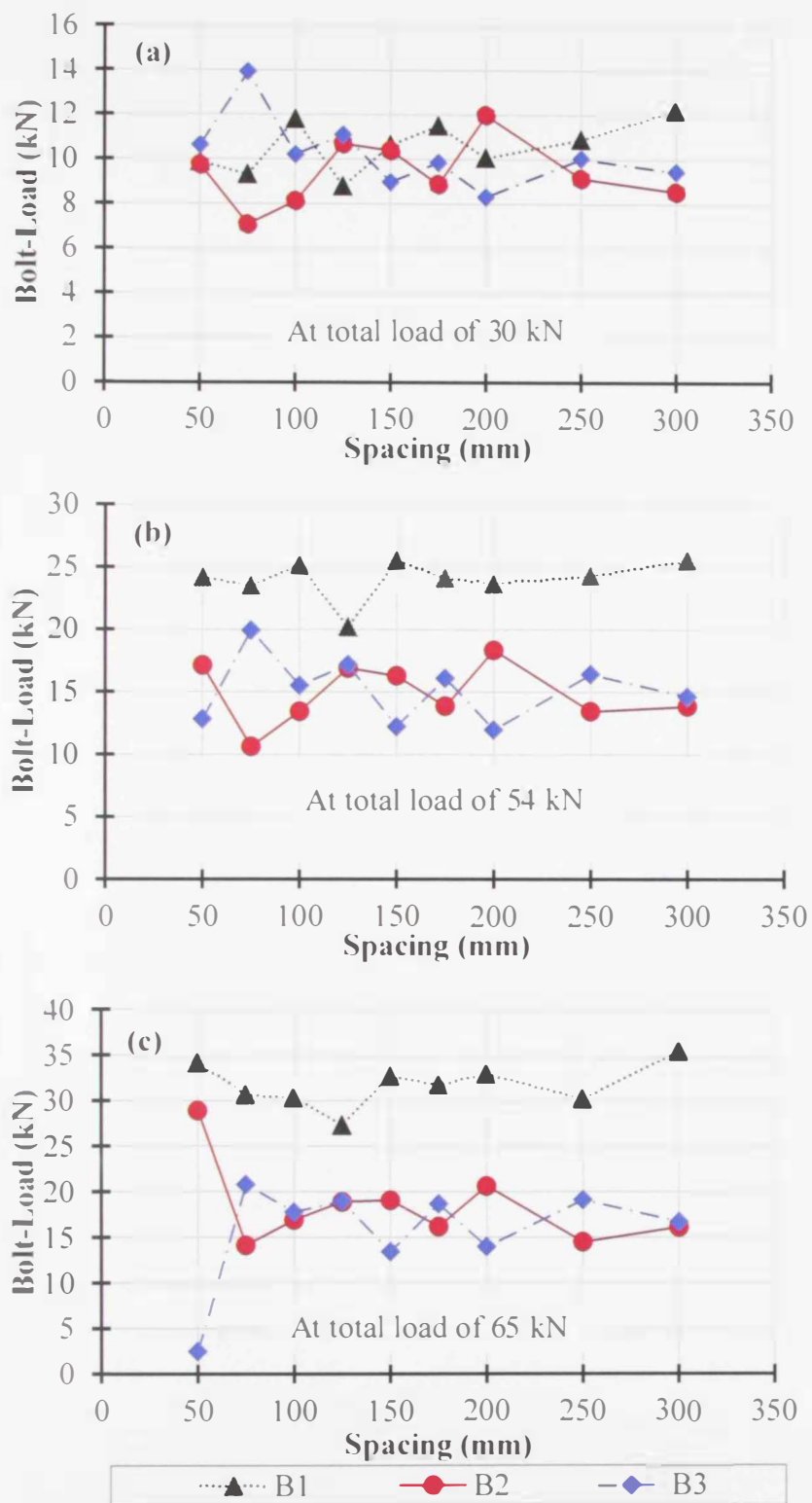
Figure 3.55: Bolt-load at tested spacing values at the: (a): elastic zone, (b) hardening zone and (c) peak load
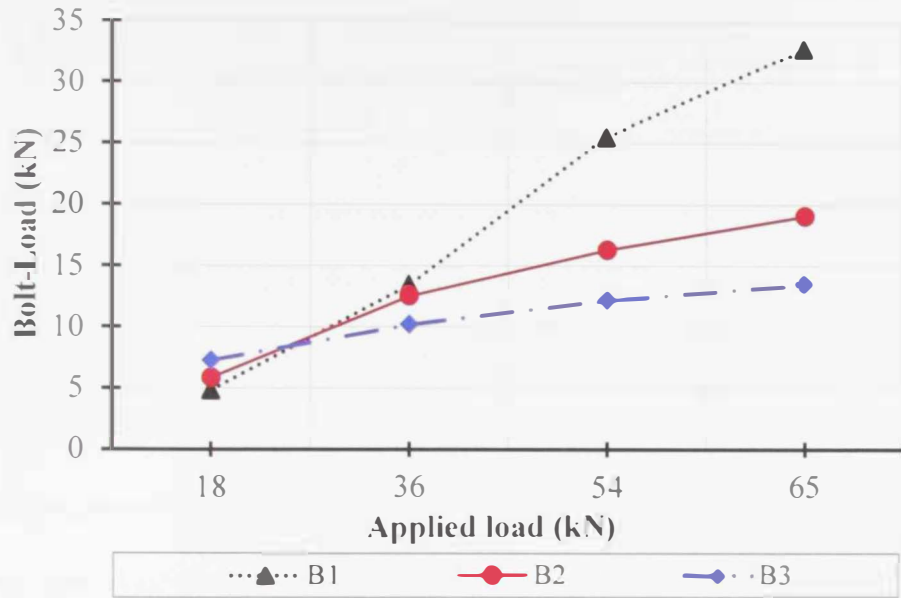
Figure 3.56: Load distribution between bolts of S_18D (Bolt spacing 150 mm)
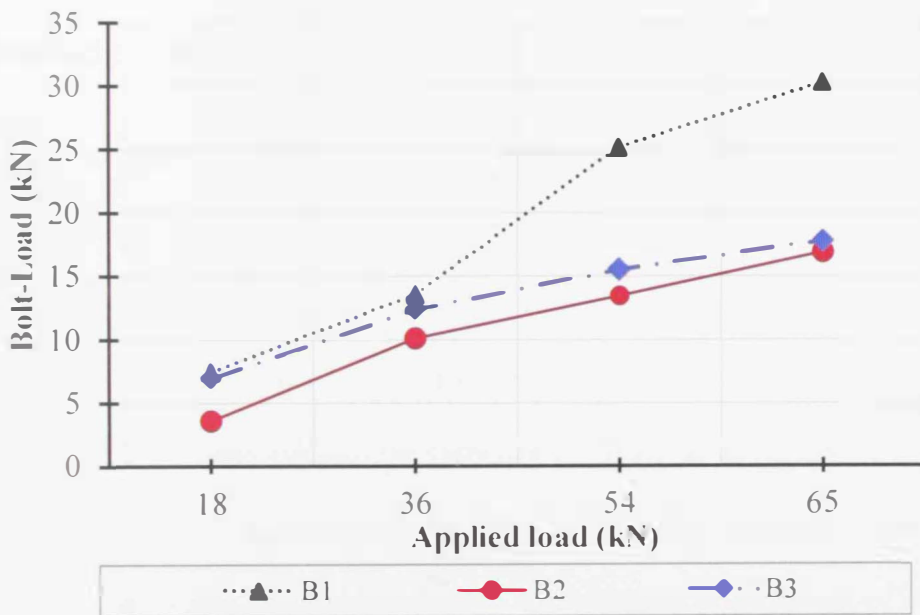
Figure 3.57: Load distribution between bolts of S_12D (Bolt spacing 100 mm)

3.3.3 Phase II: HFRP-Steel Connections using FRP Anchors

The use of the steel bolts in connecting the HFRP laminates to the targeted steel elements may raise durability concerns related to potential corrosion of the metallic components of the connection. In order to overcome this potential drawback, fiberglass studs (Fiberbolts) were selected to substitute the steel bolts due to their high corrosion resistivity. This phase of the experimental study investigates the response of the HFRP-steel double-lap connections fastened using FRP anchors. The fastening parameters tested throughout this phase include sheared edge distance (Sh) and bolt-diameter. In this section, the procedure of the experimental investigation using the Fibrebolts is illustrated. Additionally, the response of the proposed fastening technique was analyzed with respect to the various fastening parameters.

Test Procedure of Phase II

FRP anchors FB10 and FB13 with two different diameters, 10 and 13, respectively, were used in the experimental investigation. The mechanical properties of the utilized FRP anchors are presented in Table 3.3 of section 3.2.5. For each stud diameter, five different test configurations were considered in order to investigate the effect of sheared edge distance on the response of HFRP-steel connections fastened using FRP anchors. A schematic view of a typical FRP anchors connection is presented in Fig. 3.58. The loaded side of the connection consisted of one FRP anchors that was centered across the width of the HFRP laminates. Similar to the connections tested in phase I of the study, the clamped side of the connection was fastened using eight M6 steel bolts. The geometrical details of connections fastened using FRP anchors are displayed in Fig. 3.59.
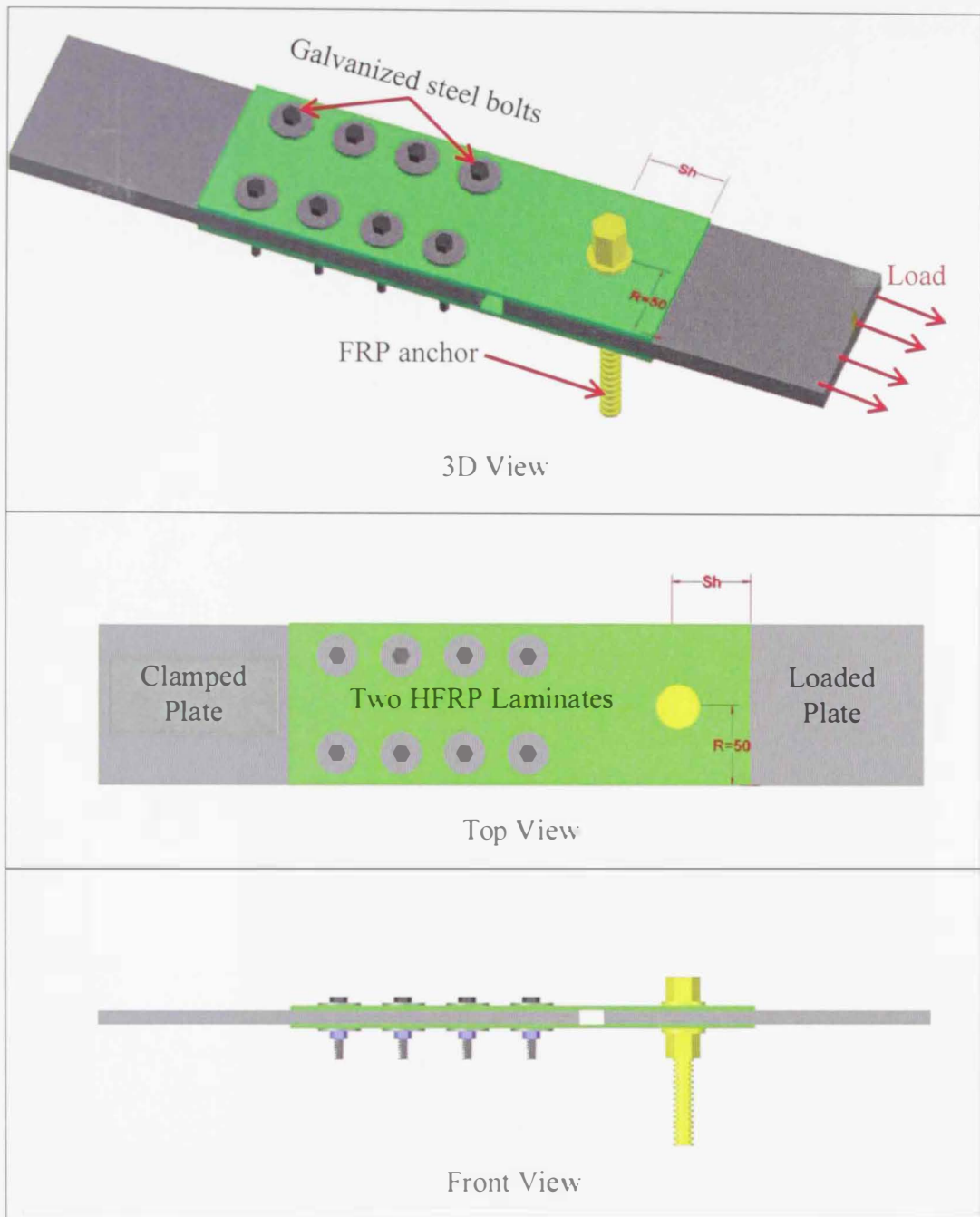
Figure 3.58: Schematic views of a typical HFRP-steel connection
using FRP anchors
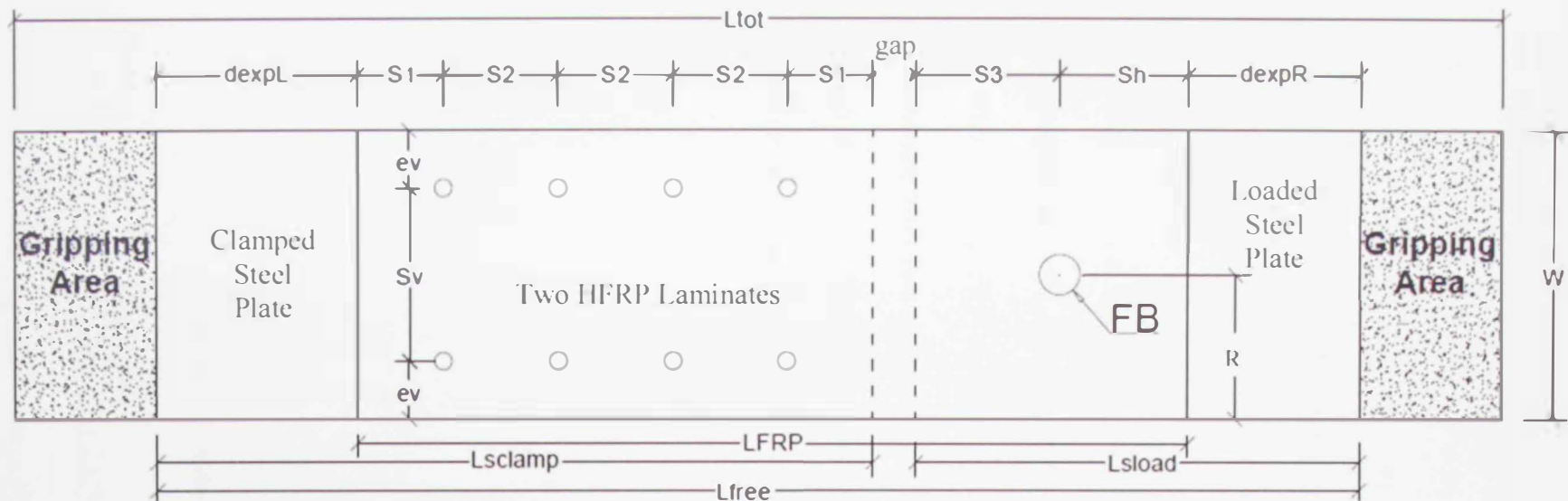
Designation	Lscalmp	dexpL	Gap	dexpR	Sh	Lsload	LFRP	Lfree	Ltot
FB10_2D			16	66	24	140	270	406	506
FB10_3D			14	69	36	155	280	419	519
FB10_4D	250	70	12	72	48	170	290	432	532
FB10_5D			10	75	60	185	300	445	545
FB10_6D			8	78	72	200	310	458	558
FB13_2D			10		30	140	270	400	500
FB13_3D			15		45	155	290	420	520
FB13_4D	250	70	10	60	60	170	300	430	530
FB13_5D			15		75	185	320	450	550
FB13_6D			10		90	200	330	460	560

Sh =	Variable (see table)
SI =	30
S2 =	40
S3 =	40
R =	50.8
W=	100
Sv=	61.6
ev=	20

Figure 3.59: Geometrical details of a typical HFRP-steel connection using FRP anchors (Dimensions in "mm")

FRP anchors were inserted in standard size holes having diameters that are 2 mm bigger than those of the bolt shank. The FRP studs and nuts were lubricated before being used in order to ease their movement as recommended in the manufacturer product sheet. The FRP nuts were tightened using a breaking type torque wrench to apply the recommended installation torque provided by the manufacturer. Specimens were loaded in tension using 100 kN MTS Machine with a rate of 1 mm/min. The longitudinal displacement of the connection was measured using two LVDTs at both sides of the specimen with a similar setup to that used in the connections with steel bolts. The experimental setup of the HFRP-steel connections using FRP anchors is presented in Fig. 3.60. Each specimen was instrumented with two strain gauges at the front and backsides of the connection to monitor the out-of-plane bending during testing. The locations of the mounted strain gauges are shown in Fig. 3.61.
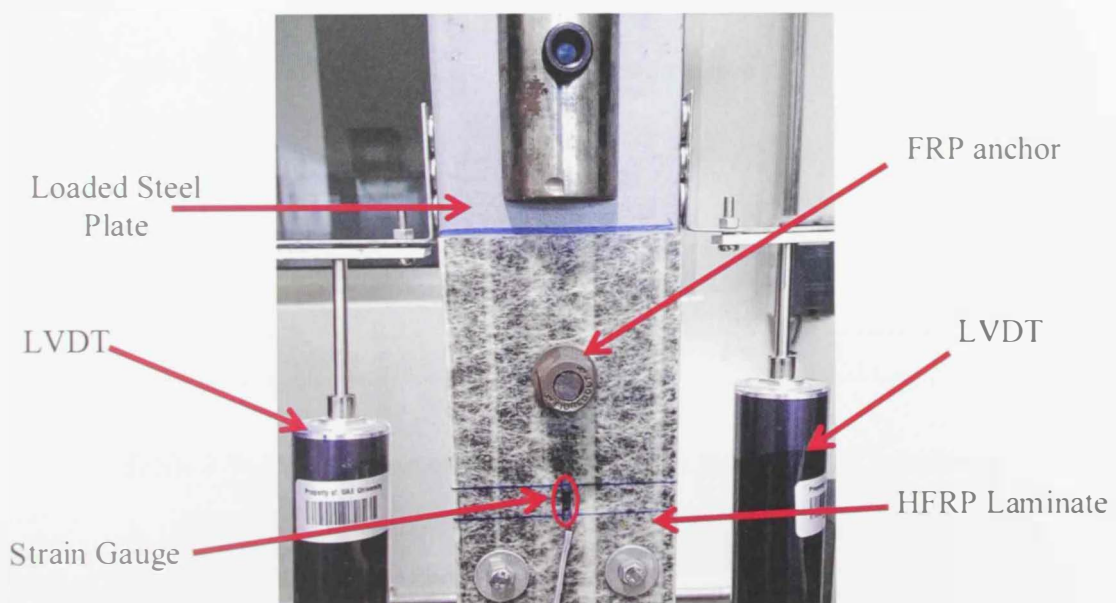
Figure 3.60: The experimental setup of HFRP-steel connections using FRP anchors
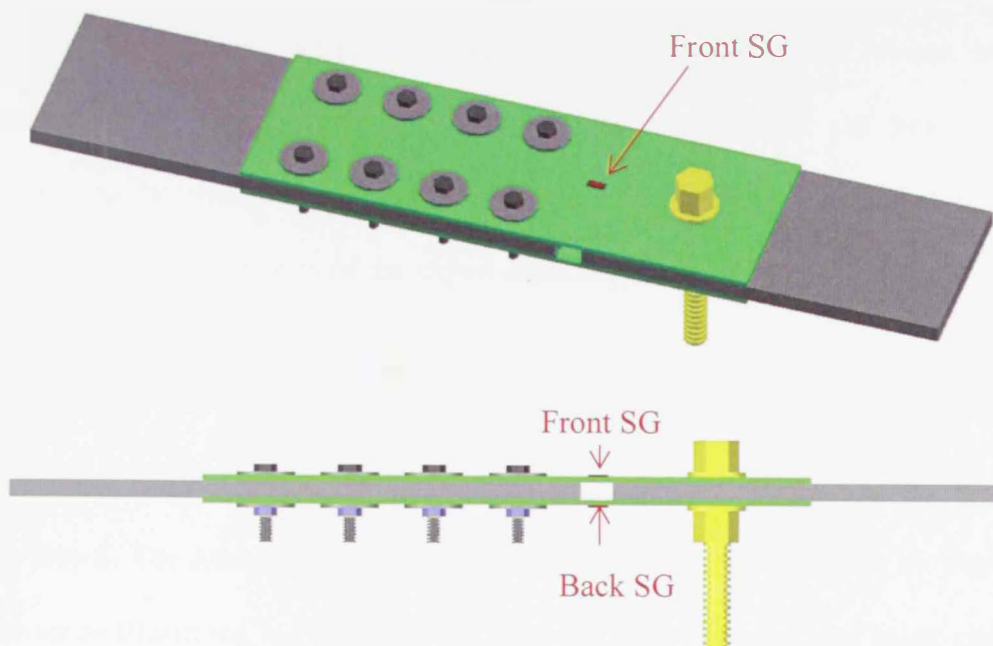
Figure 3.61: Locations of the strain gauges of the HFRP-steel connection
using FRP anchors

For each anchor diameter, five configurations were tested for sheared edge
distances that cover the range of two to six times the anchors-hole diameter. Tables
3.8 and 3.9 display the design values of the tested sheared edge distances using the
FB10 and FB13 anchors, respectively.

Table 3.8: Designed sheared edge distances for the FB10 specimens

Specimen Designation	Sheared Edge distance (mm)
FB10_2D	24
FB10_3D	36
FB10_4D	48
FB10_5D	60
FB10_6D	72

Table 3.9: Designed sheared edge distances for the FB13 specimens

Specimen Designation	Sheared Edge distance (mm)
FB13_2D	30
FB13_3D	45
FB13_4D	60
FB13_5D	75
FB13_6D	90

Specimens were designated as (FB#_yD) where the symbol (#) indicates the diameter of the stud. while (y) refers to the multiple of the hole-diameter representing the sheared edge distance. Two specimens of each configuration were tested to ensure consistency of the experimental results.

Discussion for of Results of Sheared Edge Distance (Sh)

Five configurations for the sheared edge distance of each anchor-diameter were tested. The load-displacement profiles of the FB10 connections showed close behavior as illustrated in Fig. 3.62. The figure indicates that the load value increased instantaneously with the application of the tensile load until it reached a value of about 2±0.5 kN at displacement of 0.2 mm. Following that. considerable increase in the displacement occurred (reaching a total displacement of about 2.5 mm) with relatively no increase in the applied load. This flat segment of the response curve can be attributed to the relative slippage between the HFRP laminates and steel plates. Beyond the 2.5 mm displacement. the load value increased significantly in a linear manner until it reached a peak of 13±1 kN at an average displacement value of about 7.5 mm. This stage was characterized by noticeable bearing between the FB10 anchor and the HFRP laminates. Then. the excessive stresses induced in the FRP anchor caused its sudden failure by shear as depicted by Fig 3.63. It is clear that changing the sheared edge distance from 2 to 6 times the hole-diameter using the FB10 didn't affect the ductility of the connection as all connections experienced brittle failure once the peak load was reached.
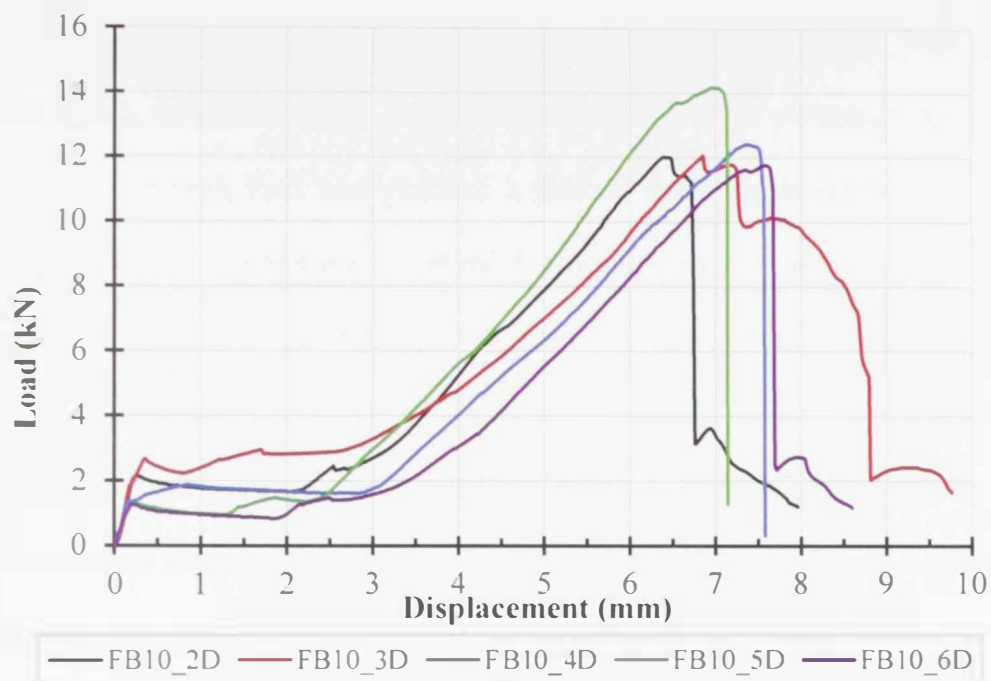
Figure 3.62: Load-displacement curves for the tested connections using FB10
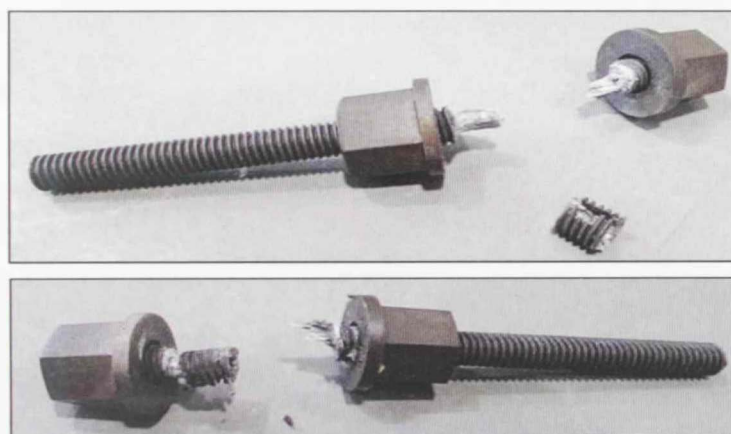
Figure 3.63: Shear failure in FB10

Figure 3.64 presents the load-displacement response curves for HFRP-steel connections fastened using the FB13 studs. Initially, all specimens with various sheared edge distance values showed a slight increase in the load value (around 3 kN) at a displacement of 0.2 mm. After that, the load value remained constant till a displacement of 3 mm in a similar manner to the behavior of the FB10 connections. At this displacement value, the bearing action between the FB13 and the HFRP

laminates started to take place causing a significant increase in the load value reaching a peak value that ranges between 19 kN and 22 kN at a displacement about 7 mm. Once the peak load was attained, a gradual reduction in the load carrying capacity of the connections was observed followed by sudden shear failure of the FRP anchors. The peak load and post-peak behavior varied from one connection to another depending on the investigated sheared edge distance. For example, specimen FB13_2D experienced sudden drop in the load value at a displacement of 8 mm with a corresponding load of 15 kN. On the other hand, connection FB13_3D showed more ductile behavior as evident by the stable post-peak response corresponding to displacement value of 8 mm through 13 mm. The failure load of the FB13_3D connection was 22 kN at a displacement of 13 mm. Using a sheared edge distance that is greater than three times the hole-diameter resulted in reduction in the peak load and connection ductility compared to those of the FB13_3D specimen.
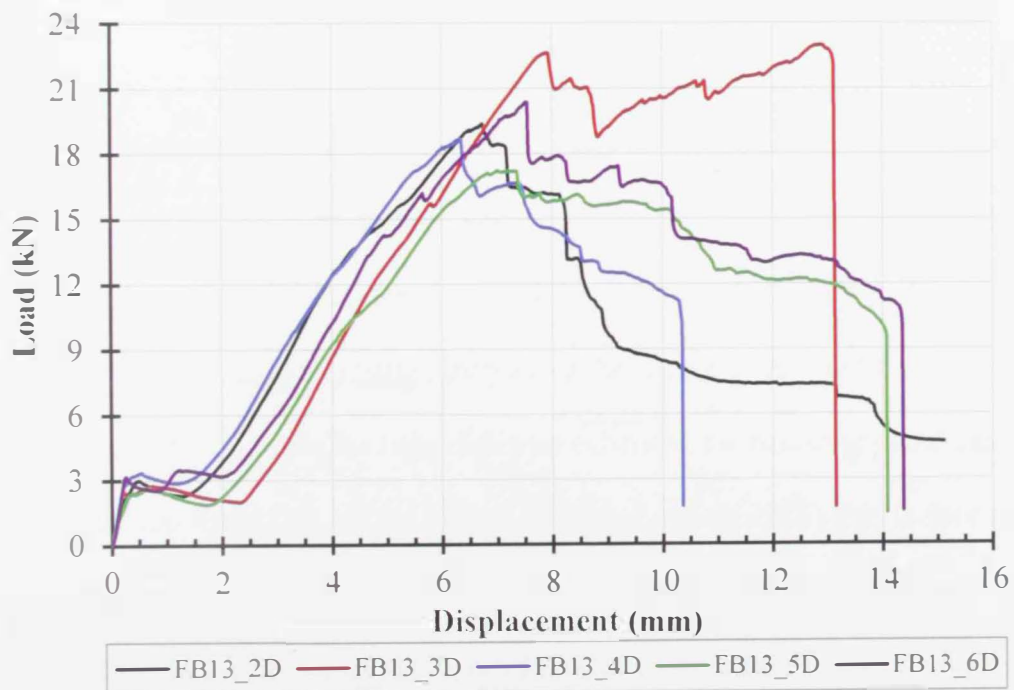
Figure 3.64: Load-displacement curves for the tested connections using FB13

Figure 3.65 presents the average peak loads for connections fastened using FB10 FRP anchors. The ultimate carrying capacity of the connection increased with increasing the sheared edge distance (Sh) from twice to five times the hole-diameter. Further increase of the sheared edge distance to six times the hole-diameter reduced the ultimate peak load of the connection from 13.5 kN to 11 kN as shown in Fig. 3.65.
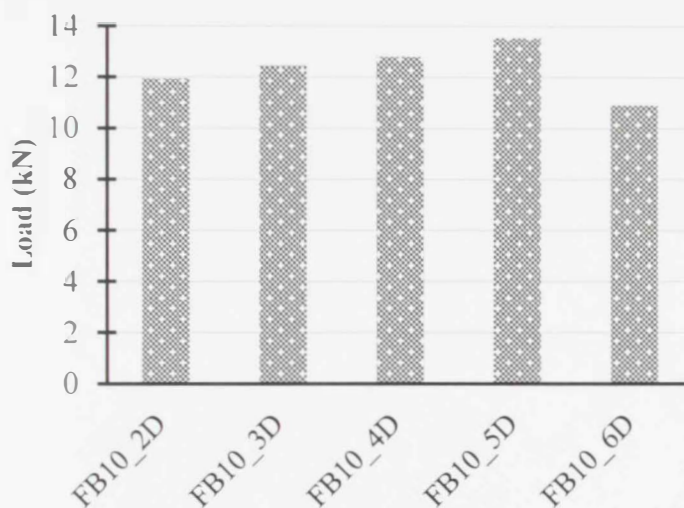
Figure 3.65: Average peak loads for FB10 connections
with various sheared edge distances

The average peak loads for the HFRP-steel connections fastened using FB13 FRP anchors are summarized in Fig. 3.66. No specific trend between the ultimate load carrying capacity of the connections and the different sheared edge distance can be observed from the plotted results. Increasing the sheared edge distance (Sh) from two (2D) to three (3D) times the hole-diameter enhanced the maximum load capacity of the connection from 18.5 kN to 23 kN. However, using a (Sh) that is four times the hole-diameter (4D) caused a reduction in the peak load of the connection. Further increase of the (Sh) from 4D to 6D resulted in a slight increase in the ultimate peak load of the connection by about 13 %. (from 19 kN to 21.5 kN). FB13_3D configuration showed a maximum peak load of 23 kN among all tested

configurations. The absence of a clear trend between the sheared edge distance and the peak loads could be attributed to the random rupture of the glass fibers constituting the material of FRP studs. Based on the results obtained in the current study, the FB13_3D is selected as the configuration with the best performance in terms of both ultimate load and ductility response.
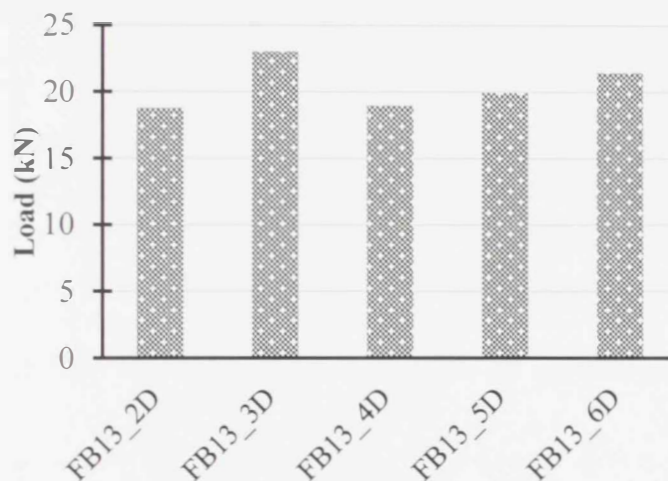
Figure 3.66: Average peak loads for FB13
connections with various sheared edge distances

It is important to highlight that the out-of-plane bending experienced by FB10 and FB13 connections was negligible as revealed by strain gauges measurements recorded for all tested connections. Figures 3.67 and 3.68 show the strain gauges measurements for representative the samples FB10_4D and FB13_3D, respectively. Although the deformation increases, this is not completely translated to elongation in the HFRP laminates, but rupture of the threaded part of the FRP anchor that absorbed considerable amount of the deformation leading to strain reduction in the HFRP. This was not the case of the steel bolts with strong threaded part relative to the HFRP laminates. Strain gauges at both sides of the both specimens recorded

tensile strains of very close values implying the minimal effect of out-of-plane bending in the connection under tensile loading.
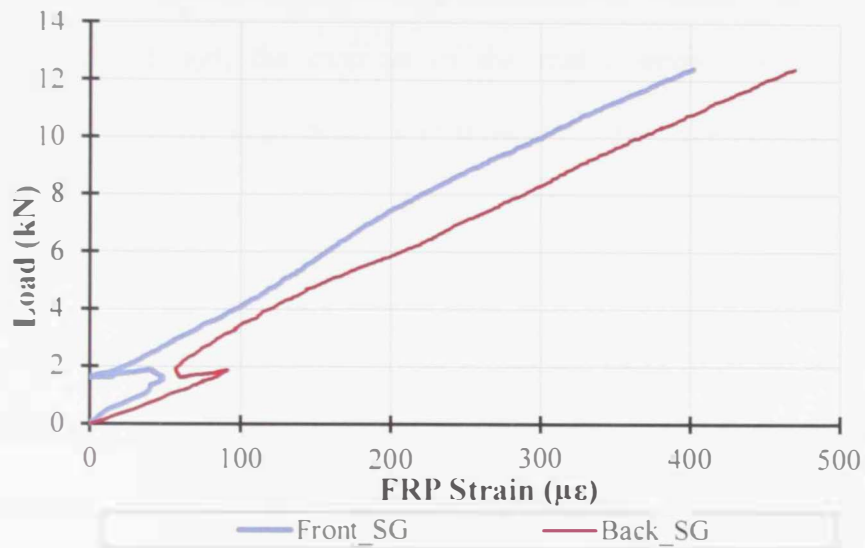
Figure 3.67: Strain gauge measurements for specimen FB10_4D
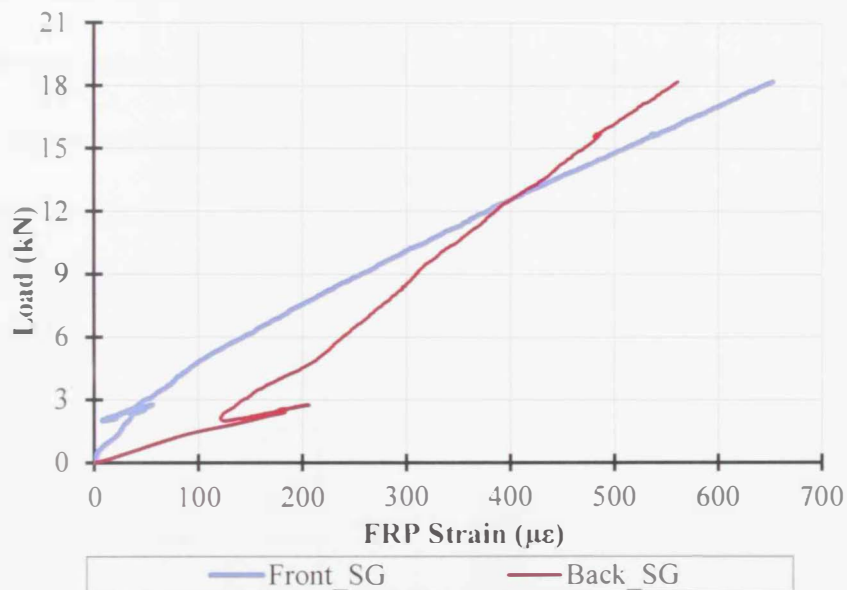
Figure 3.68: Strain gauge measurements for specimen FB13_3D

Discussion of Results of Bolt Diameter

Two different sizes of the FRP anchors were employed in this phase of the experimental program (FB10 and FB13). For comparison purposes, the average peak

loads of the HFRP-steel connections considering all tested FB10 and FB13 specimens with various sheared edge distances are plotted in Fig. 3.69. The column chart shows a 65% enhancement in the ultimate load carrying capacity of the connection associated with the increase of the stud diameter by 30%. For the proposed optimum sheared edge distance of three times the hole-diameter (3D), the recorded peak load using the FB10 was 12 kN, while that for FB13 was 23 kN (see Fig. 3.70) indicating 91.5% improvement in the load carrying capacity of the connection. It should be noted that the previously mentioned experimental peak loads are in excellent agreement with the values obtained using nominal stud diameter and the manufacturer recommended ultimate stresses presented in Table 3.3 that correspond to ultimate loads of 14.7 kN and 23.3 kN for FB10 and FB13, respectively. Additionally, the response curves shown in Fig. 3.70 indicate clearly the considerable enhancement of the FB13 connection ductility compared to that of the FB10 connection. Similar effect of the bolt diameter on the ductility of the connection was observed for all tested specimens with various sheared edge distances as depicted by Figs. 3.62 and 3.64 for FB10 and FB13 connections, respectively.
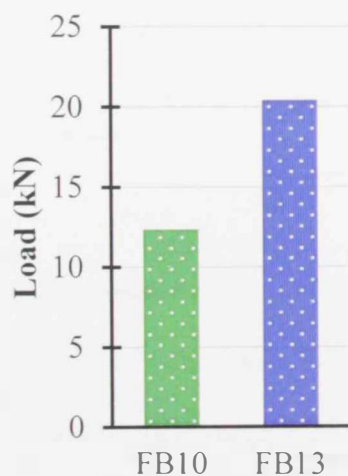
Figure 3.69: Average peak loads for FB10 and FB13
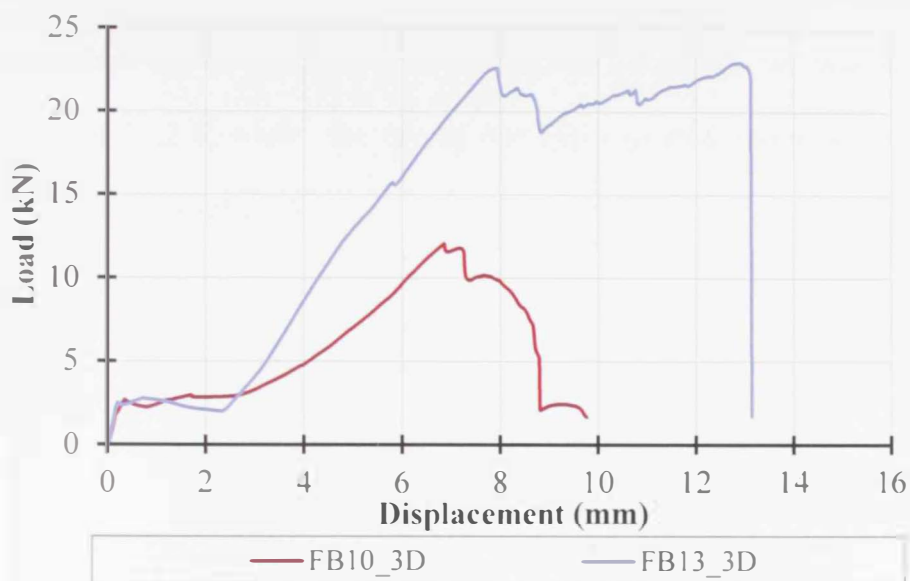
Figure 3.70: Load-displacement curves for FB10_3D and FB13_3D

3.3.4 Influence of Fastener Type on Connection Behavior

The experimental program was divided into two main phases based on the type of the fastener used to connect the HFRP laminates to the steel plates (i.e., steel bolts and FRP anchors). Comparing the best performing configurations in the two phases (W2_D8_ST and FB13_3D) several conclusions can be outlined. From strength stand point, both connections were shown to provide, almost, the same load carrying capacity with a difference that does not exceed 2% (11.7 kN for W2_D8_ST in single shear plane per bolt and 11.5 kN for FB13_3D in single shear plane per anchor), as depicted by Fig. 3.71.

As evident by Fig. 3.71, connections that use steel bolts exhibit a more ductile response compared to those with FRP anchors. Additionally, attaining the same strength requires utilization of FRP anchors of much bigger diameter compared to their steel counterparts. This is directly reflected on the size of holes to be drilled in the connected elements and the negative impact this may have on the tensile

strength of such elements. Furthermore. the steel bolts provide an economical option for designers since one steel bolt with its accessories (including two washers and a nut) cost around 0.22 \$. while the use of one FB13 (a stud and a nut) with one tightening nut cost around 7.6 \$.
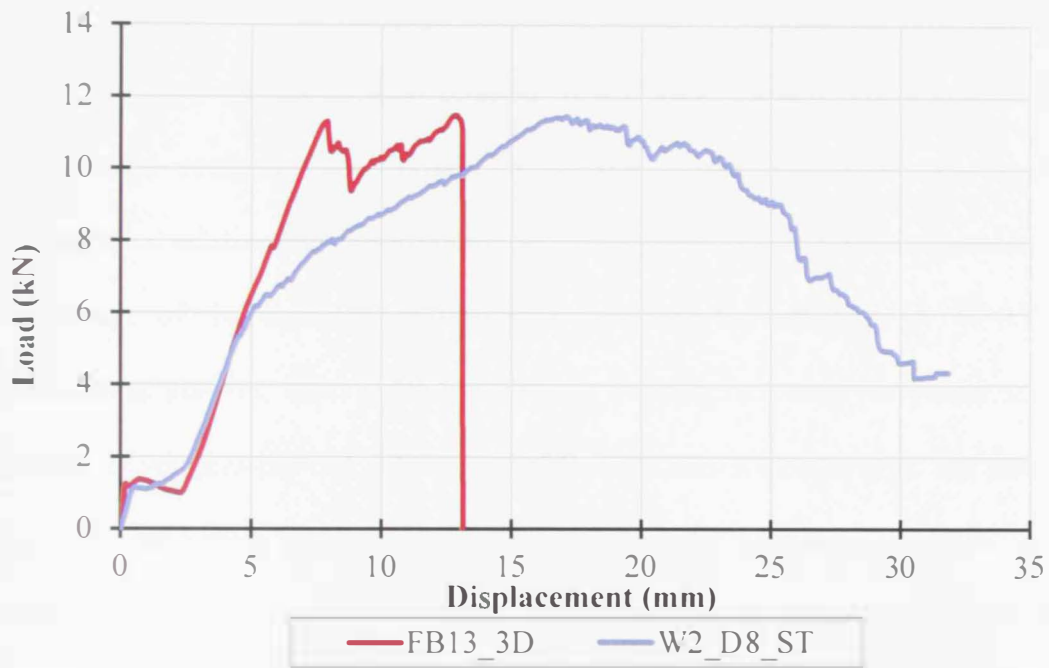
Figure 3.71: Load-displacement curves for single steel bolt in (W2_D8_ST) and FB13 anchor (FB13_3D) bearing against one HFRP laminate

On the other hand. a main drawback in the use of steel bolts could be their long-term durability which needs to be investigated carefully. Durability concerns related to the possible corrosion that may be induced in both the steel bolts and rehabilitated steel elements may adversely affect the performance of the HFRP-steel connection. To overcome the potential corrosion of the steel. FRP anchors had been introduced as a good alternative to replace the steel bolts. One of the main advantages FB13 offer. is high corrosion resistivity. since they are made of glass-fibers. Additionally. the used FB13 is much lighter than the steel bolts and hence. reduces the total imposed weight on the strengthened structure.

3.4 Summary and Conclusion

This chapter focused on investigating the interfacial behavior of the HFRP-steel fastened connections. The hybrid connections were fastened using two types of fasteners (i.e., steel bolts and FRP anchors) and subjected to axial tensile load along its longitudinal direction. An experimental program was conducted on a total of 62 HFRP-steel fastened connections in order to study and identify their response under 29 different configurations. Tensile tests were carried out to obtain the load-displacement relationships and record the associated HFRP longitudinal strains. The first phase of the experimental study investigated the response of HFRP-steel connections that use steel bolts considering various fastening parameter such as number of washers-per-bolt, clamping torque and bolt-hole clearance. Furthermore, nine different values for the spacing between the steel bolts were tested in order to propose a practical range of spacing for ideal performance of the connection. In the second phase of the experimental program, FRP anchors were employed to fasten the HFRP laminates to the steel plates. The main focus of this phase was to examine the efficiency of using FRP studs in forming hybrid connections. This phase included testing two different bolt diameters with several sheared edge distance values. In view of the experimental outcomes, the following observations and conclusions can be drawn:

- The presence of washers significantly enhanced the ductility and the load carrying capacity of the connections. Enhancements of 75% and 86% in the load capacity of the tested connections were obtained with the use of two and four washers-per-bolt, respectively, compared to those with no washers.

- The interfacial behavior of HFRP-steel connections fastened without washers differed from that observed for connections fastened with two and four washers-per-bolt. The observed softening post-peak response in the load-displacement curves of connections without washers indicated unfavorable performance of this type of connections when no washers are used.

- Connections with washers failed by a combination of failure modes including bearing at the bolt-HFRP interface, bending in the steel bolts, folding of the washers and finally tearing out and BSR in the HFRP laminates.

- The investigated clamping torque values ranging between 11 N.m. and 20 N.m. were proven to have negligible effect on the failure modes and load carrying capacity of the fastened HFRP-steel connections.

- Bolt-hole diameter significantly influenced the response of the tested connections. The use of a net fit bolt-hole reduced the connection ductility compared to standard and loose fit connections. Meanwhile, the ultimate load capacity of the tested connections was maintained unchanged regardless of the used bolt-hole diameter.

- For the considered range of bolts spacing (50 mm to 300 mm), negligible effect of spacing on the ultimate load capacity of the fastened HFRP-steel connections was observed. However, using spacing value that is twelve times the bolt-hole diameter showed best performance in terms of ductility with 10% higher displacement than other spacing values. It was also concluded that bolts' spacing had insignificant influence on the failure mechanisms of the connection.

- The influence of considered sheared edge distance on the response of HFRP-steel connections fastened with FRP anchors was negligible for both tested

diameters. This could be attributed to the fact that this particular type of connections failed by shear in the anchor before the contribution of the sheared edge distance becomes noticeable.

- The maximum recorded load capacity of all connections fastened using FRP anchors of 10 mm diameter corresponded to connections with sheared edge distance that is five times the hole-diameter.

- Using FRP anchors of 13 mm diameter with a sheared edge distance that is three times the hole-diameter enhanced the ductility of the fastened connections and resulted in the highest peak load (23 kN) among all tested sheared edge distances.

- Increasing the bolt diameter of the FRP anchors from 10 mm to 13 mm resulted in 65% increase in the ultimate load carrying capacity of the connection and enhanced its ductility.

- The load capacity of the HFRP-steel connection using a single FRP anchor of 13 mm diameter was almost equal to the one provided by a steel bolt of 6 mm diameter in a single shear setup.

- From economic standpoint, it is recommended to use steel bolts (0.22 $ per bolt) over the FRP anchors (7.6 $ per bolt) in fastening HFRP-steel connections. However, FRP anchors are expected to provide better corrosion resistivity than steel bolts.

Chapter 4: Finite Element Modeling of Fastened Hybrid FRP-Steel Connections

4.1 Introduction

The Finite Element Method (FEM) is a well-established numerical simulation technique that has been used by many researchers in different areas. It provides a risk-free approach to simulate the behavior of the connections considered in the current study. Although finite element modeling is used to evaluate the structural response, obtaining accurate predictions depends on the accuracy of the elements constituting the finite element model and the associated boundary conditions. In view of the experimental response curves presented in Chapter 3, it is clear that modeling the fastened HFRP-steel connections requires the introduction of an element that properly accounts for the interaction of the components at the HFRP-steel interface. The following sections describe in details the development of nonlinear load-slip models that can be used to simulate the interfacial behavior of the connections taking into consideration the interaction between the various failure modes that control the response of these connections. The proposed models also accounted for the fastener type (i.e., steel bolt of FRP anchor). The load-slip models were then incorporated in finite element models for the HFRP-steel connections tested in Chapter 3. The developed FE models of the connections were validated against the reported experimental results.

4.2 Finite Element Modeling of Connections with Steel Bolts

The proposed load-slip model is intended to simulate the interfacial behavior of the fastened HFRP-steel connections that are formed using steel bolts whose properties match those listed in section 3.2.3. The model was based on the

experimental load-displacement profile of W2_D8_ST connection shown in Fig. 3.25. This particular connection was chosen due to its optimal performance out of all other configurations tested in the experimental program. It should be noted that the response presented in Fig. 3.25 corresponded to two steel bolts bearing against two HFRP laminates. Thus, the average loads reported in this figure were divided by 4 to obtain reference values of one steel bolt bearing against one HFRP laminate (i.e., single-shear configuration). Furthermore, the experimental displacement values shown in the curve were corrected to exclude the influence of the steel and HFRP elongations during the test. Thus, the proposed load-slip model accounts for the various actions that take place at the steel-HFRP interface including relative slippage, bearing between the bolts and HFRP laminates, bending in the steel bolts, folding of washers and tear out of the HFRP laminates. The proposed nonlinear load-slip model is shown in Fig. 4.1, where the response curve is divided into six segments. Segment "A" relates mainly to the relative friction between the HFRP laminates and the steel plates. Part "B" of the curve represents the relative slippage between the HFRP and the steel plates due to the standard hole-size clearance. Segment "C" shows the effect of pure bearing between the bolts and the HFRP laminates. Meanwhile, part "D" demonstrates the combined effect of bearing, bending of the bolts and folding of the washers. The excessive bearing damage and initial tearing of the CFRP layers are represented by segment "E" of the curve. Finally, part "F" indicates the progressive tearing and associated BSR of the intact fibers that lead to complete failure of the connection.

The following section describes the main features of a nonlinear finite element model that was developed using the load-slip model. The accuracy of the proposed load-slip model in simulating the overall response of HFRP-steel

connections fastened with steel bolts was verified in section 4.2.2 based on comparing the numerical predictions to the experimental outcomes reported in Chapter 3. The validated finite element model was then used to simulate the behavior of the various spacing configurations in section 4.2.3.
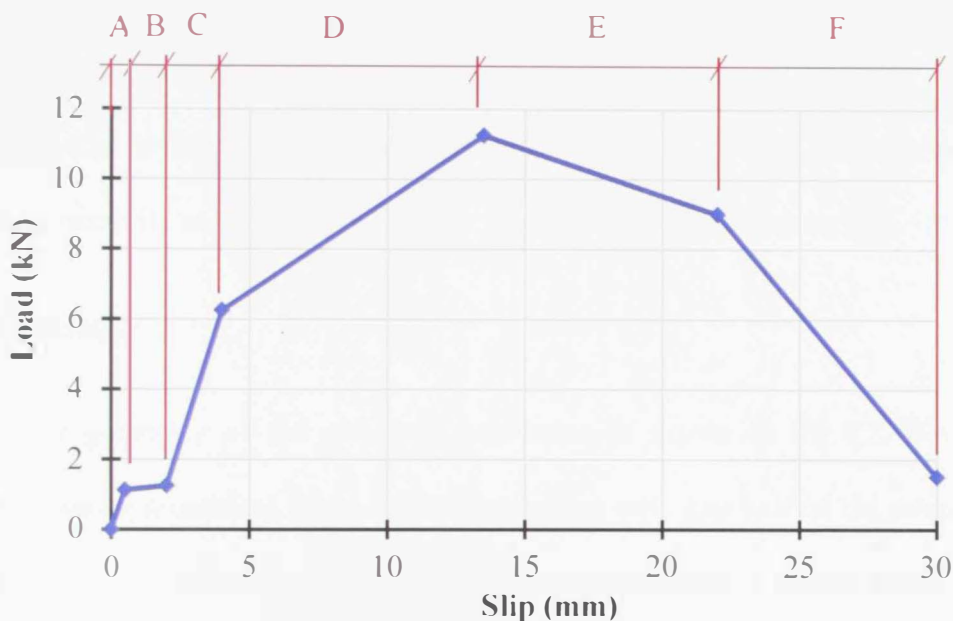
Figure 4.1: Nonlinear load-slip model of the W2_D8_ST connection

4.2.1 Description of the Finite Element Model

The general purpose finite element software package ANSYS (2009) was used to develop a three dimensional (3D) model to simulate the behavior of fastened HFRP-steel connections. The developed model took into consideration the relative slip at the HFRP-steel interface. It also accounted for both geometrical and material nonlinearities.

Geometries of the analyzed steel plates and HFRP laminates were modeled using the 8–node solid element (SOLID45), as denoted by ANSYS (2009). This element is suitable for modeling of solid structures incorporating plasticity, stress stiffening, large deflection and large strain capabilities. Meanwhile, the

unidirectional nonlinear spring element (COMBIN39) was used to model the HFRP-steel connectivity. The spring element was utilized to simulate the slip behavior at the HFRP-steel interface following the profile of the proposed load-slip model (Fig. 4.1). The spring element was used to connect two coincident node points: one of them was located on the surface of the steel plate and the other was placed on the opposite surface of the HFRP laminate. The direction of the COMBIN39 element can be selected to follow any of the three basic directions: X, Y or Z to simulate the spatial connectivity conditions between the components of the connection.

Model Geometry

The geometry of the modeled connection is shown in Fig.4.2. Since the geometry was symmetrical about the loading plane, only one half of the connection was modeled. Therefore, one HFRP laminate was considered in the FE model along with half the thickness of the steel plates. The geometry was defined using a global Cartesian coordinate system with its origin located at the mid width of the left-end of the outer surface of the clamped steel plate as presented in Fig.4.2. The longitudinal direction of the connection was directed along the X-axis, the width was parallel to the Y-axis, while the elements' thicknesses were along the Z-axis. The main geometrical parameters of the connection are its width (W), length of HFRP laminate (L_{HFRP}), length of steel plates ($L_{clamped}$) and (L_{loaded}), HFRP thickness (t_{HFRP}) and steel thickness (t_{steel}). The double node technique was used to model the interface between the steel and HFRP elements, by connecting each interface node (at the bolts' locations) on the surface of the steel plate to its counterpart node on the HFRP surface as presented in Fig.4.3. Each pair of conjugate nodes was connected using a nonlinear spring element (COMBIN39) directed along the X-direction (loading

direction). Full compatibility was implemented along the Y and Z-directions of the interface nodes. This assumption was justified due to the restrictions imposed by the clamping forces in the Z-direction and the fact that no loading was applied along the Y-direction.
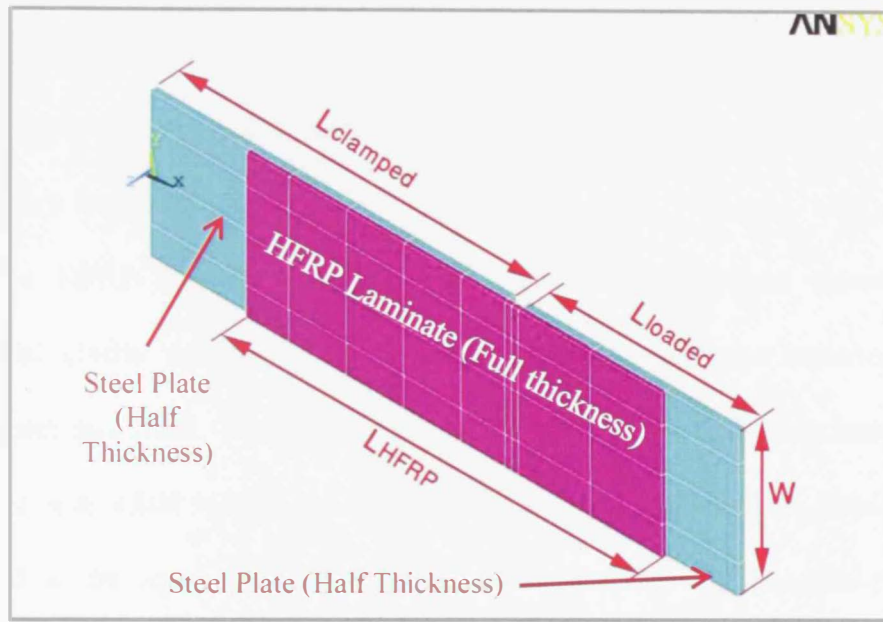
Figure 4.2: General geometry of half model of the W2_D8_ST connection
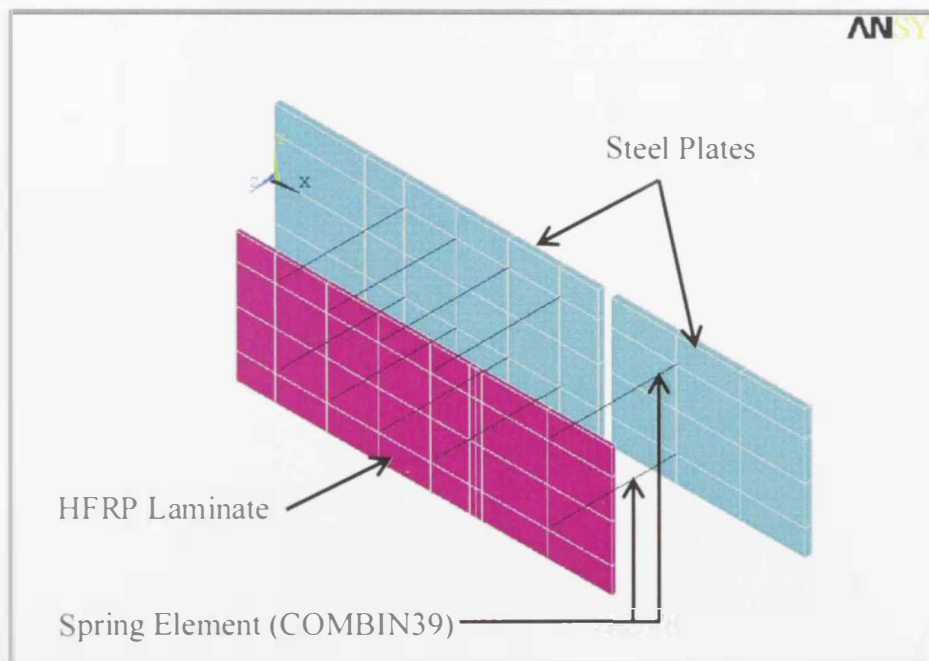
Figure 4.3: Locations of the steel bolts' springs in the modeled W2_D8_ST connection (Spacing between steel and HFRP is exaggerated for clarity of the presentation)

Material Modeling

The steel material is known to exhibit an elasto-plastic stress-strain relationship. Figure 4.4 shows the idealized multi-linear stress-strain relationship proposed by Salmon et al. (2009). This material model was adopted in the current study with the steel's elastic Young's modulus E (200,000 MPa), tangential modulus $E_t = 2\% \, E$ (4000 MPa), yield stress σ_y (300 MPa) and ultimate stress σ_u (460 MPa) and Poisson's ratio v of 0.3.

The HFRP laminates were modeled as a linear elastic material. The longitudinal elastic modulus E_x was taken as 62,190 MPa as reported in the manufacturer data sheet. The transverse elastic moduli of the HFRP laminates E_y and E_z were taken as 4,800 MPa (Kachlakev, 1998). Poisson's ratios v_{yz}, v_{zx} and v_{yx} were considered to be equal to 0.30, 0.22 and 0.22, respectively (Kachlakev, 1998, Kachlakev and McCurry, 2000).
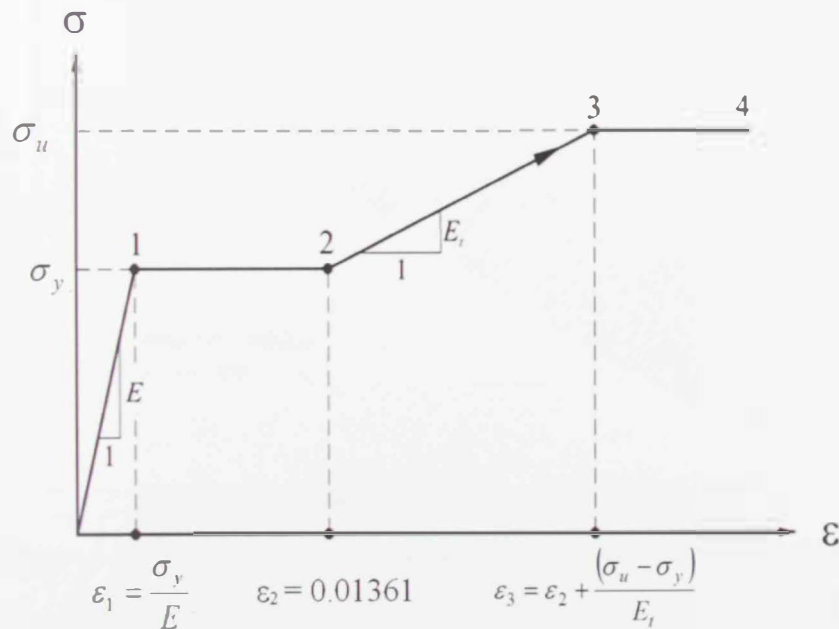
Figure 4.4: Idealized stress-strain relationship for modeling of steel material

Boundary Conditions and Loading System

Clamped boundary conditions were imposed along the exterior edge of the clamped steel plate which was connected to the fixed machine head during the experimental testing. The clamping conditions were attained through restraining all degrees of freedom, U_x, U_y and U_z at all nodal points located at the clamped edge as shown in Fig.4.5. Furthermore, symmetry boundary conditions were achieved by preventing out-of-plane translation, U_z, for all points on the steel surface perpendicular to the plane of symmetry as displayed in Fig. 4.6. All other nodes of the model were left unrestrained against any kind of translation. The numerical analysis was conducted in a displacement-controlled manner along the X-direction.
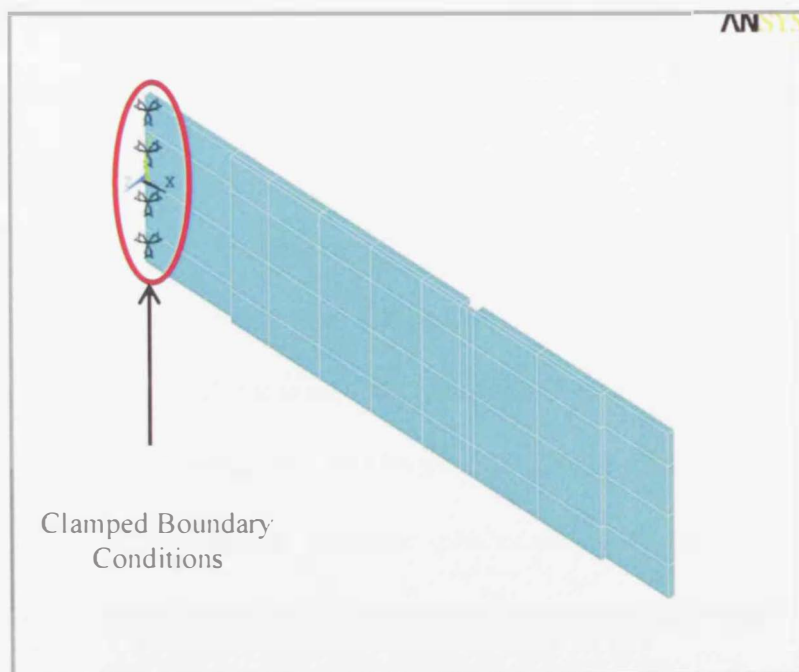
Figure 4.5: Clamping restrains at the edge of the clamped steel plate
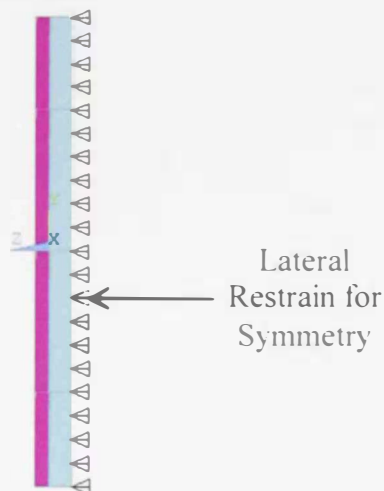
Figure 4.6: Symmetry boundary conditions for restraining lateral movement

4.2.2 Verification of the Finite Element Model

The developed FE model was used to simulate the behavior of the tested FHRP-steel connection fastened with steel bolts as described in section 4.2.1. The characteristics of the proposed spring system that simulates the stiffness of the steel bolts in responding to the applied load were adopted based on the nonlinear load-slip model shown in Fig 4.1.

Figure 4.7 shows a comparison between the experimental and numerical load-displacement response curves of the modeled W2_D8_ST connection. By examining these curves, excellent match between the experimental behavior and the numerically modeled predictions can be observed. It can be seen that the developed finite element model resulted in accurate predictions for the response of the connection through its various stages. Furthermore, comparing the experimental peak load value (45.5 kN) with that predicted by the FE model (42.5 kN) reveals a very good agreement with an error of 6.6%.
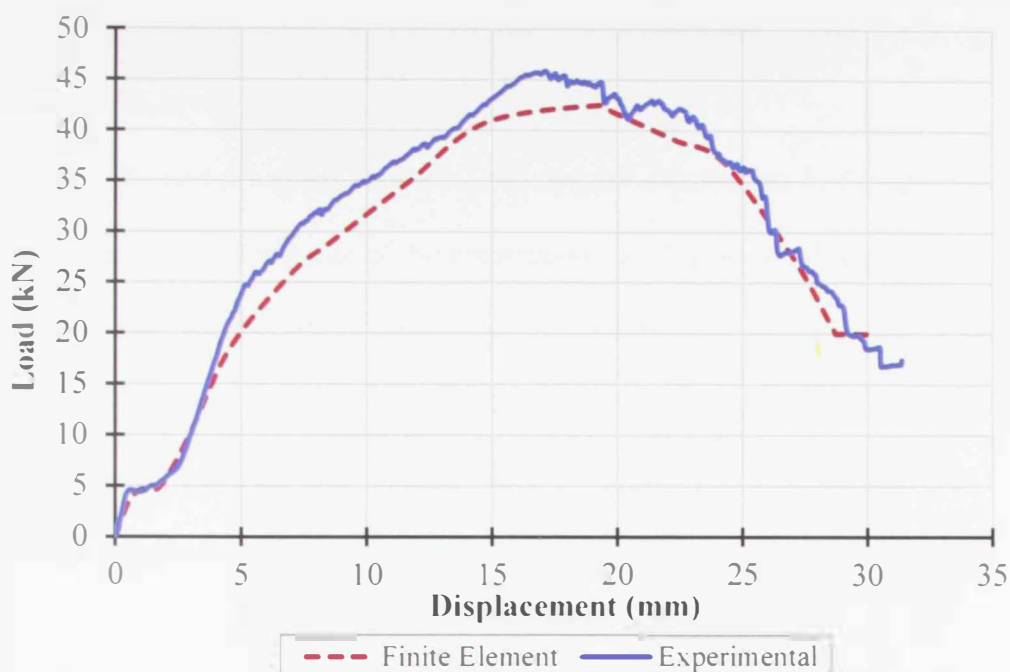
Figure 4.7: Experimental and numerical response curves for the W2_D8_ST modeled connection

The numerical predictions of the strains induced in the HFRP laminates were also used to validate the accuracy of the developed FE model and the proposed load-slip model. It is worth mentioning that the experimental phase involved measuring the longitudinal strains in the HFRP laminates at both front and back sides of the connection as shown in Fig. 3.14. Strain gauges at both sides showed similar readings as they were used to verify the negligible effect of the out-of-plan bending on the tested connections. Figure 4.8 shows the strain gauge measurements for the Front SG of W2_D8_ST_2 connection as a representative sample of the experimental results. The strain predictions, based on FE results, at the location of the Front SG are also plotted on the same strain-displacement curve. It can be noted that the trend and values of the experimental and numerical strain-displacement curves are in excellent match. The experimental and numerical load-strain curves of the same strain gauge are shown in Fig. 4.9. Plotted numerical predictions confirm

the good agreement with the experimental measurements which validates the accuracy of the developed FE model.

The FE model was also used to evaluate the distribution of the applied loads on both bolts at the loaded side of the connection (see Fig. 4.10). The predicted loads carried by each of the steel bolts in the modeled W2_D8_ST connection are displayed in Fig. 4.11. In this figure. "RB" denotes the right-sided bolt and "LB" indicates the left-sided bolt. Plotted results imply that the applied load was distributed equally between the two bolts.
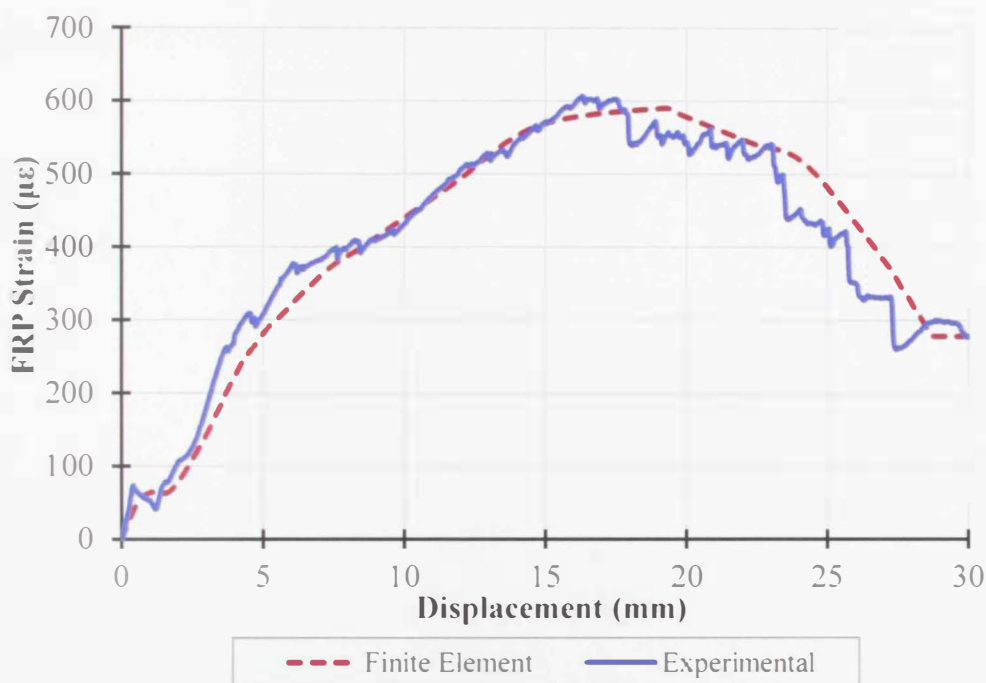
Figure 4.8: Experimental and numerical strain-displacement curves for W2_D8_ST_2 connection at the Front SG location
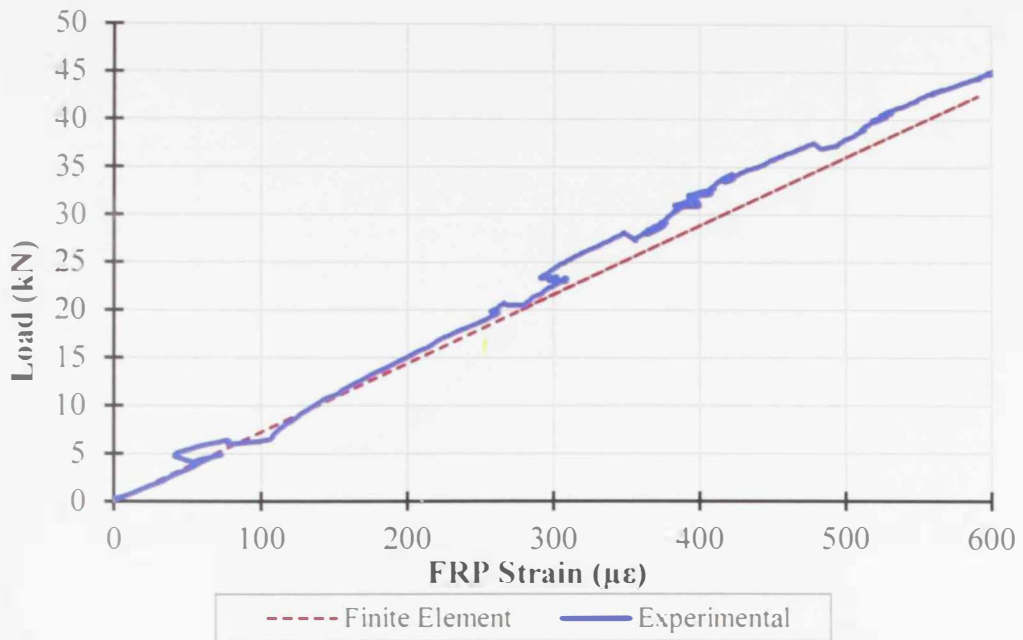
Figure 4.9: Experimental and numerical load-strain curves for W2_D8_ST_2
connection at the Front SG location

Figure 4.10: Typical locations of steel bolts in the experimental setup of the
tested W2_D8_ST connection
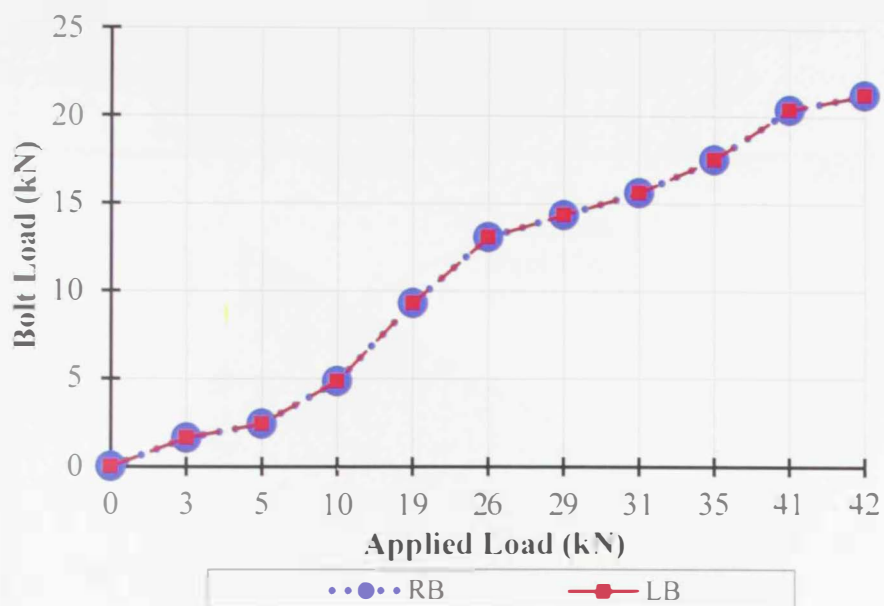
Figure 4.11: Distribution of the applied loads on the bolts of the
modeled connection

4.2.3 Application of the FE Model on Spacing Connections

The proposed load-slip model for the steel bolts shown in Fig. 4.1 was used

to predict the behavior of HFRP-steel connections with three bolts. The model was

employed to define the spring parameters when modeling the tested connections with

nine different bolt-spacing configurations. The distribution of the bolts in a typical

spacing connection is presented in Fig. 4.12. Similar boundary conditions to those

described in section 4.2.1 were imposed on the modeled connections to simulate the

real behavior during testing. Predicted results revealed a very good agreement

between the experimental and numerical load-displacement response curves of the

nine modeled connections as illustrated in Fig. 4.13 through Fig. 4.21. In terms of

peak loads, results indicated comparative values with a percentage of difference that

ranged from 0.02% to 7.01% as summarized in Table 4.1. The predicted peak loads

of the different spacing configurations confirmed the insignificant effect of bolt-

spacing on the ultimate load carrying capacity of the HFRP-steel connections as observed in the experimental testing and discussed in Chapter 3.
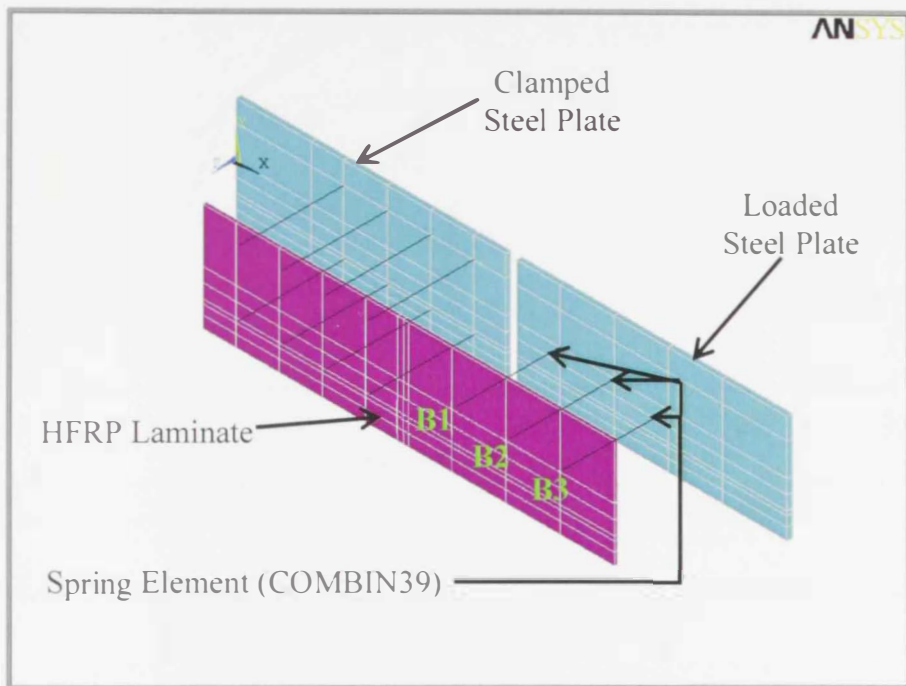
Figure 4.12: Typical locations of the springs to represent steel bolts in the modeled spacing connections (Spacing between steel and HFRP is exaggerated for clarity of the presentation)
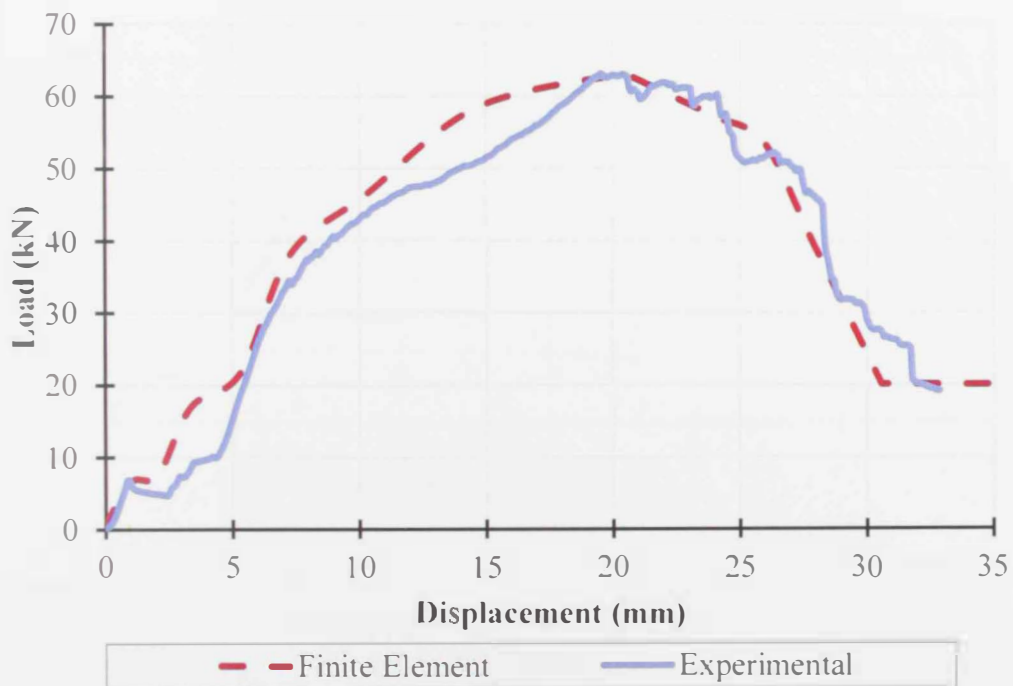
Figure 4.13: Experimental and numerical load-displacement response curves for S_6D connection
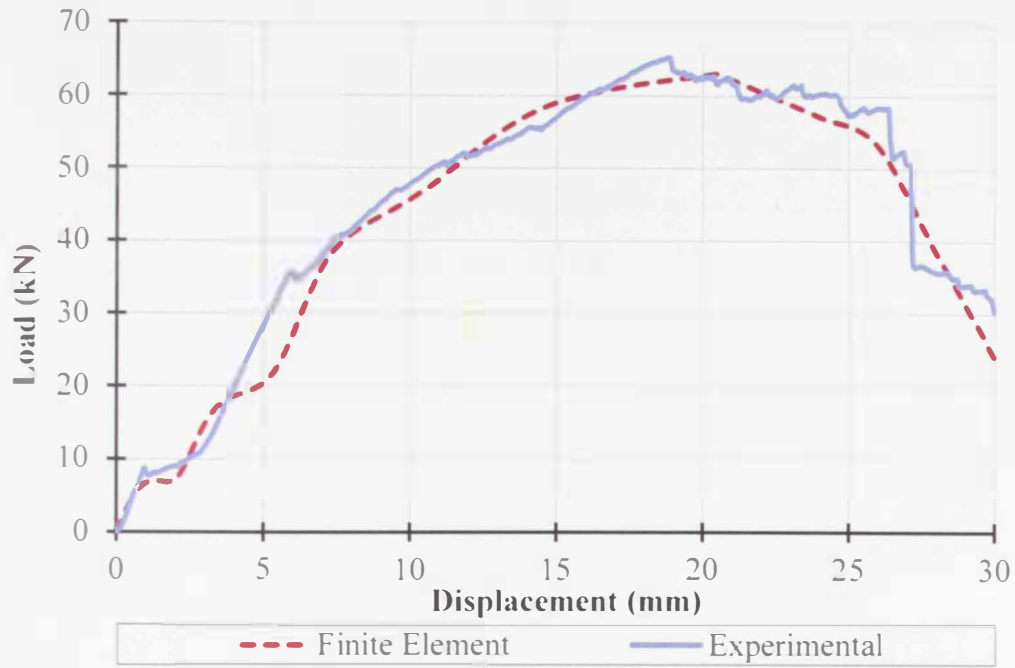
Figure 4.14: Experimental and numerical load-displacement response curves for S_9D connection
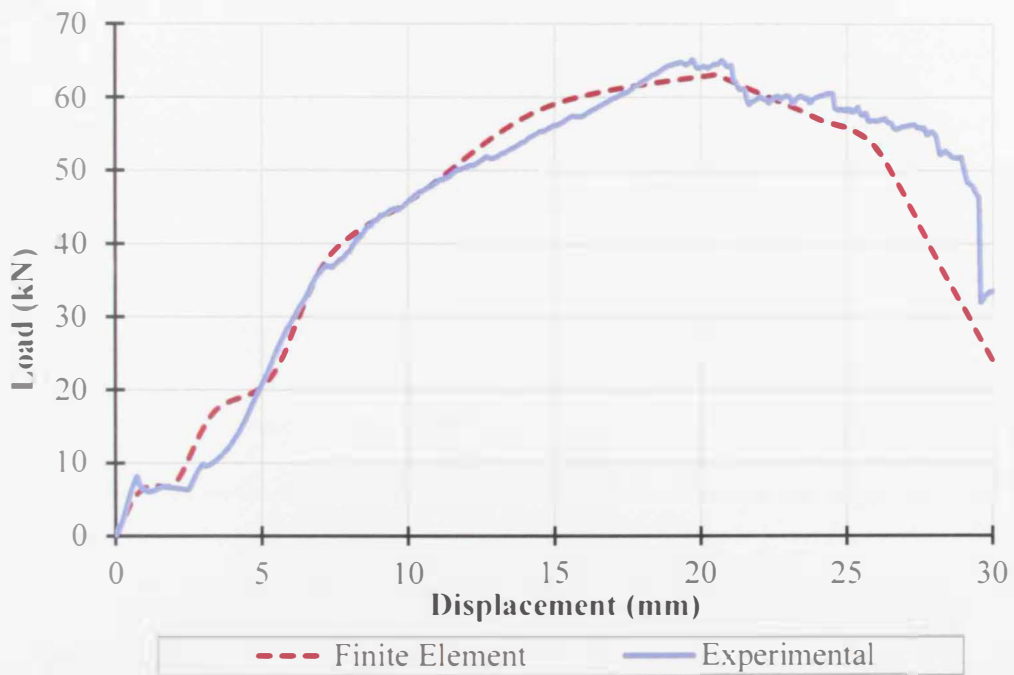
Figure 4.15: Experimental and numerical load-displacement response curves for S_12D connection
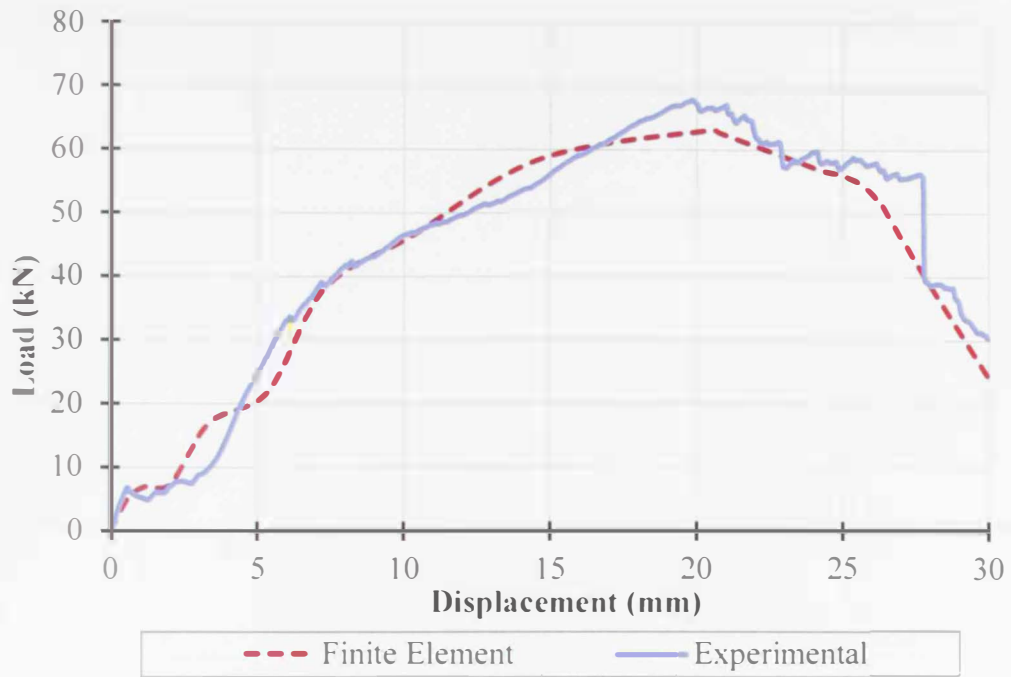
Figure 4.16: Experimental and numerical load-displacement response curves for S_15D connection
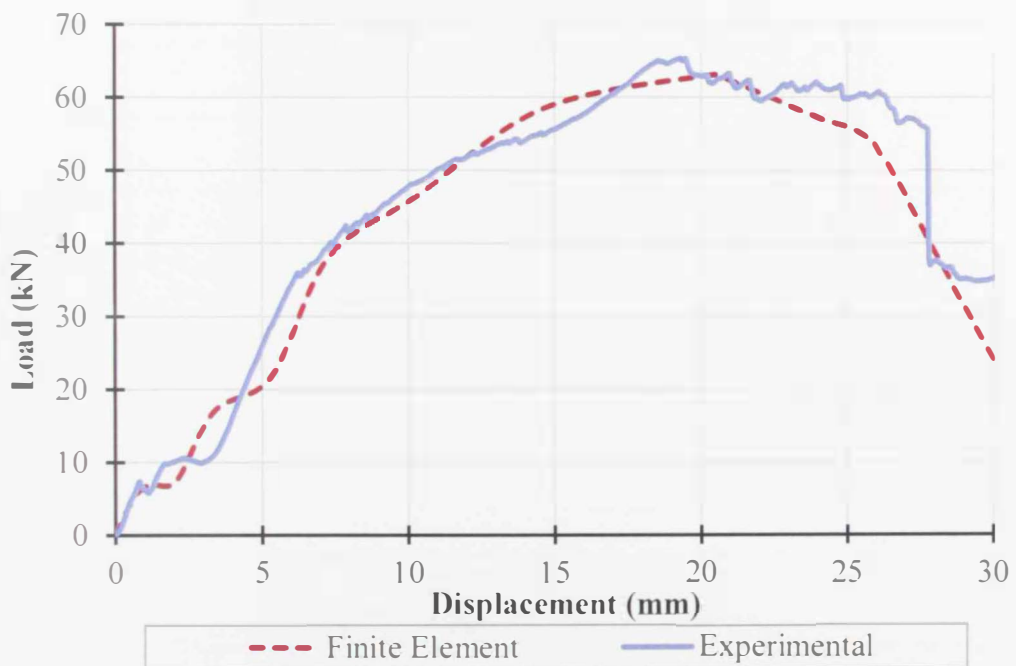
Figure 4.17: Experimental and numerical load-displacement response curves for S_18D connection
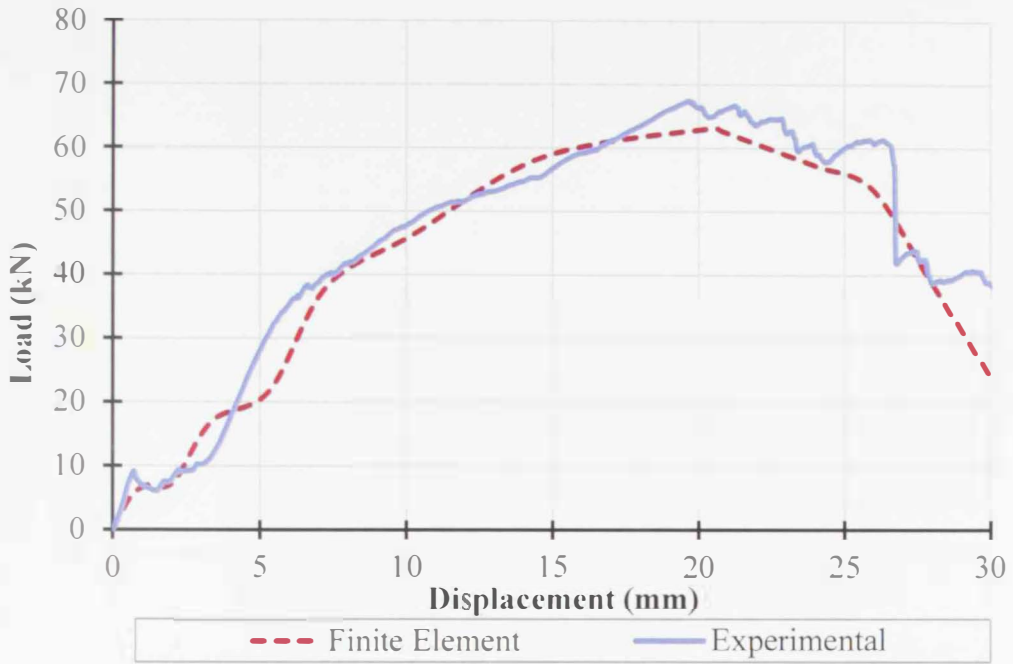
Figure 4.18: Experimental and numerical load-displacement response curves for S_21D connection
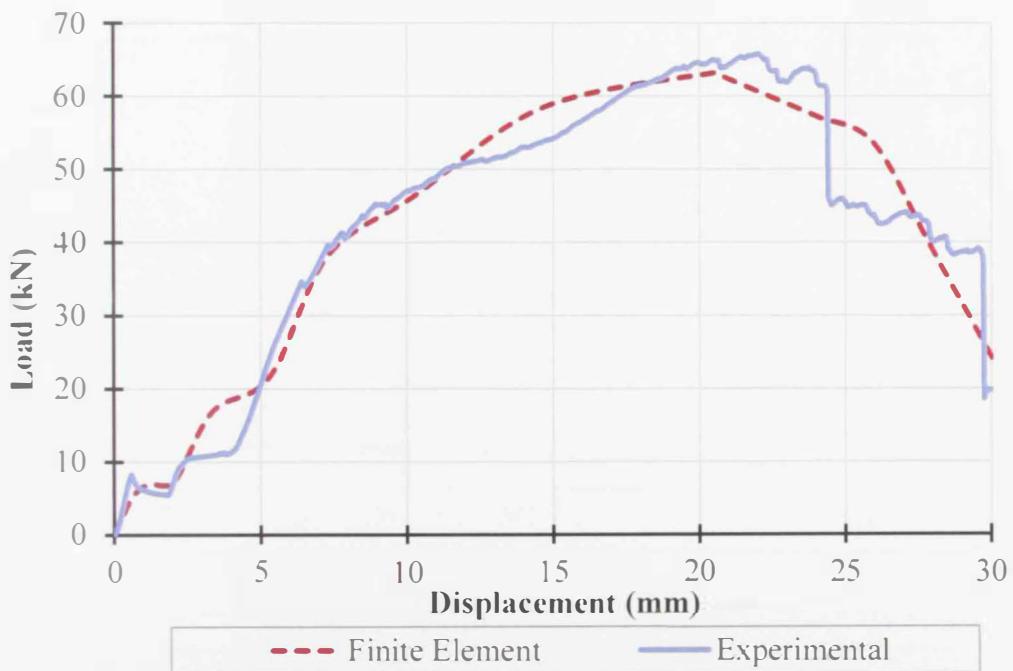
Figure 4.19: Experimental and numerical load-displacement response curves for S_25D connection
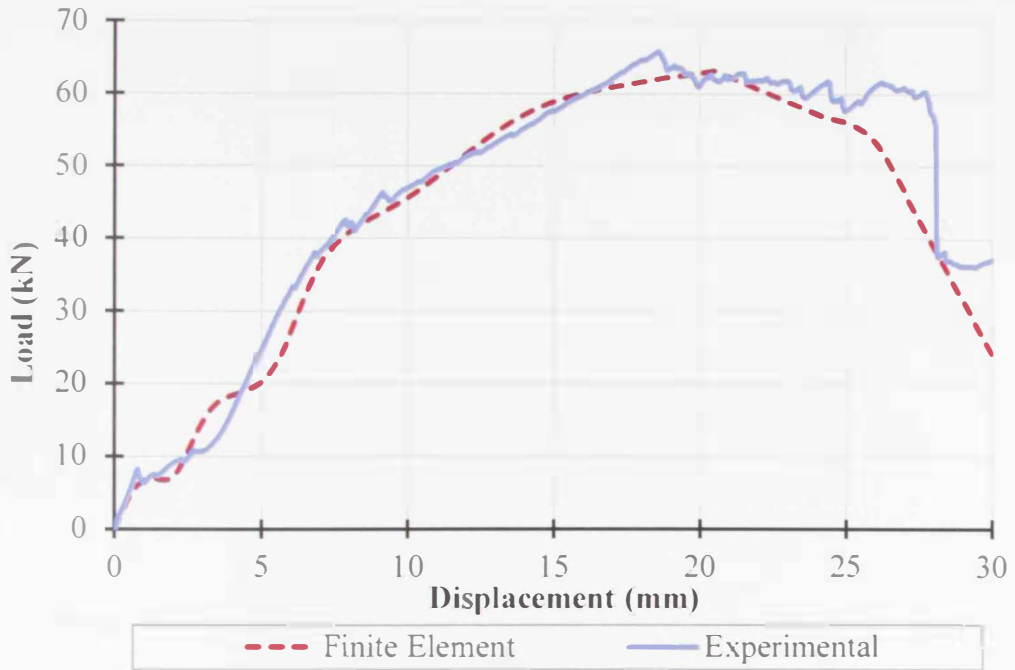
Figure 4.20: Experimental and numerical load-displacement response curves for S_31D connection
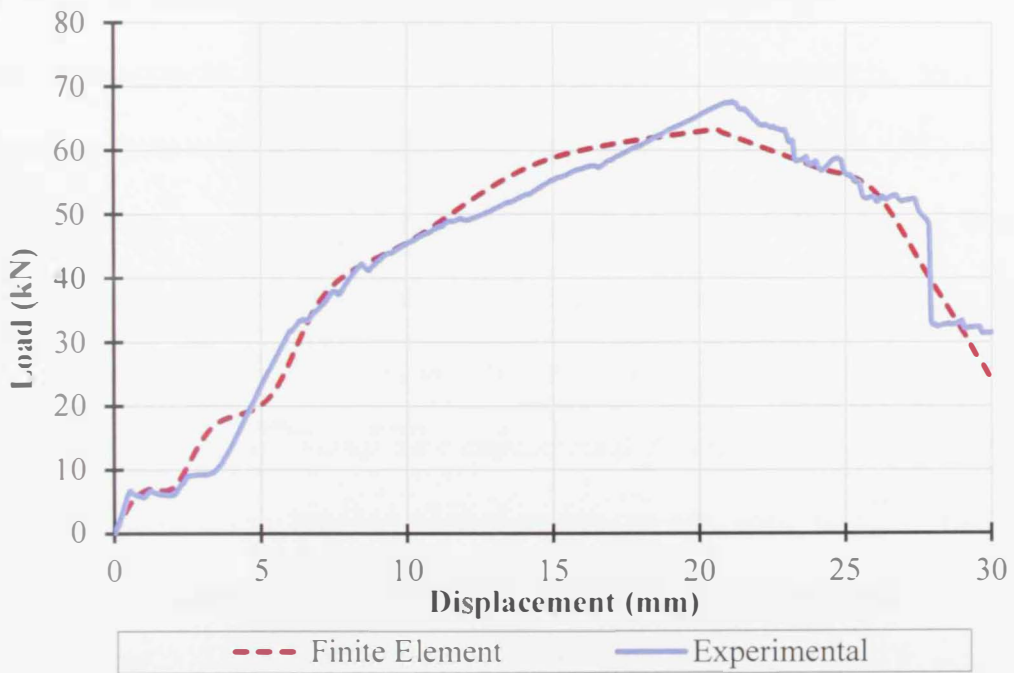
Figure 4.21: Experimental and numerical load-displacement response curves for S_37D connection

Table 4.1: Experimental and numerical peak loads for the spacing connections

Connection Designation	Peak Load (kN)		% Difference
	Experimental	Numerical	
S_6D	63.142	63.128	0.02
S_9D	65.327	63.105	3.40
S_12D	63.753	63.101	1.02
S_15D	67.863	63.108	7.01
S_18D	65.287	63.119	3.32
S_21D	67.399	63.133	6.33
S_25D	65.742	63.171	3.91
S_31D	65.863	63.206	4.03
S_37D	67.621	63.269	6.44

Strain values were also evaluated in the HFRP laminates of all modeled spacing connections configurations in order to verify the FE model accuracy. It's worth noting that the experimental setup of the spacing connections involved the use of eight strain gauges per specimen which were distributed as displayed in Fig. 3.51. The predicted strain values at the eight locations were compared to the experimental strain measurements for each spacing configuration. Unfortunately, some strain gauge measurements for connections with small spacing (S-6D to S_15D) were not reliable due to the observed damage in the strain gauges placed at or near the centerline of the connection as presented in Fig. 4.22. Records of these strain gauges were not shown to avoid confusion. Numerical strain predictions for the modeled connections were plotted versus their experimental counterparts in Fig. 4.23 through Fig. 4.31. Comparison between plotted results reveals good match between the measured and predicted strain values for almost all the modeled connections.

Figure 4.22: Photo of the damaged strain gauges in S_6D connection between "B2" and "B3"

(b) : SG3

(a) : SG4

(c) : SG7

(d) : SG8

- - - - - Finite Element　———— Experimental
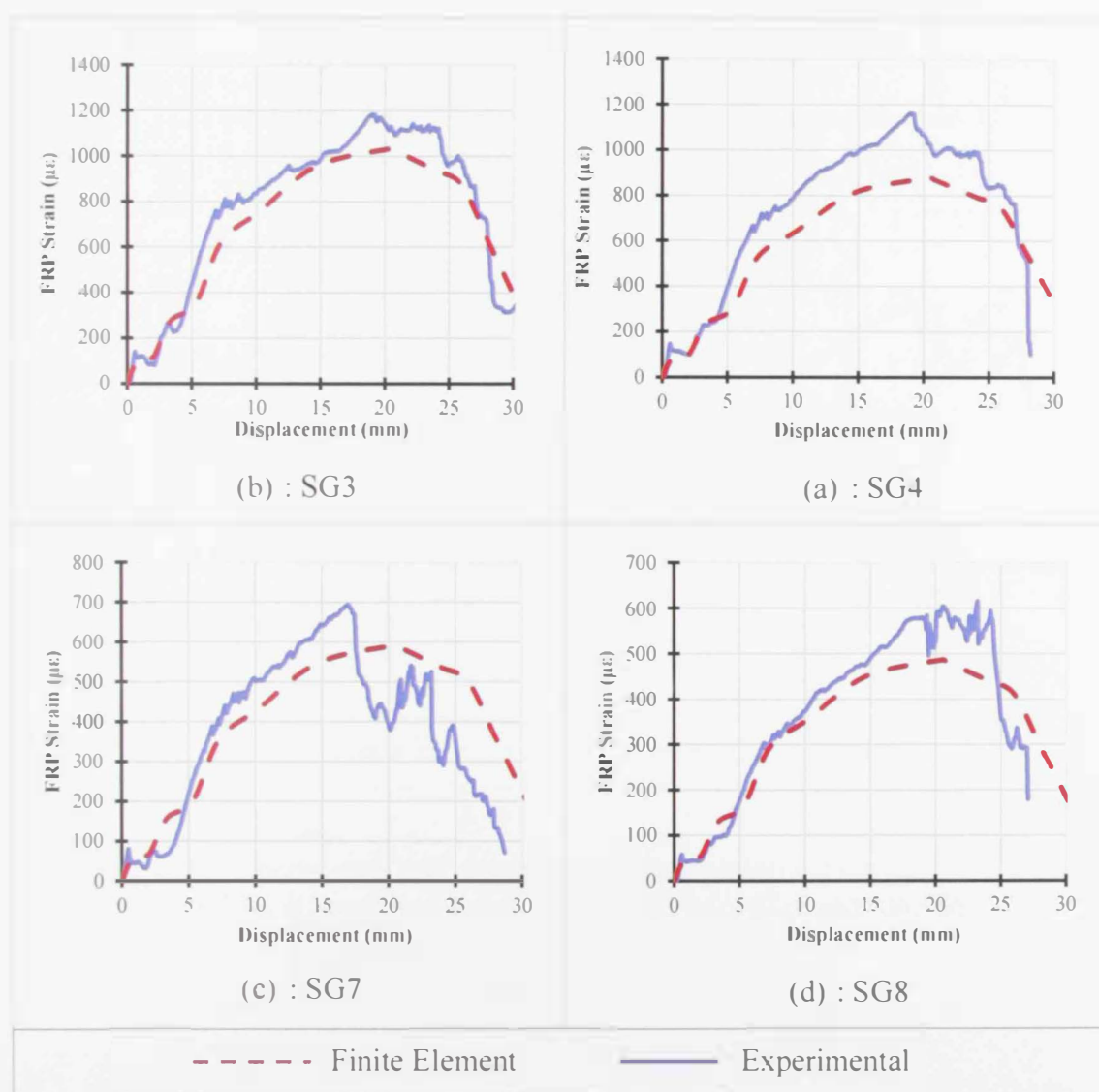
Figure 4.23: Experimental and numerical strain-displacement curves for S_6D connection at locations of: (a) SG3, (b) SG4, (c) SG7 and (d) SG8
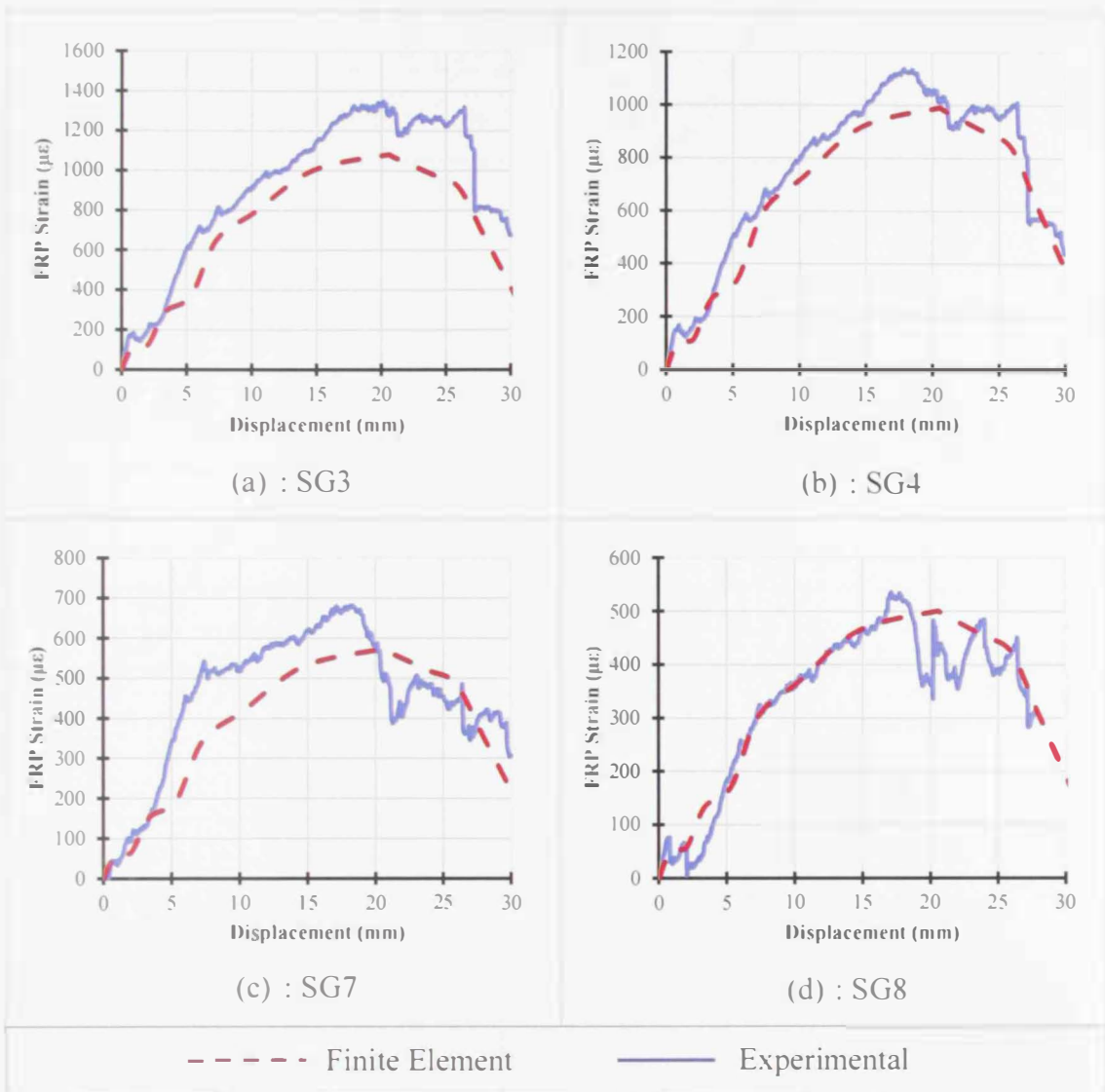
Figure 4.24: Experimental and numerical strain-displacement curves for S_9D connection at locations of: (a) SG3, (b) SG4, (c) SG7 and (d) SG8
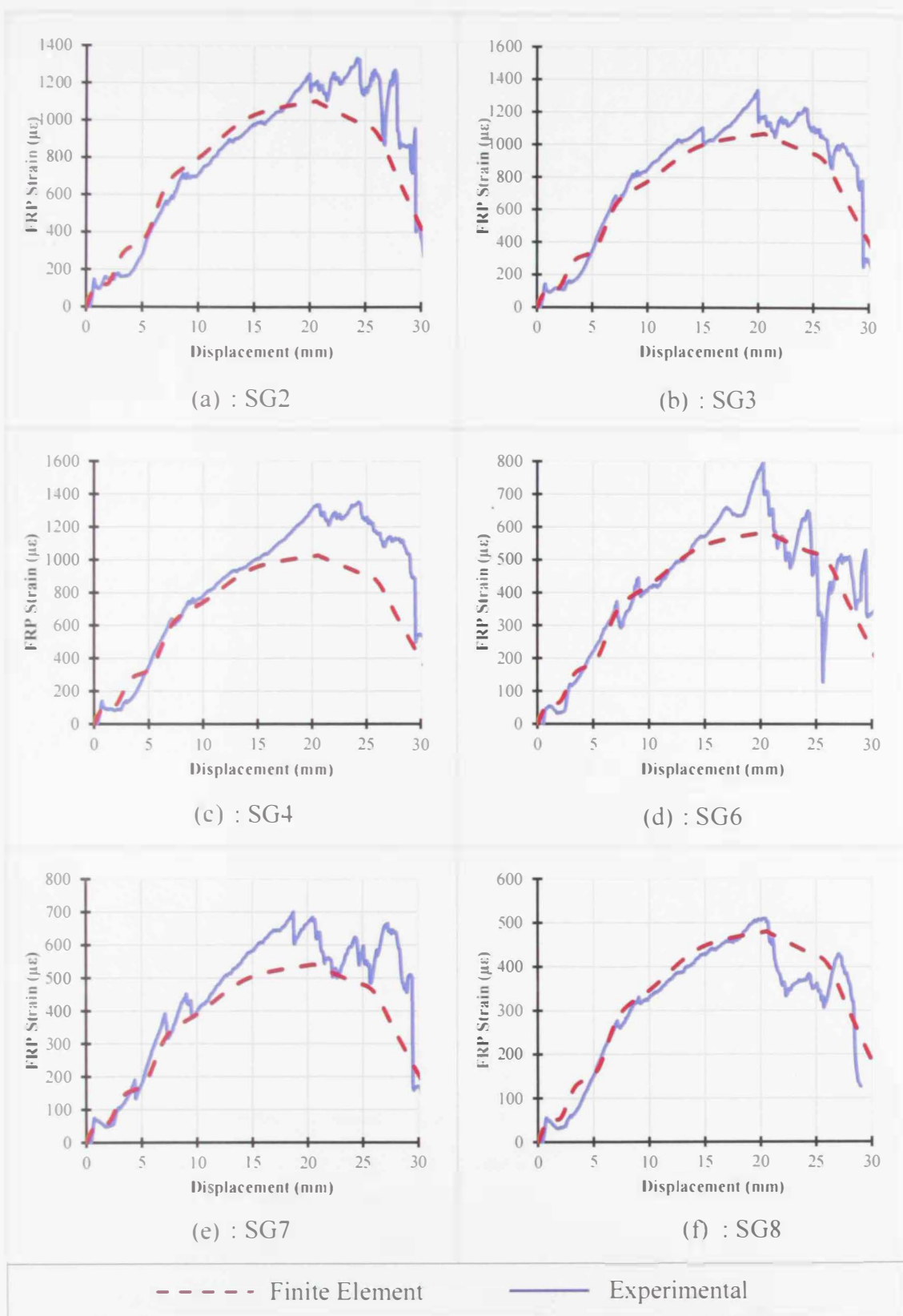
Figure 4.25: Experimental and numerical strain-displacement curves for S_12D connection at locations of: (a) SG2, (b) SG3, (c) SG4, (d) SG6, (e) SG7 and (f) SG8
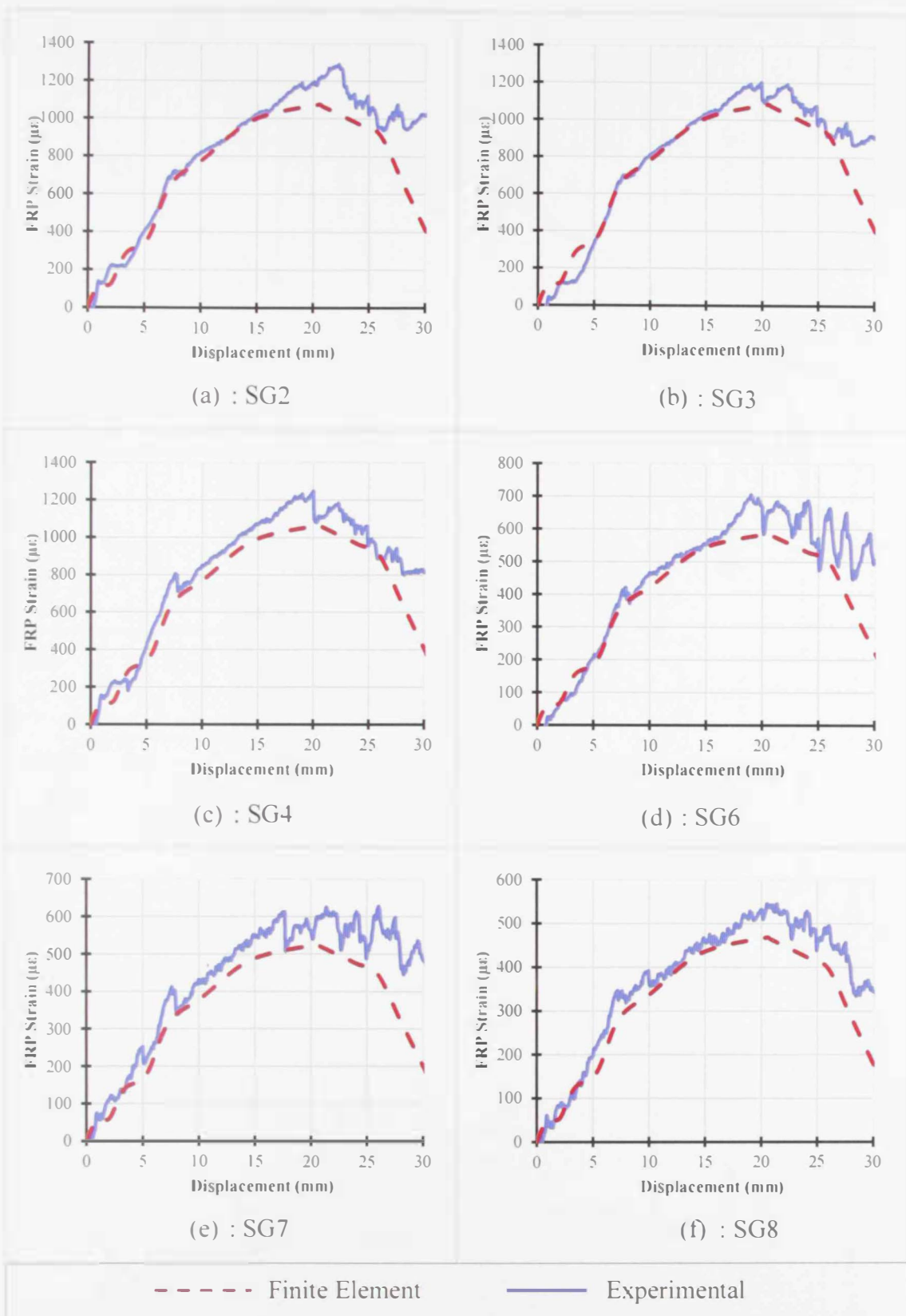
Figure 4.26: Experimental and numerical strain-displacement curves for S_15D connection at locations of: (a) SG2, (b) SG3, (c) SG4, (d) SG6, (e) SG7 and (f) SG8
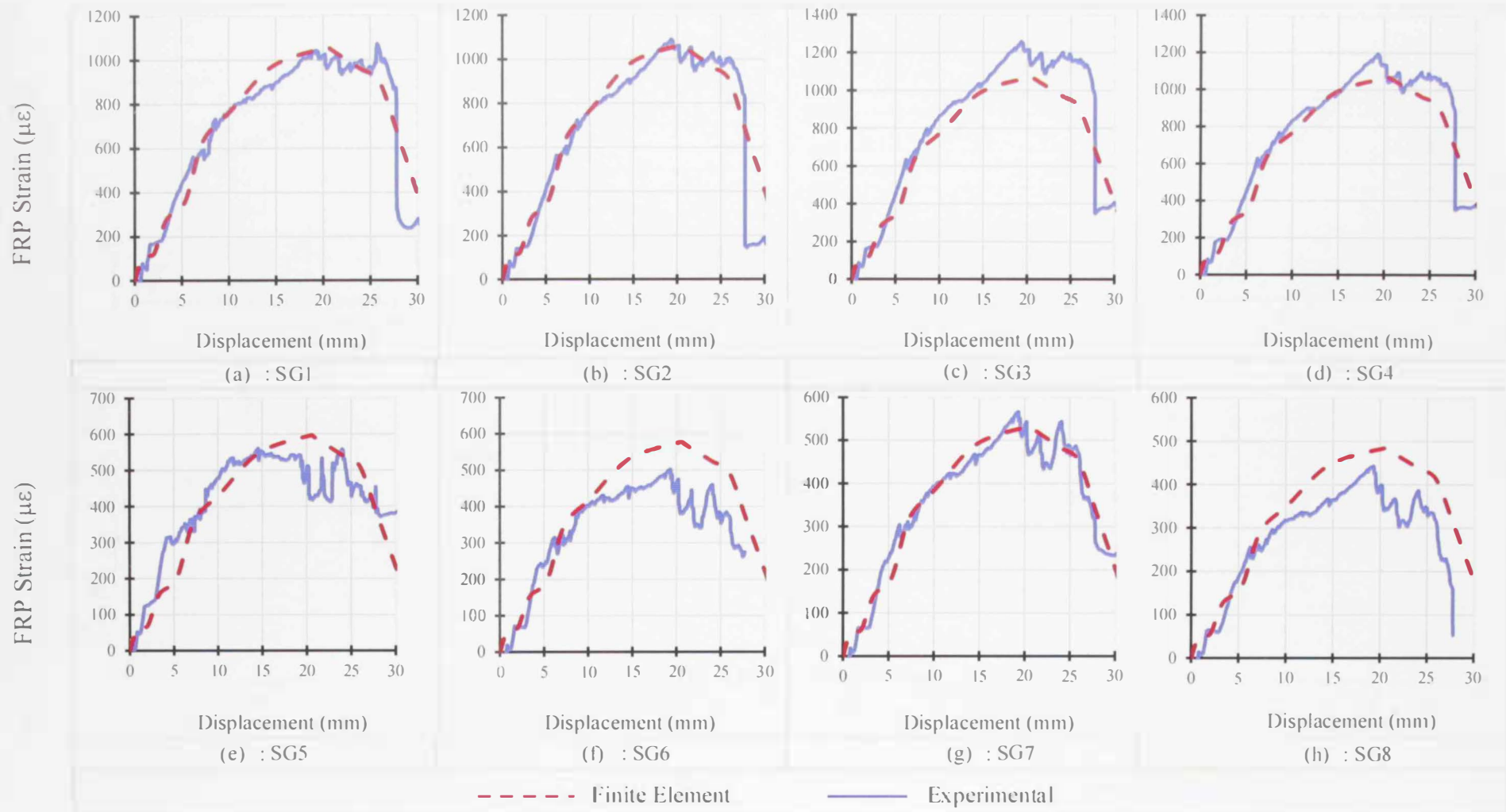
Figure 4.27: Experimental and numerical strain-displacement curves for S_18D connection at locations of: (a) SG1, (b) SG2, (c) SG3, (d) SG4, (e) SG5, (f) SG6, (g) SG7 and (h) SG8
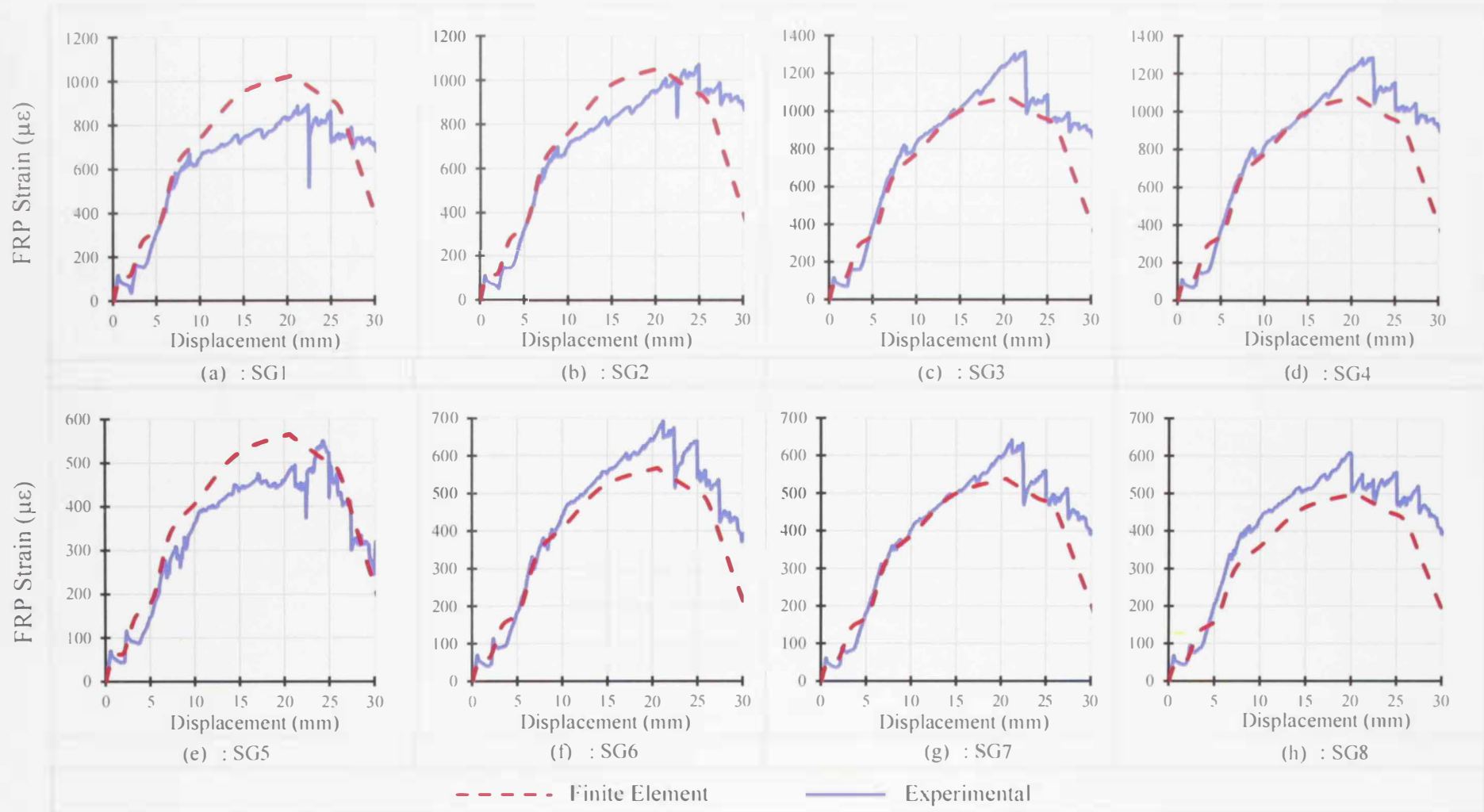
Figure 4.28: Experimental and numerical strain-displacement curves for S_21D connection at locations of: (a) SG1, (b) SG2, (c) SG3, (d) SG4, (e) SG5, (f) SG6, (g) SG7 and (h) SG8
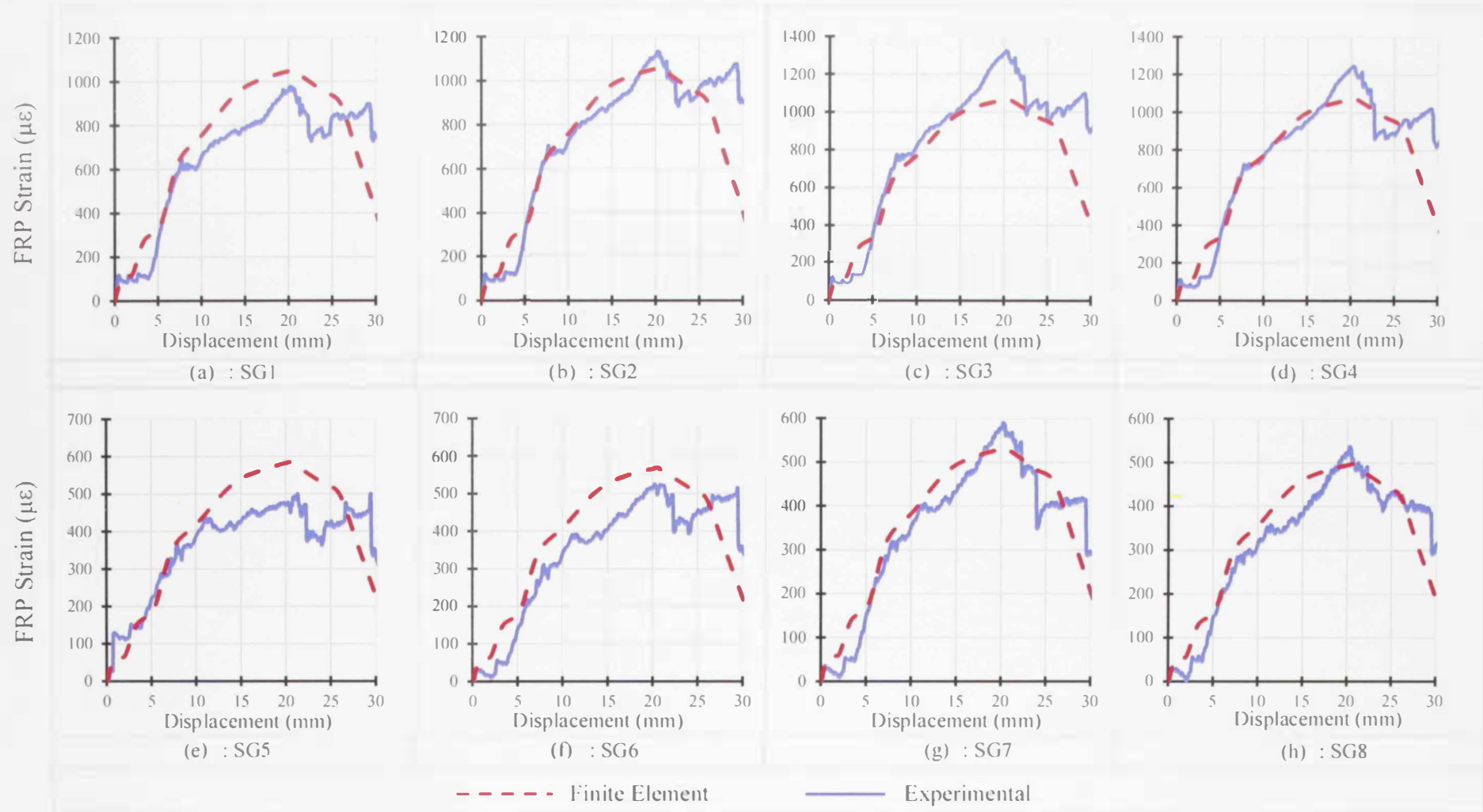
Figure 4.29: Experimental and numerical strain-displacement curves for S_25D connection at locations of: (a) SG1, (b) SG2, (c) SG3, (d) SG4, (e) SG5, (f) SG6, (g) SG7 and (h) SG8
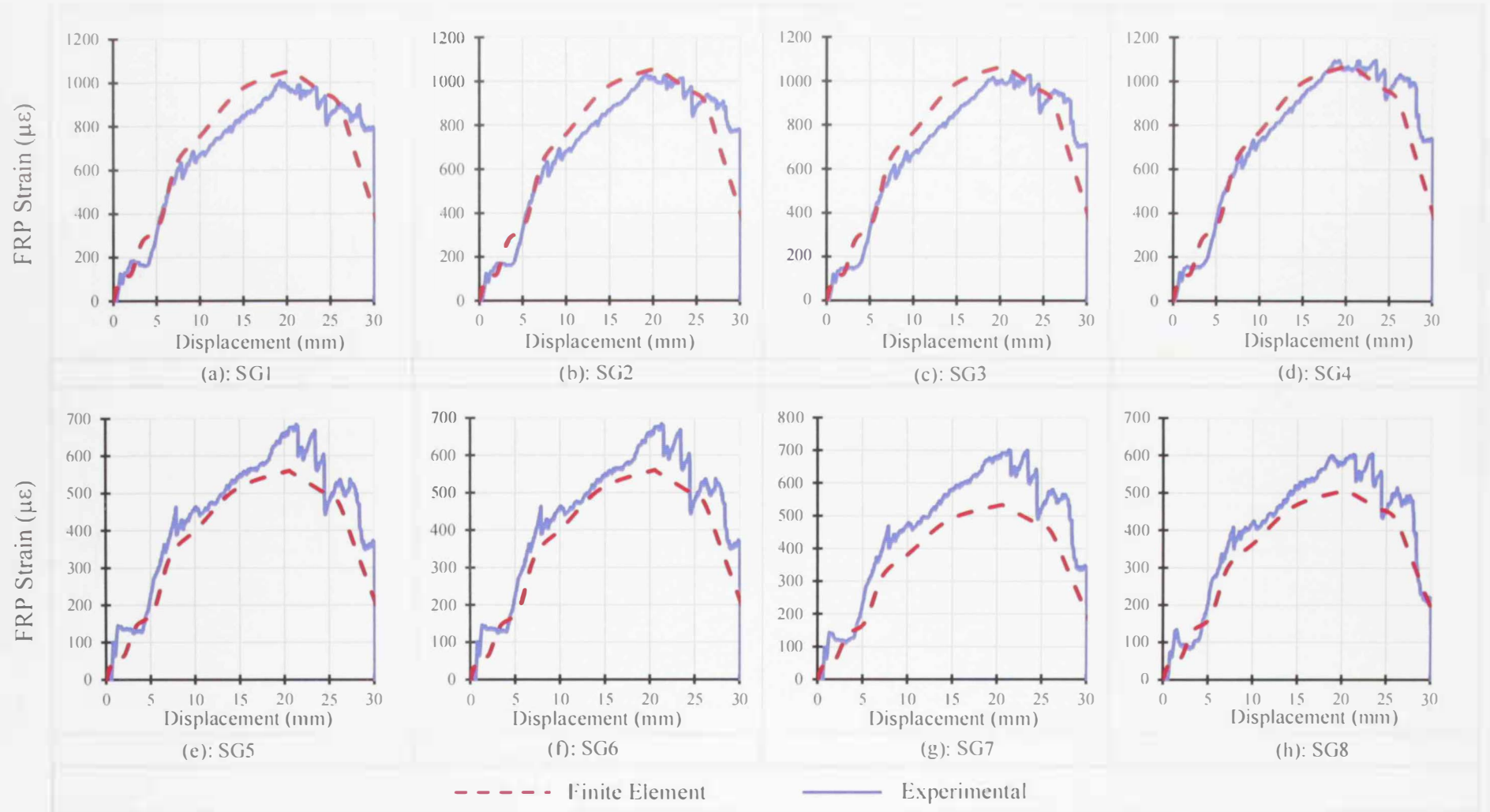
Figure 4.30: Experimental and numerical strain-displacement curves for S_31D connection at locations of: (a) SG1, (b) SG2, (c) SG3, (d) SG4, (e) SG5, (f) SG6, (g) SG7 and (h) SG8
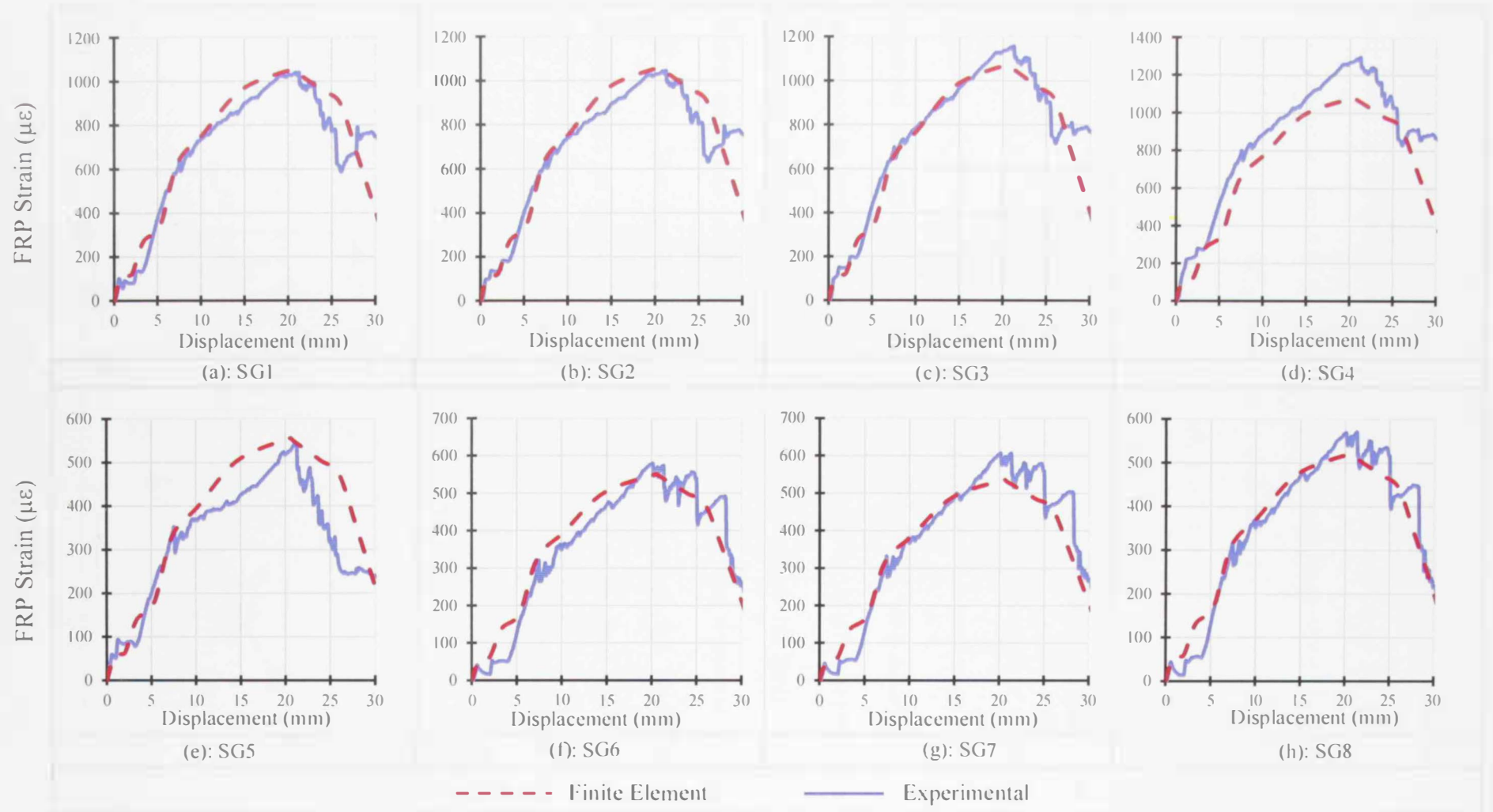
Figure 4.31: Experimental and numerical strain-displacement curves for S_37D connection at locations of: (a) SG1, (b) SG2, (c) SG3, (d) SG4, (e) SG5, (f) SG6, (g) SG7 and (h) SG8

Loads carried by each of the three bolts connecting the HFRP to the loaded steel plates in the spacing assemblies were also evaluated by the FE model. Figure 4.32 displays a sample of the numerically predicted loads carried by "B1", "B2" and "B3" of the S_12D configuration. It is clear that the load is equally distributed amongst the three connecting bolts. Each predicted bolt load was compared to its corresponding experimental value that was evaluated in section 3.3.2 of Chapter 3. Comparisons between numerically assessed bolt loads and their experimental counterparts are shown in Figs. 4.33 and 4.34 for representative configurations of S_12D and S_37D, respectively. These figures reveal a perfect match between the numerical and experimental results up to an applied load of 36 kN. This limit corresponds to the end of stage "C" of the load-slip curve (Fig. 4.1) before which the response is mainly controlled by bearing action. Beyond this limit, bending in bolts starts to take place and the applied load is distributed in an uneven fashion among the three bolts. The developed FE model underestimated the loads for "B1" and overestimated the loads of both "B2" and "B3". Similar trend was observed for all other tested configurations. This is because this simple modeling of the bolt as nonlinear spring is not capable of simulating the exact behavior of the plate with multiple holes on the same gaugline. In the experimental setup, the first bolt typically carries more load than the other ones.
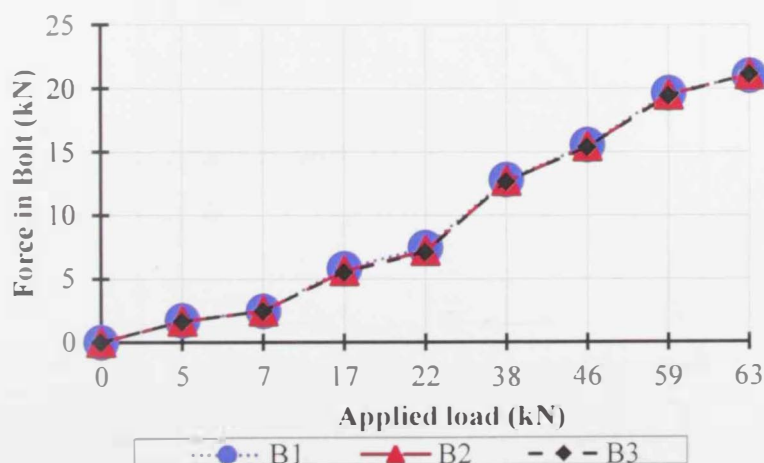
Figure 4.32: Distribution of the applied loads on the bolts of the S_12D connection
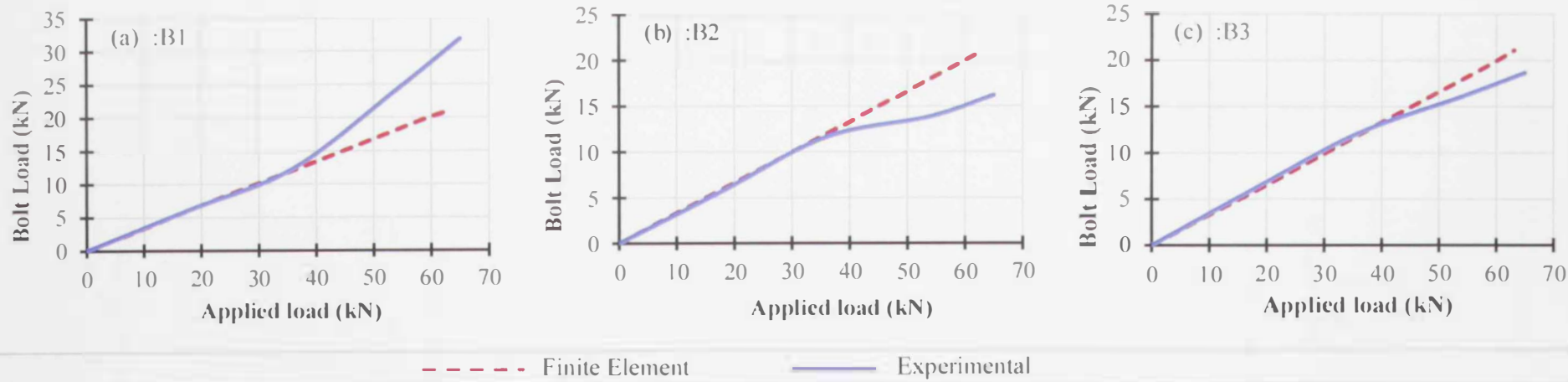
Figure 4.33: Experimental and numerical bolt load-applied load curves of S_12D for: (a) B1, (b) B2 and (c) B3
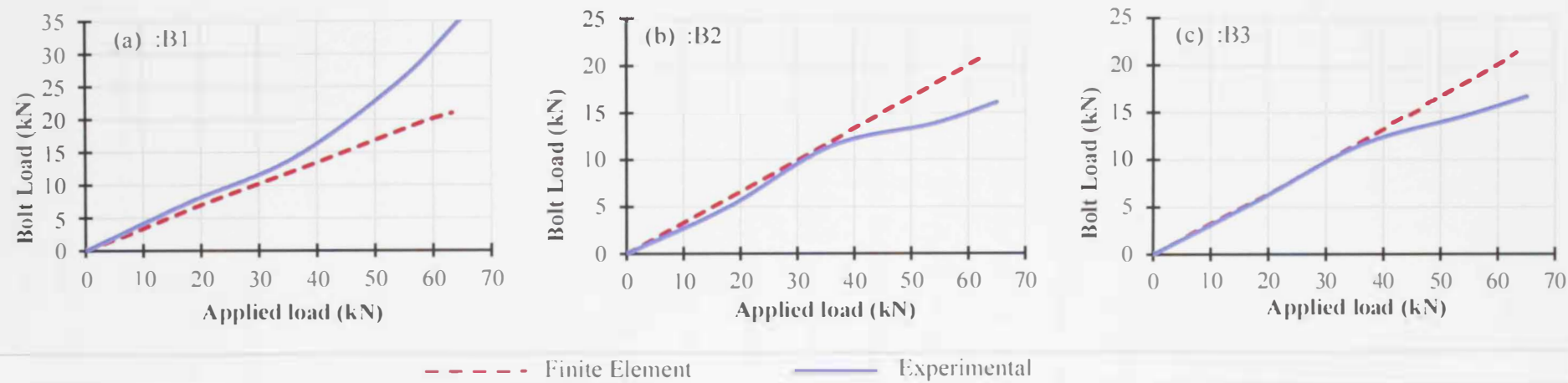
Figure 4.34: Experimental and numerical bolt load-applied load curves of S_37D for: (a) B1, (b) B2 and (c) B3

4.3 Finite Element Modeling of Connections with FRP Anchors

Connections formed using FRP anchors were modeled following similar procedures to those used in modeling connections fastened with steel bolts. Meanwhile, a new load-slip model was proposed to simulate the interfacial behavior of the HFRP-steel connection fastened with FRP anchors. As discussed in section 3.3.2, the FB13_3D configuration (with a sheared edge distance of three times the hole-diameter) was recommended for optimal performance of similar HFRP-steel connections fastened by FRP anchors. Based on the load-displacement response curve of this selected configuration, the load-slip model shown in Fig. 4.35 was developed. As the experimental load-displacement curve of FB13_3D accounted for the response of one FB13 bearing against two HFRP laminates, the load values were adjusted to represent single-shear setup. Therefore, the loads of the response curve of FB13_3D (shown in Fig. 3.64) were divided by two in order to obtain reference values of one FB13 bearing against one HFRP laminate. It should be noted that the influence of the steel and HFRP elongations during testing were excluded from the displacement values of the response curve to avoid double counting of these effects in the FE model. The various segments constituting the proposed model corresponded to five different failure modes of the FB13_3D connection. Segment "A" represents the friction between the HFRP laminates and the steel plates, while segment "B" relates to the relative slippage arising from the bolt-hole clearance. Bearing action between the FB13 and the HFRP laminates is reflected by segment "C". Part "D" represents the combined effect of bearing and bending in anchors. Finally, the ultimate shear failure of the FB13 is demonstrated by segment "E". Description and verification of the developed FE model are discussed in sections

4.3.1 and 4.3.2. Comparisons between the numerically predicted load-displacement relationships and strains and their experimental counterparts are also presented.
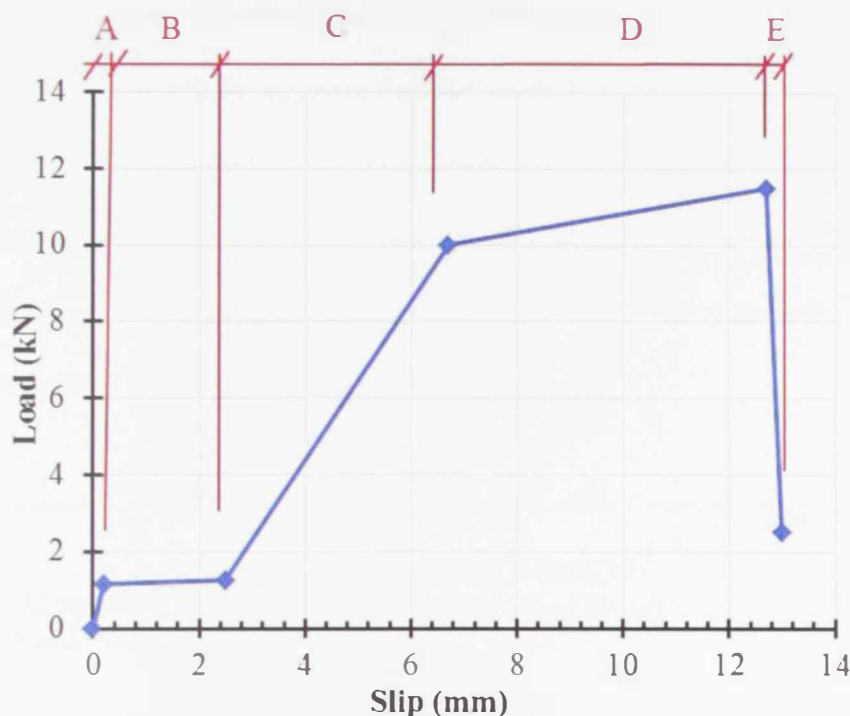
Figure 4.35: Nonlinear load-slip model of the FB13_3D connection

4.3.1 Description of the Finite Element Model with FRP Anchors

Similar to the procedure outlined in section 4.2.1, a three-dimensional model was developed using ANSYS (2009) to simulate the behavior of fastened HFRP-steel connections using FRP anchors. Considering the symmetry of the connection, one-half of the connection was modeled involving one HFRP laminate and half the thickness of the steel plates. The FE model used the previously described (SOLID45) element to model the geometry of both the HFRP laminate and the steel plates. Meanwhile, the nonlinear spring element (COMBIN39) was used to model both steel bolts and FB13 anchors located at the clamped and loaded sides of the connection, respectively. Therefore, the (COMBIN39) element was defined twice in the FE model. At the loaded steel plate, where the FB13 was employed, the load-slip model

shown in Fig. 4.35 was introduced to describe the (COMBIN39). In the meantime, the load-slip model that was developed earlier to simulate the behavior of the steel bolts (Fig. 4.1) was used to define the (COMBIN39) elements at the clamped side of the connection. It is worth mentioning that the used materials, boundary conditions and loading system were identical to those described in section 4.2.1. The numerical analysis was conducted in a displacement-control manner along the X-direction. Figure 4.36 presents the geometry of the modeled FB13_3D connection and the location of the FB13 at the loaded steel plate.
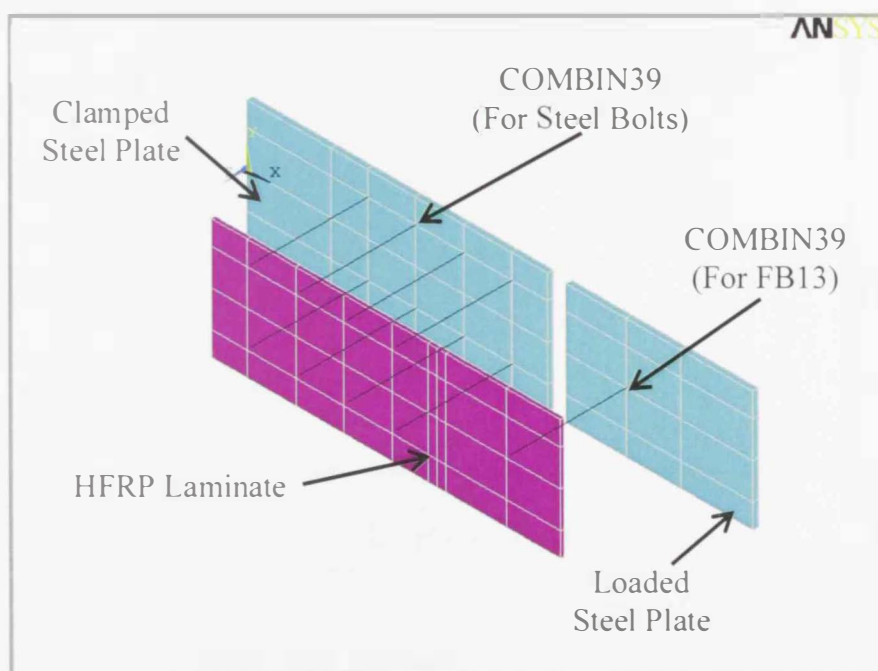
Figure 4.36: Geometry and locations of FB13 and steel bolts in the modeled FB13_3D connection (Spacing between steel and HFRP is exaggerated for clarity of the presentation)

4.3.2 Verification of the Finite Element Model with FRP Anchors

The FE model developed in section 4.3.1 was used to simulate the experimental behavior of the HFRP-steel connection fastened using FB13. To validate the accuracy of the FE model and FB13 load-slip model, a comparison was

held between the experimental and numerical load-displacement response curves of

the FB13_3D connection as shown in Fig. 4.37. An excellent match between the

experimental and the numerical response curves can be observed. It should be noted

that the (COMBIN39) spring element which was used to simulate the FB13 was

killed at a displacement of around 13 mm to reflect the sudden failure of the element

as shown in Fig. 4.35. An error of 1.85% was calculated between the predicted and

the experimental peak loads of the FB13_3D connection, which proves the accuracy

of the predictions of the FE model at the various loading stages.
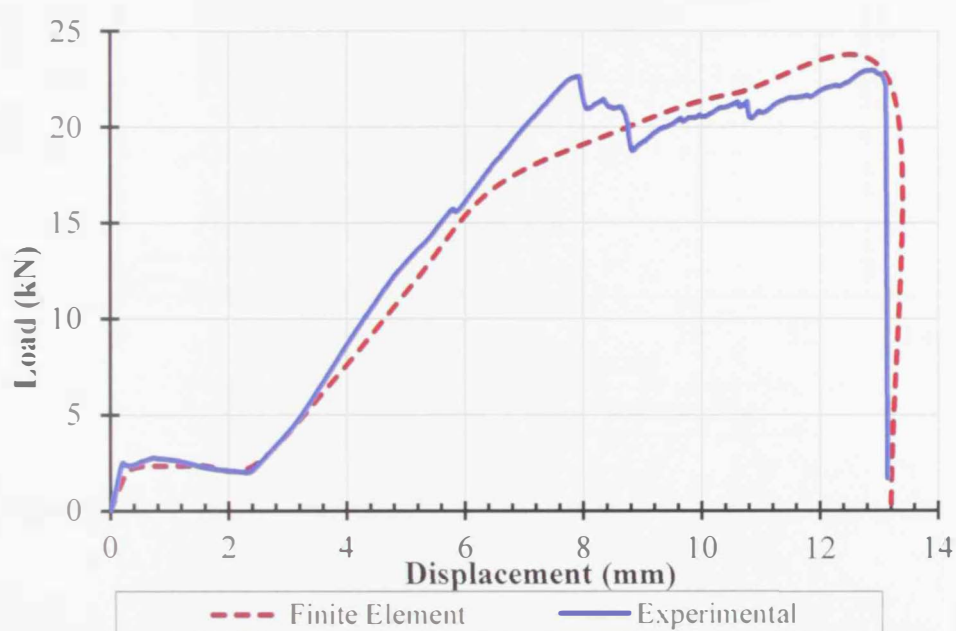
Figure 4.37: Experimental and numerical load-displacement curves for the
modeled FB13_3D connection

For further validation, a comparison between the numerically predicted

strains in the HFRP laminates and those measured experimentally was conducted.

The comparison was based on the measurements of the two strain gauges that were

attached to the front and backsides of the tested FB13_3D connection. Experimental

results revealed very close strain measurements at both gauges, thus, the recorded

strains at the Front SG were plotted against the finite element predictions in Fig.

4.38. It can be observed that the FE model provides reasonable predictions of the strains induced in the HFRP laminates. Due to its sensitivity to local effects that take place in the fibers during testing, strain measurements are always more difficult to simulate with the same order of accuracy achieved in load-displacement measurements.
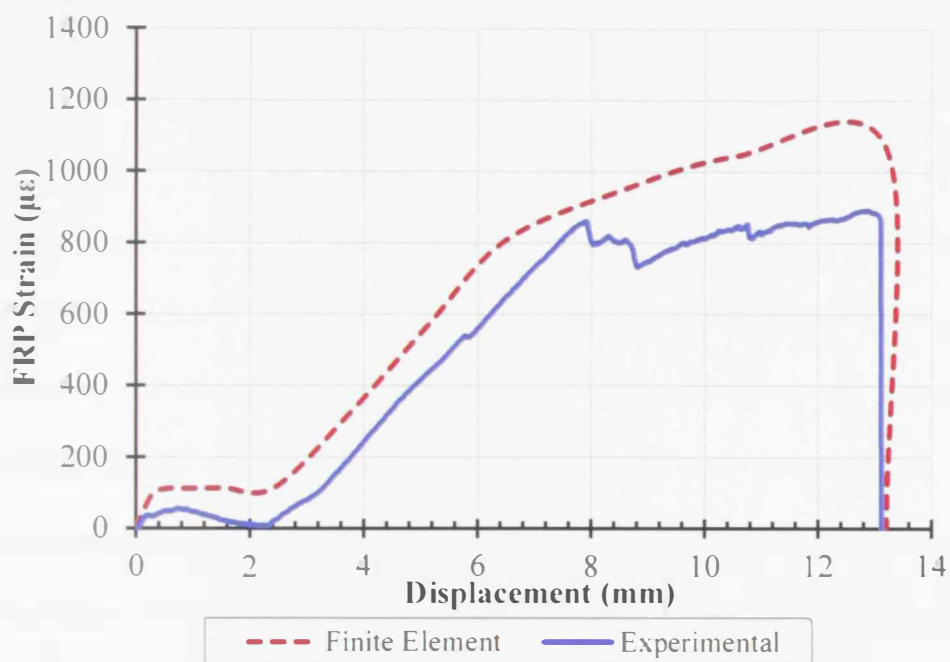
Figure 4.38: Experimental and numerical strain-displacement curves for FB13_3D connection at the Front SG location

4.4 Summary and Conclusion

The objective of this chapter was to develop 3-Dimessional nonlinear finite element models that simulate the behavior of HFRP-steel connections fastened using steel bolts and FRP anchors. This was attained through developing nonlinear load-slip models for connections fastened with two types of fasteners: steel bolts and FRP anchors. Two load-slip models were proposed to account for the different failure modes of each connection. Based on the observations and discussion presented in Chapter 3, W2_D8_ST connection with steel bolts was modeled since it showed

optimal behavior. Similarly, the FB13_3D connection was modeled to simulate the best performance of connections fastened with FRP anchors. The adopted load-slip models were incorporated into FE models using ANSYS software to address the HFRP-steel interfacial behavior. Both models were verified through comparing the numerically predicted load-displacement curves to their experimental counterparts. Results revealed excellent agreement which validated the accuracy of the proposed load-slip models and the developed FE models. The FE models were capable of predicting the load carrying capacity of the connections with acceptable margin of error of 6.6% and 1.85% for connections fastened with steel bolts and FRP anchors, respectively. Measured FRP strains were also used as an additional means to verify the accuracy of the models through comparing the numerical and experimental strain-displacement curves. Results showed reasonable agreement in both modeled connections using steel bolts and FRP anchors with lower level of accuracy to that obtained using the load-displacement measurements. Moreover, the developed load-slip model for connections with steel bolts was used to simulate the behavior of all tested assemblies with various spacing between bolts. The results revealed excellent match between the experimental measurements and predicted peak loads with a percentage error that ranges from 0.02% to 7.01%.

Chapter 5: Conclusions and Recommendations

The current study is devoted to investigate the effect of various fastening parameters on the performance and load carrying capacity of fastened HFRP-steel connections for possible use in strengthening steel members. An extensive experimental program was carried out followed by numerical modeling of the experimental findings. This chapter presents a brief summary for the main outcomes of the conducted experimental and numerical studies. Recommendations for future research studies relevant to the topic of this thesis are also stated at the end of the chapter.

5.1 Summary and Conclusions

The conducted experimental program aimed at exploring the interfacial behavior of fastened HFRP-steel connections under various fastening parameters including: fastener type and diameter, sheared edge distance, spacing between bolts, number of washers-per-bolt, clamping torque and bolt-hole diameter. The investigation was carried out in two main phases based on the type of fasteners (i.e., steel bolts and FRP anchors). A series of 62 double-lap HFRP-steel connections with different geometrical and fastening configurations were subjected to tensile loading. Load-displacement response curves and FRP longitudinal strains were monitored and recorded during testing. The main outcomes of the experimental program are highlighted in the following points:

- The presence of washers significantly enhanced the ductility and the load carrying capacity of the connections. Enhancements of 75% and 86% in the load capacity of the tested connections were obtained with the use of two and four washers-per-bolt, respectively, compared to those with no washers.

- The interfacial behavior of HFRP-steel connections fastened without washers differed from that observed for connections fastened with two and four washers-per-bolt. The observed softening post-peak response in the load-displacement curves of connections without washers indicated unfavorable performance of this type of connections when no washers are used.

- Connections with washers failed by a combination of failure modes including bearing at the bolt-HFRP interface, bending in the steel bolts, folding of the washers and finally tearing out and BSR in the HFRP laminates.

- The investigated clamping torque values ranging between 11 N.m. and 20 N.m. were proven to have negligible effect on the failure modes and load carrying capacity of the fastened HFRP-steel connections.

- Bolt-hole diameter significantly influenced the response of the tested connections. The use of a net fit bolt-hole reduced the connection ductility compared to standard and loose fit connections. Meanwhile, the ultimate load capacity of the tested connections was maintained unchanged regardless of the used bolt-hole diameter.

- For the considered range of bolts spacing (50 mm to 300 mm), negligible effect of spacing on the ultimate load capacity of the fastened HFRP-steel connections was observed. However, using spacing value that is twelve times the bolt-hole diameter showed best performance in terms of ductility with 10% higher displacement than other spacing values. It was also concluded that considered bolts' spacing had insignificant influence on the failure mechanisms of the connection.

- The influence of considered sheared edge distance on the response of HFRP-steel connections fastened with FRP anchors was negligible for both tested

diameters. This could be attributed to the fact that this particular type of connections failed by shear in the anchor before the contribution of the sheared edge distance becomes noticeable.

- The maximum recorded load capacity of all connections fastened using FRP anchors of 10 mm diameter corresponded to connections with sheared edge distance that is five times the hole-diameter.

- Using FRP anchors of 13 mm diameter with a sheared edge distance that is three times the hole-diameter enhanced the ductility of the fastened connections and resulted in the highest peak load among all tested sheared edge distances.

- Increasing the bolt diameter of the FRP anchors from 10 mm to 13 mm resulted in 65% increase in the ultimate load carrying capacity of the connection and enhanced its ductility.

- The load capacity of the HFRP-steel connection using a single FRP anchor of 13 mm diameter was almost equal to the one provided by a steel bolt of 6 mm diameter in a single shear setup.

- From economic standpoint, it is recommended to use steel bolts (0.22 $ per bolt) over the FRP anchors (7.6 $ per bolt) in fastening HFRP-steel connections. However, FRP anchors are expected to provide better corrosion resistivity than steel bolts.

Recorded experimental measurements of HFRP-steel connections fastened with steel bolts and FRP anchors were utilized to develop two nonlinear load-slip models for the interfacial behavior and associated relative slippage. Both load-slip models were utilized in developing 3D nonlinear finite element models that simulate

the behavior of the fastened connections. HFRP-steel connections with optimal performance (i.e., W2_D8_ST and FB13_3D) were modeled using AYSYS software. Developed FE models were verified through comparing the numerical load-displacement curves to their experimental counterparts. Results revealed excellent agreement which validated the accuracy of the proposed load-slip models and the developed FE models. The developed FE models were capable of predicting the load carrying capacity of the connections with acceptable margin of error of 6.6% and 1.85% for connections fastened with steel bolts and FRP anchors, respectively. Measured FRP strains were also used as additional means to verify the accuracy of the models. Results showed reasonable agreement between the numerically predicted strains and the recorded experimental ones. Moreover, the developed load-slip model for connections fastened using steel bolts was used to simulate the behavior of all tested assemblies with various spacing between bolts. The results showed excellent match between the experimental measurements and predicted peak loads with a percentage of error ranging from 0.02% to 7.01%.

5.2 Recommendations for Future Research

Based on the outcomes of the conducted experimental and numerical investigations, the following recommendations are suggested for future studies to enrich the literature of strengthening steel elements by HFRP laminates using fasteners:

- The findings of this study could be implemented on a larger scale through strengthening full-scale steel beams.

- The performance of fastened HFRP-steel connections under fatigue loading with respect to the various fastening parameters is of high importance and requires experimental and/or numerical investigations.

- The response of fastened HFRP-steel connections under creep is essential and requires experimental and/or numerical investigations.

- The behavior of the fastened HFRP-steel connections under various environmental conditions especially at elevated temperatures needs to be studied.

- The calibrated finite element model could be used in future studies.

- The experimental results of this study could be compared to test specimens where FRP laminates are bonded to steel plates using adhesive.

References

American Institute of Steel Construction (AISC). ANSI/AISC 360–10 specification for structural buildings 14th edition; 2010. Chicago, USA.

American Society of Testing Materials (ASTM) Standards. (2014) "A370-14: Standard Test Methods and Definitions for Mechanical Testing of Steel Products". USA.

American Society of Testing Materials (ASTM) Standards. (2014) "D3039_D3039M-14: Standard Test Method for Tensile Properties of Polymer Matrix Composite Materials". USA.

ANSYS User's Manual Release 12.0.1 (2009). Canonsburg, Pennsylvania, USA.

Ascione, F., Feo, L., and Maceri, F. (2010). On the pin-bearing failure load of GFRP bolted laminates: an experimental analysis on the influence of bolt diameter. *Composites Part B: Engineering*, 41(6), 482-490.

Chutima, S., and Blackie, A. P. (1996). Effect of pitch distance, row spacing, end distance and bolt diameter on multi-fastened composite joints. *Composites Part A: applied science and manufacturing*, 27(2), 105-110.

Coelho, A. M. G., and Mottram, J. T. (2015). A review of the behaviour and analysis of bolted connections and joints in pultruded fiber reinforced polymers. *Materials and Design*, 74, 86-107.

Cooper, C., and Turvey, G. J. (1995). Effects of joint geometry and bolt torque on the structural performance of single bolt tension joints in pultruded GRP sheet material. *Composite Structures*, 32(1), 217-226.

Crews, J. H. (1981). Bolt-bearing fatigue of a graphite/epoxy laminate. *In Joining of composite materials*. ASTM International.

Deutsches Institut fur Normung (DIN) Standards. (2011). "DIN EN ISO 4017 Hexagon Head Screws – Product Grades A and B". DIN-adopted European-adopted ISO Standards.

Erki, M. A. (1995). Bolted glass-fibre-reinforced plastic joints. *Canadian journal of civil engineering*, 22(4), 736-744.

Esendemir, U., and Öndürücü, A. (2011). Comparison of bolted joints with two different clearance types. *Indian Journal of Engineering and Materials Sciences*, 18(4), 283-292.

Feo, L., Marra, G., and Mosallam, A. S. (2012). Stress analysis of multi-bolted joints for FRP pultruded composite structures. *Composite Structures*, 94(12), 3769-3780.

Hai, N. D., and Mutsuyoshi, H. (2012). Structural behavior of double-lap joints of steel splice plates bolted/bonded to pultruded hybrid CFRP/GFRP laminates. *Construction and Building Materials*, 30, 347-359.

Hanauska, J., Kradinov, V., and Madenci, E. (2001). A composite double-lap joint with staggered bolts: an experimental and analytical investigation. *Composite structures*, 54(1), 3-15.

Heshmati, M., Haghani, R., and Al-Emrani, M. (2015). Environmental durability of adhesively bonded FRP/steel joints in civil engineering applications: State of the art. *Composites Part B: Engineering*, 81, 259-275.

Hollaway, L. C. (2010). A review of the present and future utilisation of FRP composites in the civil infrastructure with reference to their important in-service properties. *Construction and Building Materials*, 24(12), 2419-2445.

Hollaway, L. C., and Cadei, J. (2002). Progress in the technique of upgrading metallic structures with advanced polymer composites. *Progress in Structural Engineering and Materials*, 4(2), 131-148.

Hollaway, L.C., and Teng, J. G. (2008). Strengthening and rehabilitation of civil infrastructures using fiber-reinforced polymer (FRP) composites. First edition. Cambridge England, Woodhead Publishing Limited.

Horn, W. J., and Schmitt, R. R. (1994). Influence of clamp-up force on the strength of bolted composite joints. *AIAA journal*, 32(3), 665-667.

Kachlakev D.I. (1998). Strengthening bridges using composite materials FHWA-OR-RD-98-08. *Oregon Department of Transportation, Salem, Oregon.*

Kachlakev D.I., and McCurry D., Jr. (2000). Simulated full scale testing of reinforced concrete beams strengthened with FRP Composites: experimental results and design model verification. *Oregon Department of Transportation, Salem, Oregon.*

Kapti, S., Sayman, O., Ozen, M., and Benli, S. (2010). Experimental and numerical failure analysis of carbon/epoxy laminated composite joints under different conditions. *Materials and Design*, 31(10), 4933-4942.

Kelly, G., and Hallström, S. (2004). Bearing strength of carbon fiber/epoxy laminates: effects of bolt-hole clearance. *Composites Part B: Engineering*, 35(4), 331-343.

Khashaba, U. A., Sallam, H. E. M., Al-Shorbagy, A. E., and Seif, M. A. (2006). Effect of washer size and tightening torque on the performance of bolted joints in composite structures. *Composite Structures*, 73(3), 310-317.

Lawlor, V. P., McCarthy, M. A., and Stanley, W. F. (2005). An experimental study of bolt–hole clearance effects in double-lap, multi-bolt composite joints. *Composite structures*, 71(2), 176-190.

Martinelli, E., Napoli, A., Nunziata, B., and Realfonzo, R. (2012). Inverse identification of a bearing-stress-interface-slip relationship in mechanically fastened FRP laminates. *Composite Structures*, 94(8), 2548-2560.

McCarthy, C. T., McCarthy, M. A., and Lawlor, V. P. (2005). Progressive damage analysis of multi-bolt composite joints with variable bolt–hole clearances. *Composites Part B: Engineering*, 36(4), 290-305.

McCarthy, M. A., Lawlor, V. P., Stanley, W. F., and McCarthy, C. T. (2002). Bolt-hole clearance effects and strength criteria in single-bolt, single-lap, composite bolted joints. *Composites Science and Technology*, 62(10), 1415-1431.

Ozen, M., and Sayman, O. (2011). Failure loads of mechanical fastened pinned and bolted composite joints with two serial holes. *Composites Part B: Engineering*, 42(2), 264-274.

Realfonzo, R., Martinelli, E., Napoli, A., and Nunziata, B. (2013). Experimental investigation of the mechanical connection between FRP laminates and concrete. *Composites Part B: Engineering*, 45(1), 341-355.

Riccio, A. (2005). Effects of geometrical and material features on damage onset and propagation in single-lap bolted composite joints under tensile load: part II– numerical studies. *Journal of composite materials*, 39(23), 2091-2112.

Riccio, A., and Marciano, L. (2005). Effects of geometrical and material features on damage onset and propagation in single-lap bolted composite joints under tensile load: part I– Experimental studies. *Journal of composite materials*, 39(23), 2071-2090.

Rosales-Iriarte, F., Fellows, N. A., and Durodola, J. F. (2011). Experimental evaluation of the effect of clamping force and hole clearance on carbon composites subjected to bearing versus bypass loading. *Composite Structures*, 93(3), 1096-1102.

Salmon, C. G., Johnson, J. E., and Malhas, F. A. (2009). Steel Structures: Design and Behavior, Emphasizing Load and Resistance Factor Design, 5th Ed., Pearson Prentice Hall Publishers, Upper Saddle River, New Jersey, USA.

Sen, R., Liby, L., and Mullins, G. (2001). Strengthening steel bridge sections using CFRP laminates. *Composites Part B: Engineering*, 32(4), 309-322.

Starikov, R., and Schön, J. (2001). Quasi-static behaviour of composite joints with countersunk composite and metal fasteners. *Composites Part B: Engineering*, 32(5), 401-411.

Starikov, R., and Schön, J. (2002). Fatigue resistance of composite joints with countersunk composite and metal fasteners. *International journal of fatigue*, 24(1), 39-47.

Stockdale, J. H., and Matthews, F. L. (1976). The effect of clamping pressure on bolt bearing loads in glass fiber-reinforced plastics. *Composites*, 7(1), 34-38.

Sweedan, A. M., Alhadid, M. M., and El-Sawy, K. M. (2016). Experimental study of the flexural response of steel beams strengthened with anchored hybrid composites. *Thin-Walled Structures*, 99, 1-11.

Sweedan, A. M., El-Sawy, K. M., and Alhadid, M. M. (2013). Interfacial behavior of mechanically anchored FRP laminates for strengthening steel beams. *Journal of Constructional Steel Research*, 80, 332-345.

Sweedan, A. M., Rojob, H. N., and El-Sawy, K. M. (2014). Mechanically-fastened hybrid composites for flexural strengthening of steel beams. *Thin-Walled Structures*, 85, 250-261.

Tong, L. (2000). Bearing failure of composite bolted joints with non-uniform bolt-to-washer clearance. *Composites Part A*: Applied science and manufacturing, 31(6), 609-615.

Wang, H. S., Hung, C. L., and Chang, F. K. (1996). Bearing failure of bolted composite joints. Part I: experimental characterization. *Journal of Composite Materials*, 30(12), 1284-1313.

Xia, S. H., and Teng, J. G. (2005, December). Behaviour of FRP-to-steel bonded joints. *In Proceedings of the international symposium on bond behaviour of FRP in structures* (pp. 419-26). International Institute for FRP in Construction.

Yan, Y., Wen, W. D., Chang, F. K., and Shyprykevich, P. (1999). Experimental study on clamping effects on the tensile strength of composite plates with a bolt-filled hole. *Composites Part A*: Applied science and manufacturing, 30(10), 1215-1229.

Zhao, X. L., and Zhang, L. (2007). State-of-the-art review on FRP strengthened steel structures. *Engineering Structures*, 29(8), 1808-1823.

List of Publications

O. R. AbouEl-Hamd, A. M. I. Sweedan, K. M. El-Sawy, "Experimental Assessment of the Main Factors Controlling the Mechanical Behavior of Bolted Hybrid Connections", Proceedings of the 2nd International Conference on Infrastructure Management, Assessment and Rehabilitation Techniques (ICIMART'16), Sharjah, UAE, Mar. 8-10, 2016.